Understanding the basis of corneal shape and transparency

Patrycja Joanna Boguslawska

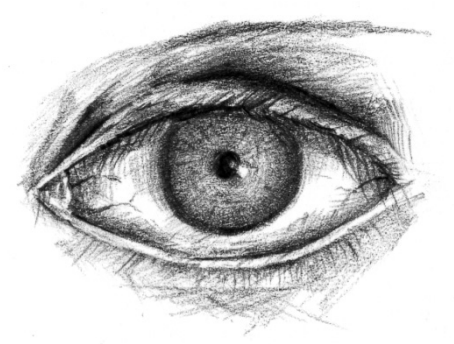

Structural Biophysics Research Group,
School of Optometry and Vision Sciences,
Cardiff University

June 2012

Form: PGR_Submission_200701

NOTICE OF SUBMISSION OF THESIS FORM: POSTGRADUATE RESEARCH

APPENDIX 1:
Specimen layout for Thesis Summary and Declaration/Statements page to be included in a Thesis

DECLARATION

This work has not previously been accepted in substance for any degree and is not concurrently submitted in candidature for any degree.

Signed ..... P. Bogucińska ..... (candidate) Date 15.07.13

STATEMENT 1

This thesis is being submitted in partial fulfillment of the requirements for the degree of MPhil

Signed ..... P. Bogucińska ..... (candidate) Date 15.07.13

STATEMENT 2

This thesis is the result of my own independent work/investigation, except where otherwise stated. Other sources are acknowledged by explicit references.

Signed ..... P. Bogucińska ..... (candidate) Date 15.07.13

STATEMENT 3

I hereby give consent for my thesis, if accepted, to be available for photocopying and for inter-library loan, and for the title and summary to be made available to outside organisations.

Signed ..... P. Bogucińska ..... (candidate) Date 15.07.13

Acknowledgements

First of all I would like to thank my supervisors, Prof. Keith Meek who gave me great opportunity to take part in this very interesting project.

I greatly appreciate the help of Dr Rob Young who was teaching me the principles of embedding procedure, preparing samples, and operating transmission electron microscope. It was a pleasure to be working with him and I am very grateful for his patience and his constant words of encouragement.

I also thank Dr Sally Hayes for her help and constant support, especially during my last experiments and while I was collecting the final data. She was always helpful and gave me many pieces of advice about tissue preparation and x-ray procedures. Her pleasant character made my work easier.

My gratitude also goes to my colleague Geraint Parfitt who had always time to help me with special programs for 3-D tomography reconstruction and data analysis.

Also I would like to thank people who I was working with and shared the same office: Basia Palka, Erin Dooley, Jon Harris, and Tariq Alhamad.

I want to express my special gratitude to my friends Professor Chris Gold from Glamorgan University and his wife Valerie. They guided me through the hardest moments and encouraged me at all times. Their confidence in my ability to complete my work kept me going.

Finally, I would like to thank my beloved husband Pawel for his constant support, motivation and encouragement throughout these years of my study.

This thesis I dedicate to my son Jakub

Abstract

Corneal transparency is a feature that can be explained by the regular arrangement of collagen fibrils and proteoglycans across the whole tissue. This special assembly promotes destructive interference of scattered light and allows only the light going forward to pass through the corneal stromal layers. There are four proteoglycans (PGs) occurring in corneal stroma: decorin, lumican, mimecan, and keratocan. Thanks to their negative charges they make a hydrated interfibrillar gel around collagen fibrils so that the fibrils do not touch each other. However, the way the proteoglycans interact with collagen to promote this spacial arrangement is not known. The first model described in this thesis was achieved from 3-D reconstruction of the tissue. We compared our results with bovine and mouse cornea and reached the conclusion that they are not arranged in any special order around the collagen fibrils. However, they are found in sufficient number in the corneal stroma to be responsible for corneal transparency. We decided to compare our results from the human to the fish cornea to get more general view of the corneal structure. The fish is known to have smaller and more closely spaced fibrils than human. The curvature of the cornea is different as the function of these two tissues is different. Fish is more flat, while the human is more spherical. The lamellar arrangement also differs between these animals. The fish cornea is more circular, while the human is orthogonal. The fibril diameter and collagen spacing is increasing towards the end of these both corneas and following on from this the transparency is reduced as we go to the periphery. We also had a chance to examine guinea pig corneas as a model of Climatic Droplet Keratopathy – a disease which is related to the loss of corneal transparency. They are similar to the human cornea in terms of the demand for ascorbic acid which is responsible for protection against UVB. The results confirmed our assumption: the animals fed on low ascorbic acid diet demonstrated some structural changes connected with UVB radiation.

Table of contents

1 INTRODUCTION 1

1.1 EYE SURFACE, CORNEA 1

1.2 CORNEAL STRUCTURE 2

1.2.1 Epithelium 3

1.2.2 Bowman's layer (anterior limiting membrane) 4

1.2.3 Stroma 4

1.2.4 Descemet's membrane (posterior limiting membrane) 7

1.2.5 Endothelium 8

1.3 COLLAGEN STRUCTURE 10

1.4 COLLAGEN BIOSYNTHESIS 13

1.5 GLYCOSAMINOGLYCANS (GAGS) 15

1.5.1 Dermatan sulphate 16

1.5.2 Keratan sulphate 18

1.6 PROTEOGLYCANS (PGS) 18

1.6.1 Decorin 21

1.6.2 Lumican 23

1.6.3 Mimecan (osteoglycin) 23

1.6.4 Keratocan 24

1.7 PROTEOGLYCAN BIOSYNTHESIS 25

1.8 PROTEOGLYCAN/COLLAGEN INTERACTION 26

1.9 CORNEAL TRANSPARENCY 27

1.10 CORNEAL METABOLISM 30

1.11 SPECIALIST TECHNIQUES USED IN THIS STUDY 31

1.11.1 Electron tomography 31

1.11.2 X-ray diffraction 32

1.12 AIMS OF THE THESIS 35

2 GENERAL MATERIALS AND METHODS 36

2.1 TRANSMISSION ELECTRON MICROSCOPY (TEM) 36

2.1.1 Sample preparation – fixation and dehydration 36

2.1.2 Sectioning procedures 37

2.1.3 Staining of ultrathin sections 40
2.2 X-RAY DIFFRACTION STUDY 41
2.2.1 Introduction 41
2.2.2 Sample preparation 41
2.3 LOW-ANGLE X-RAY DIFFRACTION 41
2.3.1 Data collection 41
2.3.2 Data analysis 42
2.4 HIGH ANGLE X-RAY DIFFRACTION 46
2.4.1 Data collection 46
2.4.2 Data analysis 47
2.5 HISTOLOGY 49
2.5.1 Sample preparation 49
2.5.2 Processing the tissue for wax embedding 50
2.5.3 Sectioning the tissue 50
2.5.4 Clearing (de-waxing) and rehydration of the tissue 51
2.5.5 Haematoxylin and eosin staining 52
2.6 SPECTROPHOTOMETRY 53
2.6.1 Sample preparation 53
2.6.2 Data collection 53
2.6.3 Data analysis 55
3 A STUDY OF PROTEOGLYCANS/COLLAGEN INTERACTION IN THE HUMAN CORNEA BASED ON ELECTRON MICROSCOPY 57
3.1 INTRODUCTION 57
3.2 AIMS AND OBJECTIVES 57
3.3 MATERIALS AND METHODS 58
3.3.1 Sample preparation: human corneas 58
3.3.2 Sectioning of corneas 59
3.3.3 TEM data collection 59
3.4 RESULTS 61
3.4.1 Data analysis using eTomo programme (with IMOD software package) 61
3.4.2 Creating tomography reconstruction (a model of human cornea) in EM3D 64
3.4.3 Analyzing proteoglycan/collagen interactions in the model 65
3.5 DISCUSSION 67

3.6 CONCLUSION 71
3.7 FUTURE WORK 72

4 A STUDY OF CORNEAL STRUCTURE AND COLLAGEN ORIENTATION IN SEA FISH CORNEAS (HAKE, MACKEREL, SALMON, SEABASS) 74

4.1 INTRODUCTION 74
4.1.1 The structure of the fish cornea 74
4.1.2 The function of the fish cornea 76
4.1.3 Aquatic environment of four selected species (hake, mackerel, salmon, seabass) 78
4.2 AIMS AND OBJECTIVES 80
4.3 MATERIALS AND METHODS 81
4.3.1 Sample preparation: fish corneas 81
4.3.2 Histology 82
4.3.3 High angle x-ray data collection and analysis 83
4.3.4 Low-angle x-ray data collection and analysis 84
4.3.5 Spectrophotometry 84
4.4 RESULTS 85
4.4.1 Histology 85
4.4.2 High-angle results 93
4.4.3. Low-angle results 99
4.4.3 Spectrophotometry 102
4.5 DISCUSSION 106
4.6 CONCLUSION 110
4.7 FUTURE STUDY 112

5 A STUDY OF CLIMATIC DROPLET KERATOPATHY IN GUINEA PIGS CORNEAS AS A MODEL OF HUMAN DISEASE 113

5.1 INTRODUCTION 113
5.2 AIMS AND OBJECTIVES 115
5.3 MATERIALS AND METHODS 116
5.3.1 Sample preparation: guinea pigs 116
5.3.2 Low-angle x-ray data collection and analysis 118

5.3.3 TEM data collection 118
5.4 RESULTS 119
5.4.1 Low-angle x-ray results 119
5.4.2 Electron microscopy results 121
5.5 DISCUSSION 123
5.6 CONCLUSION 126
5.7 FUTURE STUDY 127
6 CONCLUDING DISCUSSION 128
REFERENCES: 138

List of figures

Figure 1.1. A cross-section diagram of the human eye (picture after Meek, 2002). 1

Figure 1.2. A cross-section image of the corneal layers; a) photo from the light microscope: EPI – epithelium, BW - Bowman's layer, stroma (occupies 90% of the corneal thickness), DES – Descemet's membrane and ENDO – endothelium (picture after Beuerman and Pendoza, 1996); b) schematic diagram of the human corneal layers including their average dimensions (picture after Michelacci, 2003). 3

Figure 1.3. A diagram of corneal stroma showing keratocytes and collagen arranged into the lamellae in the extrafibrilar matrix (picture adapted from Ehlers et al., 2006). 5

Figure 1.4. Models of endothelium ion transport across its basal and apical membranes; a) shows the activity of basolateral Na + /K + pump and effects of activity HCO3-/Na+ cotransporters (Jentsch et al., 1984); b) reflects Na + /K + exchange as well as HCO3-/Cl- cotransporters (Bonanno and Giasson, 1992). 8

Figure 1.5. Cells in the endothelium layer viewed from the apical side showing typical hexagonal pattern (picture reproduced from Fischbarg, 2006). 10

Figure 1.6. Schematic structure of collagen; a) one alpha chain consists of glycine and two other amino acids; b) triple helix formed by three α-helices bond together (picture after Oyster, 1999). 11

Figure 1.7. Sketch of the hierarchical structure of the collagen molecule in cornea; picture a) and b) after www.steve.gb.com/science/extracellular_matrix.html, and picture c) after http://www.grendahl.com/eyeworks/index.html). 12

Figure 1.8. Structure of procollagen molecule including: A – N-terminal propeptide, B – short, non-triple-helix that contains the site of the N-terminal peptide which is cleaved, C – the main triple helix domain with the repeating sequence Gly-X-Y, D – another telopeptide, E – the C-terminal peptide with the disulfide bonds, removed during biosynthesis (picture after Michelacci, 2003). 14

Figure 1.9. A diagram of biosynthesis of collagen including intracellular events: 1) synthesis of pro-α chains, 2) hydroxylation of prolines and lysines, 3) glycosylation of hydroxylysines, 4) subsequent isomerization which enable pro-α chains to 5) create triple-helix; extracellular events: 6) transport procollagen molecule in the secretory vesicles to the extracellular matrix (ECM), 7) removing the propeptides from procollagen, and 8) assembling the collagen molecule into fibril (picture adapted from Alberts et al., 2002). 15

Figure 1.10. Imagined model of the illustrative proteoglycan showing typical features of the PG molecule. GAGs composed of hexosamine (GlcN-glucosamine or GalN-galactosamine) and hexuronic acid (GlcA-glucuronic acid or IdoA-iduronic acid) are shown as two chains joined to the protein core. GAGs consists of G-G-X (galactosyl-galactosyl-xylosyl) trisaccharide units bound to the serine (Ser) on the protein core. They carry CS/DS (chondroitin sulphate/dermatan sulphate) and HS

(heparan sulphate) chains. This picture shows potential phosphate group (P), oligosaccharides (OS) and keratan sulphate (KS) among the PGs molecule. PGs in the core protein carry many other domains like: A – anchoring domain, whose role is to attach the PGs to the other molecules in extracellular matrix or to the cell surface, D – other domains which can perform any other functions (picture after Kjellen and Lindahl, 1991). 19

Figure 1.11. Classification of the small leucine-rich proteoglycans SLRPs where: C means the cysteine and x means any amino acid (diagram after McEwan et al., 2006). 20

Figure 1.12. Image of the electron microscope in bovine corneal stroma. Arrows show fine proteoglycan filaments, which are frequently regularly spaced and orthogonal to the collagen fibrils. Collagen fibrils are banded structues running approximately horizontally (picture after Scott and Haigh, 1988). 21

Figure 1.13. Three dimensional organization of decorin (*white*) interacting with a triple helix of collagen (*yellow*). The concave surface of decorin consists of charged residues with basic (*blue*) and acidic amino acid residues (*red*). In this model the glycosaminoglycan attachment site on asparagine (N-linked oligosaccharide) and serine domains are seen as *purple* and *green* residues, respectively (picture adapted from Iozzo, 1999). 22

Figure 1.14. A schema showing proteoglycans binding sites (a, b, c, d, e) on collagen fibrils (diagram after Scott, 1995). The letters mean as follows: GDRGETGPAGP is an 11-amino acid sequence (at least one copy of each binding site); QS – ordered quarter-staggered array bands of polar amino acids; BP – bar-code pattern 'fibril', which is asymmetric and labelled with letters from a to e; CS – chondroitin sulphate; KS – keratan sulphate. 26

Figure 1.15. Two images presenting *Lattice Theory* of corneal transparency; a) section shows cornea as a lattice where collagen fibrils are arranged in a perfect order (after Ameen et al., 1998); b) picture shows hexagonal lattice where each of the fibrils scatter the light independently (picture adapted from Maurice, 1957). 28

Figure 1.16. Diagram showing factors important in maintaining transparency of normal corneal endothelium (picture after Edelhauser, 2006). 30

Figure 1.17. An example of the model generated using electron tomography: 3-D reconstruction of the virus based on 2-D projections (adapted from Harris et al., 2006). 32

Figure 1.18. A diagram displaying the reflections of the cylindrical collagen fibrils placed in an X-ray beam (picture after Meek and Fullwood, 2001a). 34

Figure 2.1. Slot grid, mainly used for tilting the specimen under TEM. 38

Figure 2.2. Special plastic bridge used for storing the grids on the film unfolded within the holes. 39

Figure 2.3. Reichert-Jung 'Ultracut E' Ultramicrotome station. 39

Figure 2.4. Diamond Light Source (picture adapted from the Diamond web page:http://www.diamond.ac.uk/Home/About.html) 41

Figure 2.5. Low-angle x-ray pattern from the centre of a normal fish cornea (a vertical transect selected thorough the centre of the pattern was chosen to create an intensity profile – shown as dashed black rectangle). 42

Figure 2.6. a) An intensity profile of the x-ray pattern; b) the same pattern folded around the centre producing average intensity profile of the two halves. 43

Figure 2.7. A linear background was removed from image profile of scattering intensity. This action left only the low-angle reflection of the cornea. 44

Figure 2.8. The Bessel function fitted to the 3rd order of collagen in the profile of scattering intensity. 45

Figure 2.9. Typical WAXS pattern from corneal collagen (picture adapted from Boote et al., 2004). 46

Figure 2.10. a) Normalized X-ray scatter intensity around the intermolecular collagen reflection: isotropic scatter (collagen) and aligned scatter (collagen); b) only the aligned scatter (collagen) displayed without background (picture after Boote et al., 2004). 48

Figure 2.11. Sample of polar coordinates created by conversion of the aligned collagen by shifting the intensity profile by 90 degrees (taking into consideration the fact that collagen fibrils scatter X-rays at right angles to the fibril axis (picture after Boote, et al., 2004). 49

Figure 2.12. The Microtome (Leica, Microm HM 325) 51

Figure 2.13. Fume hood with all the stains ready for staining procedure. 52

Figure 2.14. Pye Unicam SP8-100 Spectrophotometer 53

Figure 2.16. The sample chamber designed for spectrophotometry study. 55

Figure 3.1. Schematic representation of the components from a model of proteoglycan/collagen interaction. This picture shows collagen fibrils as yellow cylinders arranged in regular lattice. Proteoglycans (seen as grey lines) are connected to the next nearest collagen fibril creating the hexagonal pattern around each of them (adapted from Müller et al., 2004). 58

Figure 3.2. Picture presenting the parts of the cornea where the sections were taken: central part of the cornea, peripheral cornea, sclera and limbus. 59

Figure 3.3. Image showing relationship between series of 2D images obtained from TEM and 3D objects made in special software package IMOD. 60

Figure 3.4. Picture taken at tilt 0° under transmission electron microscope (first picture from the whole tilt series). 61

Figure 3.5. Image showing colloidal gold particles (surrounded by the green circles) act as fiducial markers placed on the surface of the specimen. 62

Figure 3.6. Screenshot showing the interface of the eTomo program which is used for making the initial alignment. 63

Figure 3.7. Screenshot from the tomogram positioning stage of eTomo program. 63

Figure 3.8. Screenshot showing the interface of EM3D programme (longitudinal collagen fibres and small proteoglycans between them which were drawn using this tool as red elements). 65

Figure 3.9. Model of normal human cornea arranged in longitudinal section. Collagen fibrils are shown as long cylindrical strings, whereas small proteoglycans concentrate along their axis are marked with claret and purple colour, a) face view of the model, b) side view of the same model. 66

Figure 3.10. A diagram showing interaction between collagen fibrils and proteoglycans in corneal stroma (p means protein core of PGs). KS and CS/DS proteoglycans occur as duplexes which means they have at least two glycan chains. CS/DS GAG chains are longer than KS GAG chains (picture adapted from Scott, 1992a). 67

Figure 3.11. A diagram showing the relationship between two neighbouring collagen fibres and proteoglycans acting as a bridge (see full description in text), the pluses on the picture are the positive charged ions and the blue dots are the water molecules (after Lewis et al., 2010). 69

Figure 3.12. A longitudinal view of 3D reconstruction of bovine cornea, the collagen fibrils are marked with blue and proteoglycans are coloured with yellowish, thin threads around them; a) face view of the model; b) side view of the same model (adapted from Lewis et al., 2010). 70

Figure 3.13. Picture showing three-dimensional reconstruction of collagen/proteoglycans arrangement in the mid stroma of the mouse cornea: a) longitudinal section; b) transverse section. The collagen fibrils are marked with blue colour and the proteoglycans are coloured yellow. Scale bar = 50nm (adapted from Parfitt et al., 2010). 71

Figure 3.14. A human corneal stroma exposed to exceeding critical electron dose (there are visible distinct pattern of burning tissue – seen as white bubbles, mostly on the left hand side of the picture). 73

Figure 4.1. Image presenting the structure of the fish eye in cross-section (Collin and Collin, 2001). Individual elements are described in the text. 75

Figure 4.2. Two diagrams comparing the accommodation in human and fish cornea. These two pictures show the difference in shape of the cornea in different environment (picture adapted from Hawryshyn, 1998). The letters in the diagram refer to the following: *t* is the thickness of the lens, *d* is the lens diameter. 77

Figure 4.3. Picture showing the location of the lens muscle (Nicol and Somiya, 1989). 78

Figure 4.4. Picture showing four of the fish species used in our study: a) mackerel; b) seabass; c) hake; and d) salmon (pictures not to scale). 79

Figure 4.5. A diagram showing the way the cornea was cut for the histology study 82

Figure 4.6. Leica DM RA2 microscope. 83

Figure 4.7. A diagram showing the way the cornea was scanned for collection of the high-angle x-ray patterns. The arrows show the direction of the monochromatic x-ray beam. 83

Figure 4.8. A diagram showing the transect scan across the centre of the cornea collected for low-angle x-ray pattern. The arrow shows the direction of monochromatic x-ray beam. 84

Figure 4.9. The hake cornea. Cornea is divided into two layers: outer layer (dermal cornea) and inner layer (scleral cornea) – both are visible in the picture. The outer layer – spectacle is attached to the scleral cornea. The picture shows also the cartilaginous sclera at the edge of the cornea, and the annular ligament appearing as a third layer of the cornea. 87

Figure 4.10. The hake cornea (the close-up). In the picture there is well seen the division between two corneal layers: outer and internal layer. 88

Figure 4.11. The hake cornea. The general view showing the basis cross section through the whole tissue. 88

Figure 4.13. The salmon cornea. On the picture there is very well seen the homogenous structure of the tissue and the cartilaginous sclera at the edge of the cornea. 90

Figure 4.14. The general view of the salmon cornea. 90

Figure 4.15. The picture showing the seabass cornea with two distinguished separate layers: the outer layer – spectacle and the inner layer. The spectacle is fused (attached) to the sclera cornea hence there are two clearly visible separate layers.On both sides is visible cartilaginous sclera. 91

Figure 4.16. The seabass cornea with all the structures described in the picture. 92

Figure 4.18. A diagram displaying how the features on the graphs from the high-angle x-ray pattern correspond to the position in the fish cornea. 94

Figure 4.19. The graphs showing: a) total, b) aligned, and c) beta scatter, d) vector polar plot of the hake cornea (the annulus is marked as the red line around the cornea). Picture: a, b and c has also the scale of density shown in the key. 96

Figure 4.20. The graphs showing: a) total; b) aligned; and c) beta scatter; d) vector polar plot of the salmon cornea. Picture: a, b and c has also the scale of density shown in the key. 97

Figure 4.21. The graphs showing: a) total; b) aligned; and c) beta scatter, d) vector polar plot of the seabass cornea. Picture: a, b and c has also the scale of density shown in the key. 98

Figure 4.22. Two graphs showing results from low-angle x-ray scatter: a) interfibrillar spacing, b) fibril diameter of mackerel cornea. Pictures indicate the results for left and right eye. 100

Figure 4.23. Two graphs showing results from low-angle x-ray scatter: a) interfibrillar spacing, b) fibril diameter of salmon cornea. Pictures indicate the results for left and right eye. 101

Figure 4.24. The graphs showing the average variation in transmission as a function of the wavelength, at different positions across the fish corneas from the left eye in: a) hake; b) mackerel; and c) salmon. The key presents the position of collected data from the: nasal, centre, and the temporal part of the cornea. 103

Figure 4.25. The graphs showing the variation in transmission by plotting it as a function of position for a given wavelength (550nm was chosen as it is near the centre of the visible spectrum) across the fish corneas from the left eye in: a) hake; b) mackerel; and c) salmon. The key presents individual corneas: 3 hake's specimens, 4 mackerel's, and 3 salmon's. The values on the horizontal axis mean as follows: minus – nasal, 0 – around centre, and plus – temporal side of the cornea. 104

Figure 4.26. The graphs showing the average variations in transmittance as a function of distance from the centre of the cornea and the transmission of light (as a percentage). The wavelength chosen to calculate these variations is seen in the key (550nm was chosen as it is near the centre of the visible spectrum). The values on the horizontal axis mean as follows: minus – nasal, 0 – around centre, and plus – temporal side of the cornea. 105

Figure 4.27. Vector polar plot of the hake cornea (the annulus is marked as the red line around the cornea). 108

Figure 4.28. Diagrams showing the right eye of: a) fish – aligned vector polar plot of hake; b) aligned vector polar plot of human (after Boote et al., 2006).; and c) a model of theoretical arrangement of collagen aligned in predominant directions in human cornea (after Boote et al., 2006). The rhombic shape does not occur in the fish eye as it does not need as high visual acuity as terrestrial eyes (this shape seems to be a feature of the terrestrial eyes). They have also the suturing lamellae which are thought to help flatten the peripheral cornea to make a smoother transition with the sclera (Aghamohammadzadeh et al., 2004). This act is not necessary in the fish cornea..... 110

Figure 5.1. Picture showing the last stage (grade 3) of Climatic Droplet Keratopathy with clearly visible haziness in the lower part of the cornea and small yellow droplets spread within the eye (after Urrets-Zavalia et al., 2007)..... 114

Figure 5.2. Image showing typical droplets found in CDK (3rd grade) surrounded by Bowman's membrane under EM (after Gray et al. 1992). 115

Figure 5.3. Diagram presenting relationship between two different diets and UVB exposure on animals divided into four experimental groups. 117

Figure 5.5. Group A (normal dose of ascorbate, UVB exposure): a) interfibrillar spacing contour map; b) fibril diameter contour map. The collagen interfibrillar spacing (a) and fibril diameter (b) is shown in nanometres in the colour scale on a side of each graph..... 120

Figure 5.6. Group D (low dose of ascorbate, no UVB exposure): a) interfibrillar spacing contour map; b) fibril diameter contour map. The collagen interfibrillar spacing (a) and fibril diameter (b) is shown in nanometres in the colour scale on a side of each graph..... 121

Figure 5.7. Group C (normal dose of ascorbate, no UVB exposure): a) interfibrillar spacing contour map; b) fibril diameter contour map. The collagen interfibrillar spacing (a) and fibril diameter (b) is shown in nanometres in the colour scale on a side of each graph. 121

Figure 5.8. a) Normal dose AA (UVB) – centre (x3000); b) normal dose AA (no UVB) – centre (x3000). 122

Figure 5.9. a) Normal dose AA (UVB) – peripheral (x3000); b) normal dose AA (no UVB) – peripheral (x3000) 122

Figure 5.11. a) Low dose AA (UVB) – peripheral (x3000); b) low dose AA (no UVB) – peripheral (x3000). 123

List of tables

Table 1. Composition of the stroma in human cornea (table adapted from Meek, 2008)..... 6

Table 2. The most typical collagens in the human body (table after Hulmes, 2008)..... 12

Table 3. Structure of different glycosaminoglycan chains (table after Prydz and Dalen, 2000). 17

1 Introduction

The eye is a complex organ composed of many small elements, which have evolved to allow us to see the shape, colour and size of objects, both far and near. In brief the eye is our window to the world. The capability to see everything clearly depends on how well these elements can work together. Light waves from different objects enter the eye first through the cornea, the dome shaped, transparent element at the front of the eye globe.

1.1 Eye surface, cornea

The cornea is the most external layer of the eye, it allows the light rays to enter the interior of the eye and bends the light rays to that they can be brought to a focus on the retina. The retina then converts the light rays into electrical impulses which are transmitted to the brain through the optic nerve (Fig. 1.1).

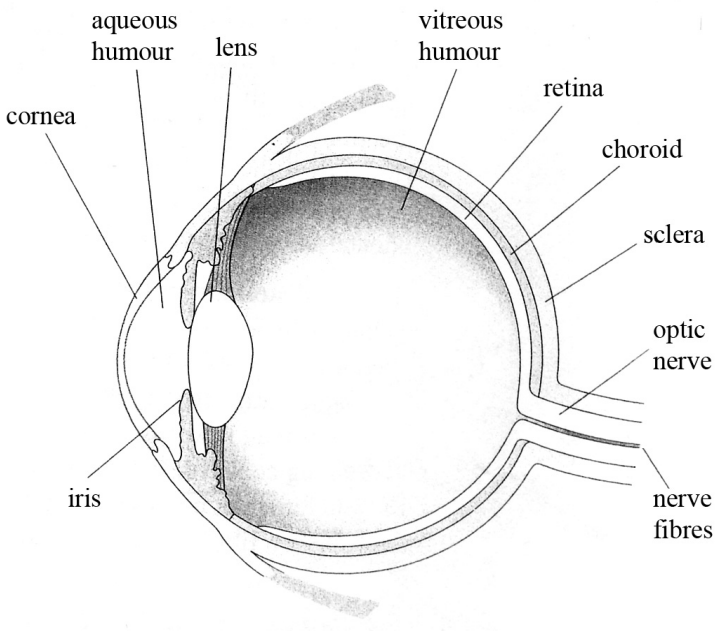

Figure 1.1. A cross-section diagram of the human eye (picture after Meek, 2002).

The surface of the cornea is dust-free and moist because of the tear film coating the front of the eye. This very thin layer protects the eye by preventing it from corneal infection caused by foreign bodies, and bacteria. The tear film creates a smooth optical surface over the cornea and supplies oxygen and other nutrients that the cornea can use in its biological function. At every blink the tear film is renewed and its structure is rebuilt immediately while the eye is open (Alberts et al.; 2002, Ehlers et al., 2006). The posterior part of the cornea is also in contact with moisture because of the watery and very clear intraocular fluid called *aqueous humor*. The curvature of cornea is maintained by the pressure from this fluid behind the cornea.

Surrounding the cornea is the tough, fibrous, "white" opaque tissue of the eye known as the sclera. It protects the delicate structures inside the eye from physical injury and acts as an attachment for the muscles around the eye, muscles which control the movement of the eye (Alberts et al., 2002).

The cornea forms only 15% of the outer layer of the eye ball, whereas the sclera creates the remaining 85%. Both layers meet at a region called the limbus (Meek, 2008). The anterior border of the limbus is a line connecting two ends: Bowman's layer and Descemet's membrane. The posterior border of the limbus in turn is a line where the tissue goes from being transparent to opaque. In the basal layer of the limbal epithelium there are limbal stem cells, which allow the epithelium to regenerate. The limbus tissue contains blood vessels which are arranged into a deep network. The collagen fibrils from the corneal stroma, in the limbus form an annular structure. This arrangement maintains the curvature of the cornea and the cornea-sclera section (Ehlers et al., 2006).

1.2 Corneal structure

Anatomically, along with sclera, the cornea is one of the simplest tissues in the eye. It contains only a few types of cells and its structure is homogenous. The cornea is

avascular and spherical in shape near the visual axis and flattered in the periphery. The cornea is transparent and the sclera is completely opaque. In human the cornea is about 0.7mm thick at the periphery decreasing to about 0.5mm at the centre (Meek, 2008). The diameter of the adult cornea is about 11mm, slightly smaller vertically than horizontally. The central curvature of the surface is 7.8mm which is 44 diopters (Ehlers et al., 2006). The cornea is composed for the most part of connective tissue (containing collagen in the form of fibrils) with a thin layer of the epithelium on the surface (Oyster, 1999). Mainly, the cornea is built up of five parallel layers: the epithelium, Bowman's layer, the stroma, Descemet's membrane, and the endothelium (Fig. 1.2).

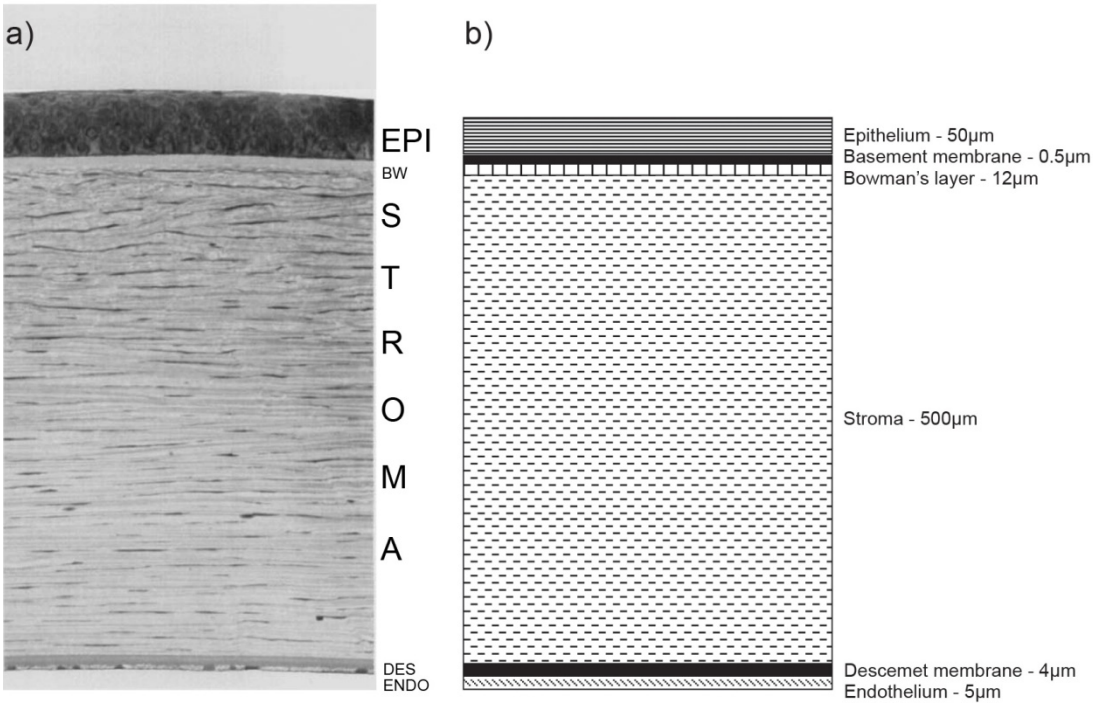

Figure 1.2. A cross-section image of the corneal layers; **a)** photo from the light microscope: EPI – epithelium, BW - Bowman's layer, stroma (occupies 90% of the corneal thickness), DES – Descemet's membrane and ENDO – endothelium (picture after Beuerman and Pendoza, 1996); **b)** schematic diagram of the human corneal layers including their average dimensions (picture after Michelacci, 2003).

1.2.1 Epithelium

The epithelium constitutes about 10% of the corneal thickness and it is divided into three layers that differ in morphology: an outer *squamous layer*, a *wing cells* layer, and

a deeper layer of *basal cells*. Its thickness is around 50μm. The most outer *squamous layer* – the oldest – is sloughed regularly into the tear film. These superficial cells are flattened and join to each other and to the wing cells by *desmosomes* – special adhesion structures in vertebrate epithelial cells that bind cells to their neighbours. These cells communicate through *gap* junctions, across which small molecules can pass (Ehlers et al., 2006). *Wing cells* are irregular in shape with small projections resembling wings that give the cells their name. They were originally the *basal cells* (Oyster, 1999). They push the old cells to the outer surface of the epithelium. The *basal cells* – the newest – are laid next to Bowman's layer and these are the only cells to undergo mitosis (Beuerman and Pendoza, 1996). These are about 15μm in diameter and packed closely alongside. All the cells in epithelium live about 10 days, before being shed in the *squamous layer* in the process called *apoptosis,* a form of programmed cell death (Oyster, 1999).

1.2.2 Bowman's layer (anterior limiting membrane)

Bowman's layer is amorphous, and from 8-12μm thick. It contains short fibrils of Type I collagen which are embedded in a proteglycan matrix (Beuerman and Pendoza, 1996). On the anterior surface of Bowman's layer is the basal lamina of the epithelium which is composed largely of Type I, III, V, and VII collagen and proteoglycans. Type V collagen is found more often than Type I in Bowman's layer. The collagen in Bowman's layer makes an irregular meshwork of fibrils which are thinner than those from the stroma (Ehlers et al., 2006).

1.2.3 Stroma

The stroma constitutes about 90% of the corneal thickness. It is composed mainly of water but the most abundant of the dry constituents is the protein collagen, mainly Type

I and other constituents (Table 1). It also has a smaller amount of Type III, V, VI, XII, and XIV and other nonfibrillar collagen - Type XIII and XVIII (Meek and Quantock, 2001b, Michelacci, 2003, Robert et al., 2001). Types XII and XIV are FACITs collagens (Fibril Associated Collagens with Interrupted Triple helices). Collagen is a major component of all connective tissue, such as tendons, ligaments, bones, skin. The stroma consists of keratocytes which are fibroblasts – cells producing collagen and proteoglycans (PGs) into the extrafibrillar matrix (Fig. 1.3). Keratocytes constitute almost 10% of the stromal volume and their density decreases with age.

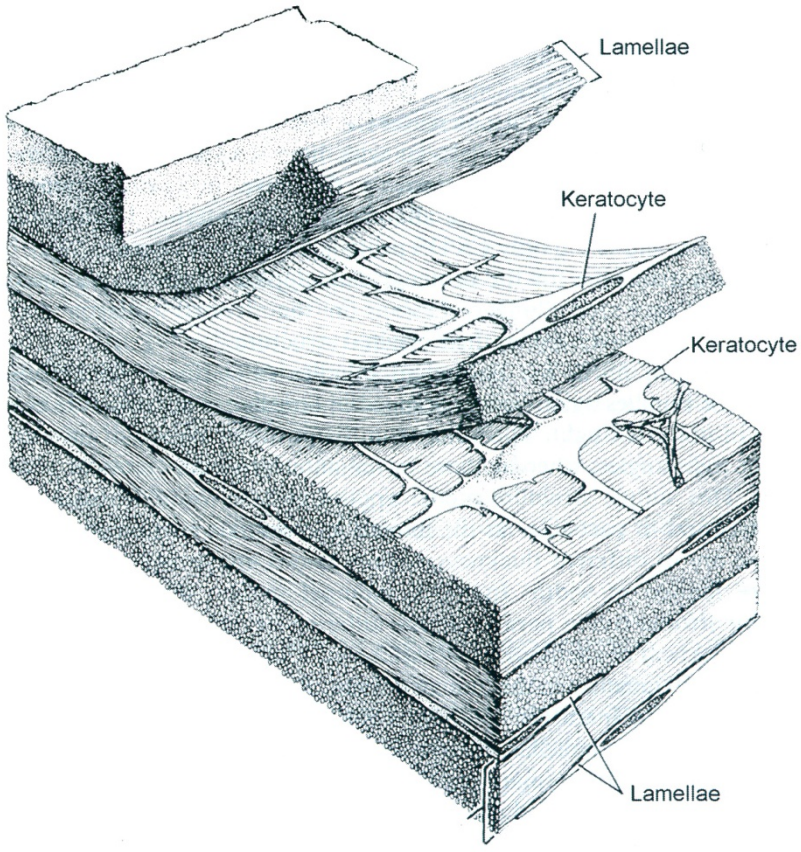

Figure 1.3. A diagram of corneal stroma showing keratocytes and collagen arranged into the lamellae in the extrafibrilar matrix (picture adapted from Ehlers et al., 2006).

Glycosaminoglycans (GAGs) as a part of the proteoglycans (PGs) occur in four main forms: chondroitin sulphate (CS), dermatan sulphate (DS), heparan sulphate (HS) and keratan sulphate (KS), where KS and DS are the predominant PGs in the corneal

stroma. The corneal proteoglycans belong to the family of small leucine-rich proteoglycans (SLRPs). These were named according to their carbohydrate side chains and are known as keratan sulphate (KS) proteoglycans: lumican (11 leucine-rich repeats, single KS side chain), keratocan (10 leucine-rich repeats, 3 KS side chains) and mimecan (5 leucine-rich repeats, 1 KS side chain), and chondroitin sulphate/dermatan sulphate (CS/DS) proteoglycans: decorin – 9 leucine-rich repeats, single CS/DS side chain. The stroma's cells also contain free ribosomes, endoplasmatic reticulum, and a Golgi complex (Beuerman and Pendoza, 1996, Ehlers et al., 2006).

Constituents of the corneal stroma	Wet weight (%)
Matrix water	64.8
Cellular water	11.4
Collagen	14.6
Other proteins (including cellular components)	8.2
Proteoglycans	1.0

Table 1. Composition of the stroma in human cornea (table adapted from Meek, 2008).

In human central cornea, the collagen fibrils are preferentially aligned towards the insertion points of the four rectus muscles. These aligned stromal collagen fibrils are thought to give the cornea additional strength needed to resist changes during any eye movements. In addition to the inferior/superior and medial lateral lamellae, there are other preferentially aligned structures in the peripheral cornea that could help to

maintain the corneal curvature in the eye globe where the cornea meets limbus (Hayes et al., 2007).

As animals live in different environments (terrestrial, aquatic and aerial), they have a different collagen organization of the corneal stroma. The stroma of a vertebrate's cornea is always built up of collagen layers. Each single layer is formed by collagen fibrils running parallel to the others and creating the corneal matrix with the glycosaminoglycans. The fish cornea (and other aquatic vertebrates) has not only one stroma but often even three stromas (mainly in a deep-sea fishes) with different thickness. Some fish posses as the second stroma only one layer of collagen fibres which is called the spectacle (dermal cornea or dermal stroma). This thin layer is situated between epithelium and the typical stroma and is continuous with the skin. The spectacle allows the fish eye to move as if under the protection of safety goggles (Collin and Collin, 2001). The avian cornea displays a diversity in structure and arrangement of collagen layers during embryonic development. Chick corneas possess a primary and secondary stroma with different collagen organisation, which is not seen in any other non-avian embryonic corneas (Quantock and Young, 2008). Their corneas become transparent between 14 and 18 days of development, when the stroma starts to become thin and dehydrate. The collagen fibril number density also changes along with the chicken getting older. The fibrils become organized first in the anterior stroma and reaching day 18 the fibrils are the same in anterior and posterior stroma (Connon et al., 2004).

1.2.4 Descemet's membrane (posterior limiting membrane)

Descemet's membrane is a thick basal lamina which is secreted by the endothelium (Beuerman and Pendoza, 1996). It is about 10μm thick. The main component is Type

VIII collagen which is responsible for the toughness and resistance of the cornea (Tamura et al., 1991).

1.2.5 Endothelium

The endothelium is a single layer of cells. The endothelial cells have a hexagonal shape and are about 20µm wide. This layer is about 5µm thick. The main function of endothelium is to control the passage of water and molecules between the corneal stroma and the *aqueous humor* (it acts as a barrier). Connection between nutrient-rich aqueous humor and the corneal stroma is maintained by the presence of tight junctions by which some ions and macromolecules are permitted to diffuse from the aqueous humor into the stroma. That is why the corneal endothelium is known as a *leaky* barrier (Edelhauser, 2006). The cells in the endothelium are very active because they have a large amount of mitochondria in their cytoplasm, which allows this tissue to be engaged in fluid transport. The other feature of activity is that they have an ion pump which can move ions across the plasma membrane against the concentration gradient (Fig. 1.4). This results in water movement within the cornea so the water can be removed from the stroma.

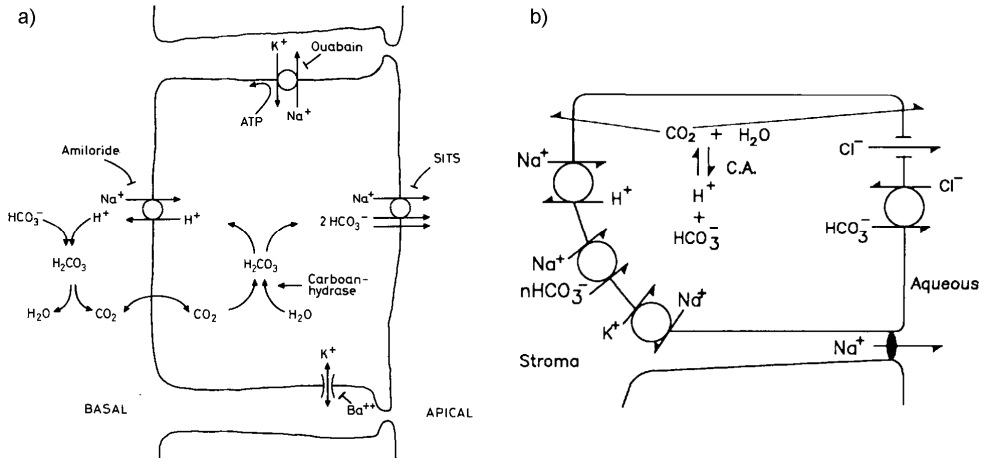

Figure 1.4. Models of endothelium ion transport across its basal and apical membranes; **a)** shows the activity of basolateral Na + /K + pump and effects of activity HCO3-/Na+ cotransporters (Jentsch et al., 1984); **b)** reflects Na + /K + exchange as well as HCO3-/Cl- cotransporters (Bonanno and Giasson, 1992).

A good example of the water flow in the cornea is a sodium/potassium pump which transports sodium ions (Na^+) out of, and potassium ions (K^+) into, the cell using Na^+/K^+ -ATPase enzyme (Fischbarg, 2006). Transendothelial fluid transport in cornea is dependent upon Na^+/K^+ ATPase located on the basolateral membrane of the endothelium. This enzyme delivers enough energy to drive the ion flux, which is stopped by ouabain and causes stromal swelling (Armitage, 1999).

A large number of models of stromal hydration control so far have been suggested and updated to describe the endothelial transport, among others by Bonnano and Giasson (1992), Bonnano and Srinivas (1997), Bonnano (2003), Fischbarg et al. (1985), Fischbarg, (1997, 2003), Fischbarg and Maurice, (2004), Fischbarg and Diecke, (2005), Hodson and Miller (1976). These models are based on the 'pump-leak' hypothesis: which assumes the electrochemical equilibrium across the endothelium is maintained on the one hand by the active transfer of one of the main ions such as: Na, K, Cl, and HCO_3^- in one direction and on the other hand by transfer of ions of the opposite charge in opposite direction (Fischbarg and Maurice, 2004). As Na^+ leaves the endothelial cells via sodium/potassium pump activity, it returns again to them through the basolateral membrane. Thus, in order to equalize its electrochemical gradient, cotransport or exchange of other ions is appearing, such as H^+. There is a basolateral Na^+/H^+ exchanger, inhibited by amiloride, which gives the cells re-entry of Na^+, together with control of intracellular pH (by removing additional protons). There are two possible sources of HCO_3^-. One is the simple diffusion of CO_2 from the intracellular space into the cells. Hence CO_2 with water is converted by carbonic anhydrase into HCO_3^- and ion H^+. (Armitage, 1997; Stiemke et al., 1995). The other is HCO3-/Na+ and HCO3-/Cl- cotransport across the apical membrane, which regulates correct stoichiometry within basolateral and apical membrane (Fig. 1.4).

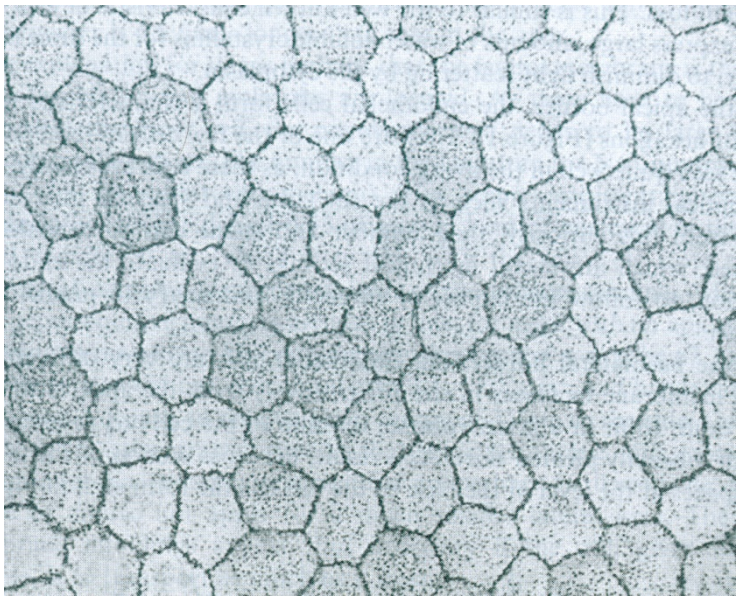

Figure 1.5. Cells in the endothelium layer viewed from the apical side showing typical hexagonal pattern (picture reproduced from Fischbarg, 2006).

The water transport is maintained as a result of sodium and bicarbonate transport. The proper maintenance of hydration has a very important role in transparency (Meek, 2008). The endothelial cells show some regularity (Fig. 1.5) but they vary both in size and shape with age. They become more irregular in shape and their density decreases in old age and in contact lens wearer. This happens because cells that were lost with time cannot be replaced with new ones, so gaps are filled by cell migration and expansion. Compared with the normal cells, more cells now have seven sides (Oyster, 1999).

1.3 Collagen structure

Collagen is the most abundant protein in the body. It has great tensile strength. Collagen is a fibrous structural protein composed of three polypeptide chains. Each chain consist of amino acids which are arranged in a regular sequence: $(Gly\text{-}X\text{-}Y)_n$, where Gly is glycine and X and Y can be any amino acid, and $_n$ is 337-343 (varies in different collagen types). In one sixth of the total sequence is Gly-Pro-Y or Gly-X-Hyp, where

Pro is proline and Hyp is hydroxyproline. This sequence forms a right-handed triple helix (Fig. 1.6).

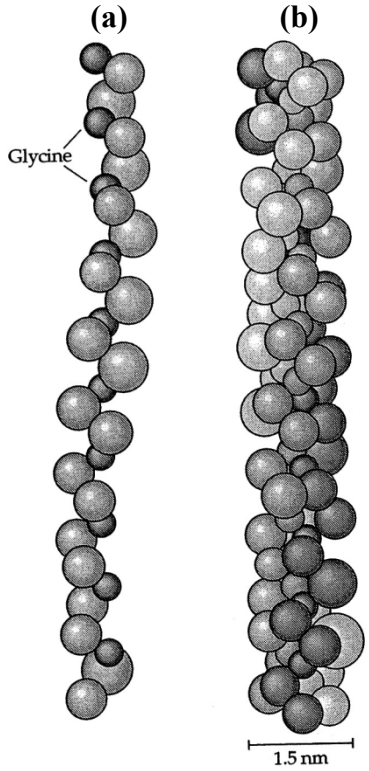

Figure 1.6. Schematic structure of collagen; **a)** one alpha chain consists of glycine and two other amino acids; **b)** triple helix formed by three α-helices bond together (picture after Oyster, 1999).

Each chain is an alpha helix. Proline strengthens the helical structure in each α chain because of its ring structure and glycine allows three helical α chains to wind around one another and create a collagen superhelix (Alberts et al., 2002). Collagen molecules are built of three identical α chains – these are either homotrimeric, or different α chains – heterotrimeric. There are about 28 different collagens in the human body and they are divided into subfamilies: fibrillar collagens, fibril associated and related collagens (e.g. FACIT – Fibril Associated Collagens with Interrupted Triple Helices), basement membrane and associated collagens. The main fibrillar collagens contain collagen Type I, II, III, V and XI (Table 2).

Types of the collagen	Appearance in the human body
Type I	Skin, tendon, bone, ligaments, cornea, lung, vasculature-artery walls, scar tissue, myofibrils
Type II	Cartilage, vertebral disc, vitreous humour of the eye
Type III	Embryonic skin, lung, blood vessels, intestines, uterus
Type V	In association with Type I collagen, cornea
Type XI	In association with Type II collagen, cartilage

Table 2. The most typical collagens in the human body (table after Hulmes, 2008).

The most common collagen in the cornea and sclera is Type I collagen, a heterotrimer which has two different alpha helices. The collagen triple helix is about 1.5 nm in diameter and is usually referred to as the collagen molecule. The collagen molecules are packed into an organized bundle termed a fibril. Fibrils create fascicles where every fibril goes parallel to one another, forming layers of uniform collagen thickness and spacing, called lamellae (Fig. 1.7).

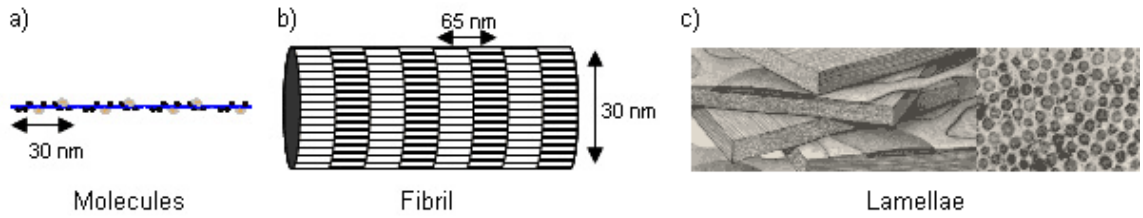

Figure 1.7. Sketch of the hierarchical structure of the collagen in cornea: **a)** collagen molecule, **b)** collagen fibril, **c)** lamellae (source: www.grendahl.com).

Collagen fibres are produced by a type of cell found in all connective tissue, called a *fibroblast*. A corneal fibroblast, called a keratocyte, is a large cell with a flattened shape, and many processes spreading out into the stroma. Keratocytes build an irregular meshwork, touching each other by their processes (Oyster, 1999).

1.4 Collagen biosynthesis

Collagen is synthesized in the rough endoplasmic reticulum (RER) from procollagen – its precursor molecule with N- and C- terminal propetides. In the further biosynthesis of collagen the C-terminal propeptides are removed (Fig. 1.8).

Each polypeptide chain is synthesized from *pro-α-chains* which are encoded by the COL1A1 or COL1A2 genes. Each of these *pro-α-chain* constituents is able to organize a very specific form of each fibrillar collagen, either homo- or heterotrimers. For example, type I collagen as a heterotrimer consists of two proα1(I) chains and one proα2(I) chain (McLaughlin and Bulleid, 1998). Procollagen migrates from the membrane-bound ribosome to the rough endoplasmic reticulum (RER) and here is modified in a series of post-translational processes. The first step is a change from proline to 3- or 4-hydroxyproline (enzymes: prolyl 3- or 4-hydroxylase-assisted), and from lysine to hydroxylysine (enzyme: lysyl hydroxylase-assisted) in the process called hydroxylation -adding the hydroxyl group (OH^-) to the chemical compound (McLaughlin and Bulleid, 1998, Michelacchi, 2003, Robert et al., 2001). This stage is essential to provide stability to the triple helix at body temperature.

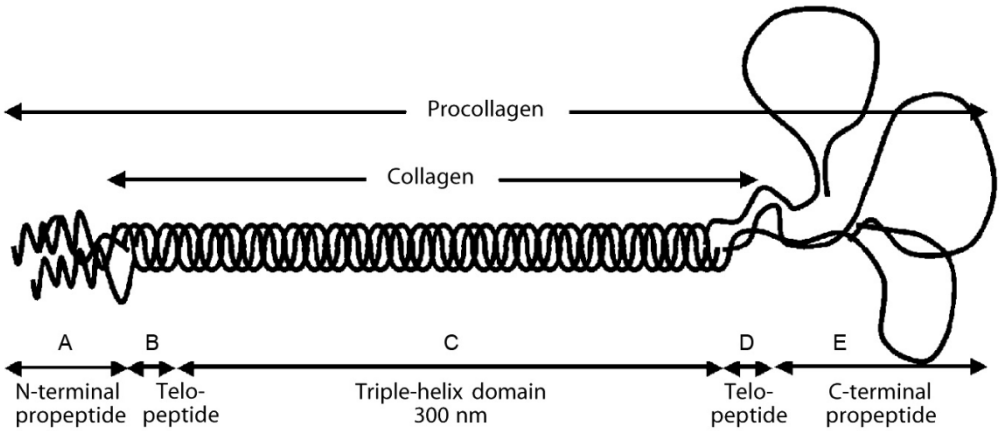

Figure 1.8. Structure of procollagen molecule including: A – N-terminal propeptide, B – short, non-triple-helix that contains the site of the N-terminal peptide which is cleaved, C – the main triple helix domain with the repeating sequence Gly-X-Y, D – another telopeptide, E – the C-terminal peptide with the disulfide bonds, removed during biosynthesis (picture after Michelacci, 2003).

Very important in maintaining the thermal stability of the triple helix is the hydroxylation of proline, and the presence of glycine at every third position (Robert et al., 2001, Scott, 1988). The rest of the amino acids transformation include: N- and O-linked glycoslation of hydroxylysine – a process which attaches mono- and di-saccharides to proteins (which requires: the: hydroxylysyl galactosyltransferase enzyme and galactosylhydroxylysyl glucosyltransferase enzyme); trimerization – a process where monomer molecules react together in a chemical reaction to become a polymer chain; into protein; prolyl cis-trans isomerization – a process in which one molecule is transformed to the other by rearrange the atoms, but the atoms are still the same (it requires: peptidyl prolyl cis-trans isomerase enzyme).

The triple helix formation goes from the C-terminal end to the N-terminal end. The procollagen molecules pass from rough endoplasmic reticulum (RER) through the *trans*-Golgi network (where they are packed in secretory vesicles) and sent to the extracellular matrix. Here, thanks to metalloproteinases (which belong to the ADAMTS-metalloproteinase with thrombospondin type 1, 2, 3-14) and BMP1/Tolloid-like proteinases, the procollagen propeptides are removed (Fig. 1.9).

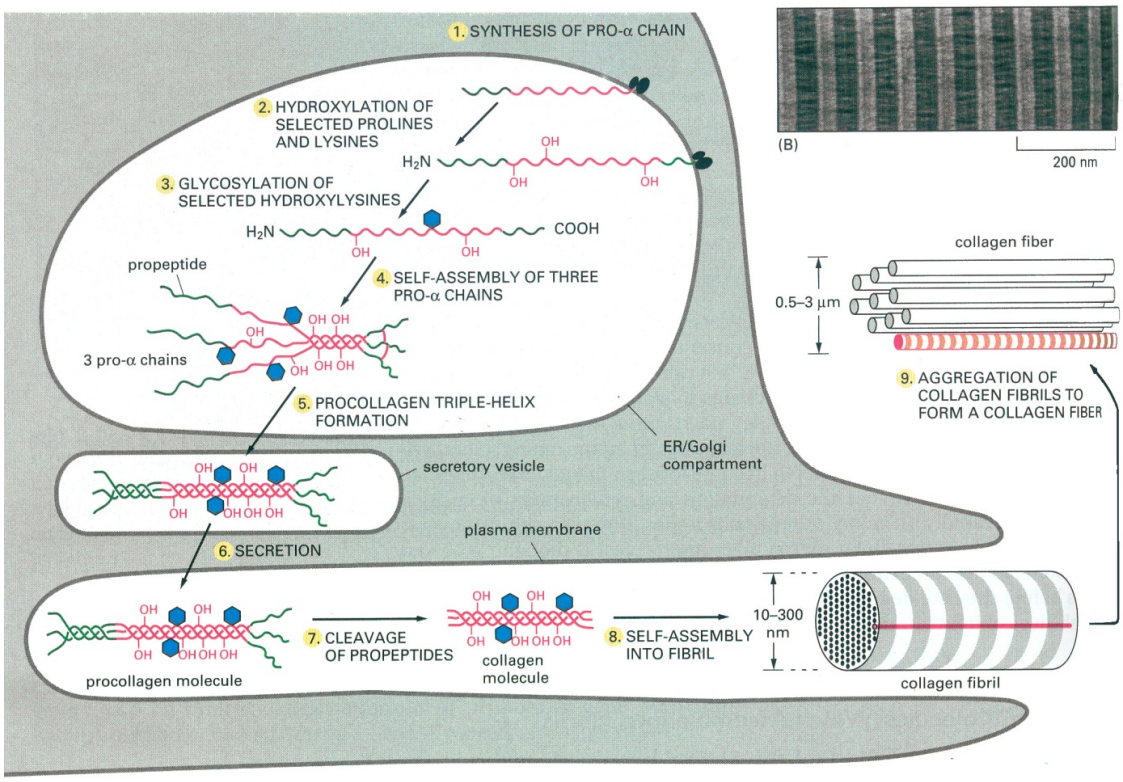

Figure 1.9. A diagram of biosynthesis of collagen including intracellular events: **1)** synthesis of pro-α chains, **2)** hydroxylation of prolines and lysines, **3)** glycosylation of hydroxylysines, **4)** subsequent isomerization which enable pro-α chains to **5)** create triple-helix; extracellular events: **6)** transport procollagen molecule in the secretory vesicles to the extracellular matrix (ECM), **7)** removing the propeptides from procollagen, and **8)** assembling the collagen molecule into fibril (picture adapted from Alberts et al., 2002).

The final step in the production of collagen fibrils is to create covalent cross-links which can stabilize the whole structure of the collagen. This process can happen thanks to lysyl oxidase (LOX, LOXL, LOX1, 2, 4) – an extracellular enzyme that catalyzes the formation of aldehydes from lysine or hydroxylysine residues. These aldehydes are highly reactive and undergo many spontaneous chemical reactions with each other or with lysines and hydroxylysines, and create covalent cross-links (Hulmes, 2008).

1.5 Glycosaminoglycans (GAGs)

Glygosaminoglycans are long, unbranched polysaccharide chains that consist of repeating disaccharide units. One of the two sugars in the repeating disaccharide is always an amino sugar – hexosamine: N-acetyl glucosamine (GlcNAc) or N-acetyl

galactosamine (GlaNAc), generally connected to the sulphate group. The second sugar is usually an uronic acid: glucuronic (GlcA) or iduronic (IdoA) or the hexose: D-galactose (Gal). Glycosaminoglycans are involved in many biological functions within the human body, such as: cell proliferations, differentiations, cell-cell and cell-matrix interactions. These last two include: control of enzyme activities, regulation of cell growth, metabolism, adhesion and modulation of assembly and function of extracellular matrices (Trowbridge and Gallo, 2002, Volpi, 2006).

GAGs have a very high density of negative charges because of the combination of the carboxyl group (CO_2H) and the sulphate group (SO_3^-), which are negatively charged themselves. There are four main groups of GAGs: 1. hyaluronan, 2. chondroitin sulphate (CS) and dermatan sulphate (DS), 3. heparan sulphate (HS), 4. keratan sulphate (KS). Keratan sulphate is composed mainly of N-acetylglucosamine and D-galactose. Heparan sulphate consists of D-glucuronic, L-iduronic acid and glucosamine or glucose. Chondroitin sulphate contains N-acetylgalactosamine, D-glucuronic and/or L-iduronic acid. Dermatan sulphate is the chondroitin sulphate but without L-iduronic acid. The individual GAGs and also these described in subsection 1.5.1 and 1.5.2 are presented in Table 3.

1.5.1 Dermatan sulphate

Dermatan sulphate consists of disaccharide units creating long linear polysaccharides and contains hexosamine, N-acetyl galactosamine (GalNAc) joined by β 1-4 linkage or glucuronic acid (GlcA) joined by β 1-3 linkage, and iduronic acid (IdoA). Dermatan sulphate is a form of chondroitin sulphate, distinguished by the presence of IdoA rather than GalNAc. Dermatan sulphate forms dermatan sulphate proteoglycans (DSPGs) by covalent linkage via an O-xylose to serine of the core protein.

GAG	Hexuronic or Iduronic acid	Galactose	Hexosamine	Disaccharide composition
Heparan sulphate/Heparin	D-glucuronic acid (GlcA) L-Iduronic acid (IdoA)	-	D-glucosamine (GlcNAc)	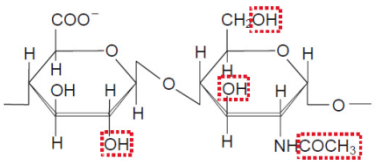 **GlcA β(1→4) GlcNAc α((1→4)** 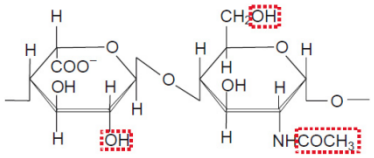 **IdoA α(1→4) GlcNAc α(1→4)**
Keratan sulphate	-	Galactose (Gal)	D-glucosamine (GlcNAc)	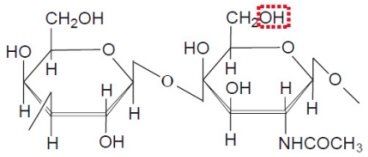 **Gal β(1→4) GlcNAc β(1→3)**
Chondroitin sulphate	D-glucuronic acid (GlcA)	-	D-galactosamine (GalNAc)	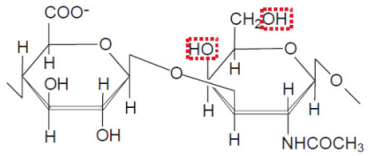 **GlcA β(1→3) GalNAc β(1→4)**
Dermatan sulphate	D-glucuronic acid (GlcA) L-Iduronic acid (IdoA)	-	D-galactosamine (GalNAc)	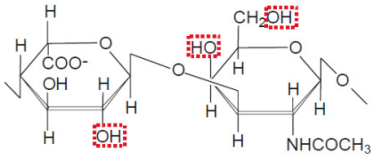 **IdoA β(1→3) GalNAc β(1→4)**
Hyaluronic acid	D-glucuronic acid (GlcA)	-	D-glucosamine (GlcNAc)	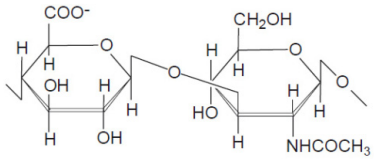 **GlcA β(1→3) GlcNAc β(1→4)**

Table 3. Structure of different glycosaminoglycan chains (table after Prydz and Dalen, 2000).

Dermatan sulphate is found in the small leucine-rich PGs in cornea such as decorin and biglycan, the same as in other PGs: thrombomodulin, endocan, epiphycan and versican. Dermatan sulphate is involved in creating the extracellular matrix

assembly by intercellular signalling and structural integrity (Trowbridge and Gallo, 2002).

1.5.2 Keratan sulphate

Keratan sulphate is the sulphated glycosaminoglycan that regulates stromal hydration in corneal stroma (Chakravarti, 2006, Funderburgh, 2000). Keratan sulphate from cornea belongs to class KSI and is N-linked between N-acetylglucosamine and asparagine (Asn) residues in the core protein. In contrast, class KSII occurring in cartilage has an O-linkage from N-acetylgalactosamine and serine, or threonine (Tai et al., 1997, Volpi, 2006).

Production of keratan sulphate is maintained by adding galactose (Gal) and N-acetylglucosamine (GlcNAc) with the presence of glycosyltransferase enzymes to the growing polymer. The other part in biosynthesis is adding the sulphate group to galactose by the sulphotransferase enzymes. Sulphation of GlcNAc can occur only on the terminus chain of the keratan sulphate during its elongation. Keratan sulphate has been found in three corneal small leucine-rich PGs: lumican, mimecan, and keratocan. There are numerous other proteins where it has also been described, such as: fibromodulin, aggrecan, PRELP (proline arginine-rich end leucine-rich repeat protein) in cartilage, osteoadherin in bone etc. (Funderburgh, 2000).

1.6 Proteoglycans (PGs)

Proteoglycans (PGs) are molecules with sulphated glycosaminoglycan side chains (GAGs) covalently joined to the protein core (Fig. 1.10). The group of PGs was so named because the protein core is attached to GAG domains with high negative charges which can be separated by ion-exchange chromatography from any other molecules. The size of the core protein can vary from 10 kDa to >500 kDa and the quantity of

GAGs could be from one to >100 (Prydz and Dalen, 2000). In their biosynthesis, the serine amino acid of the protein core is joined to a special link tetrasaccharide (consisting of xylose – Xyl, galactose – Gal, galactose – Gal, glucuronic acid – GlcA) of the GAGs. The rest of the chain is created by adding one sugar at a time. This amino sugar is different in various GAGs, e.g.: in heparan sulphate (HS) it is N-acetylglucosamine (GlcNAc), in chondroitin sulphate/dermatan sulphate it is N-acetylgalactosamine (GalNAs) and in keratan sulphate is as an additional N-acetylglucosamine (GlcNAc) and galactose (Alberts et al., 2002, Prydz and Dalen, 2000, Ruoslahti, 1988).

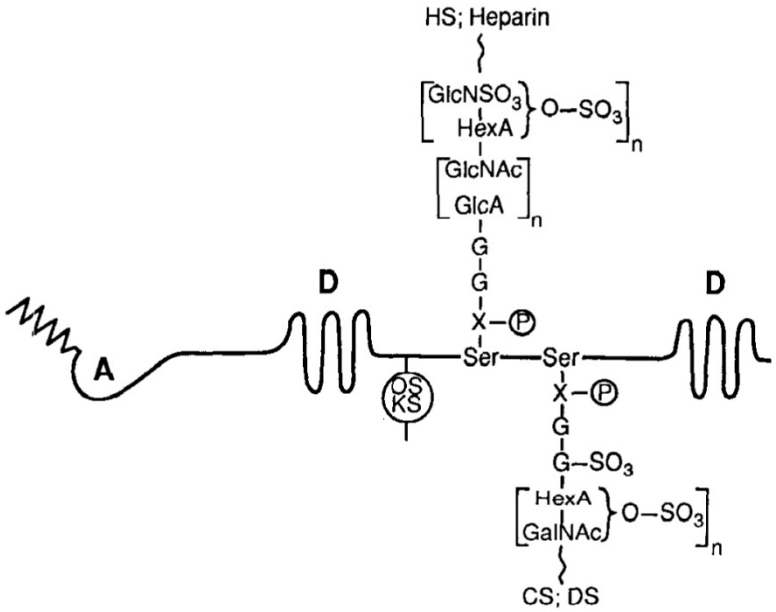

Figure 1.10. Imagined model of the illustrative proteoglycan showing typical features of the PG molecule. GAGs composed of hexosamine (GlcN-glucosamine or GalN-galactosamine) and hexuronic acid (GlcA-glucuronic acid or IdoA-iduronic acid) are shown as two chains joined to the protein core. GAGs consists of G-G-X (galactosyl-galactosyl-xylosyl) trisaccharide units bound to the serine (Ser) on the protein core. They carry CS/DS (chondroitin sulphate/dermatan sulphate) and HS (heparan sulphate) chains. This picture shows potential phosphate group (P), oligosaccharides (OS) and keratan sulphate (KS) among the PGs molecule. PGs in the core protein carry many other domains like: A – anchoring domain, whose role is to attach the PGs to the other molecules in extracellular matrix or to the cell surface, D – other domains which can perform any other functions (picture after Kjellen and Lindahl, 1991).

There are four proteoglycans occurring in the corneal stroma: **decorin, lumican, mimecan (osteoglycin) and keratocan** (Michelacci, 2003, Kao and Liu, 2003). These

four are the small leucine-rich repeat proteoglycans (SLRPs) which are composed of a single polypeptide chain (protein core) with an N-terminal cysteine-rich cap, and several leucine-rich repeat fragments (LRRs), and usually a C-terminal disulphide bonded cap. The length of the LRRs in the family of SLRPs is between 20 and 39 amino acids and follows the same, regular pattern of short-long-long domains in the whole LRR (Hulmes, 2008, McEwan, 2006). Several subfamilies of SLRPs may be distinguished by the number of repeat regions and by the spacing of cysteines (Fig. 1.11).

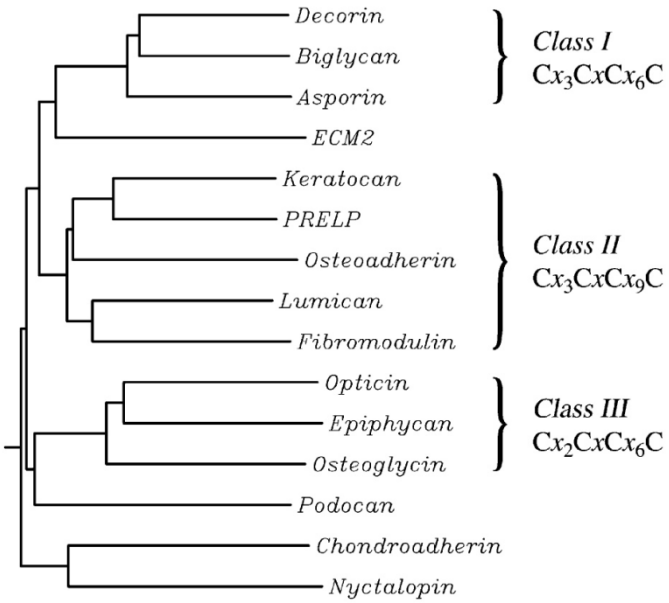

Figure 1.11. Classification of the small leucine-rich proteoglycans SLRPs where: C means the cysteine and x means any amino acid (diagram after McEwan et al., 2006).

There are different glycosaminoglycans (GAGs) which produce these four main proteoglycans in the cornea: keratan sulphate – appears in lumican, keratocan, and mimecan, and chondroitin sulphate and dermatan sulphate – are found together in decorin (Hulmes, 2008). Proteoglycans along with collagen are responsible for corneal transparency. Keratan sulphate proteoglycans which are more abundant in the posterior stroma, regulate the diameter of collagen fibrils and dermatan sulphate proteoglycans control the spacing between fibrils and the adhesion properties of corneal collagen

(Michelacci, 2003). Decorin which is the only chondroitin sulphate/dermatan sulphate proteoglycan in the cornea, is more abundant in the anterior stroma than in the posterior (Ehlers et al., 2006). In the electron microscope (using the specific reagent – Cupromeronic blue to stain for PGs) collagen fibrils show a characteristic banded structure and run parallel to each other, where proteoglycans appear regularly along the collagens as dark thin orthogonal filaments (Fig. 1.12).

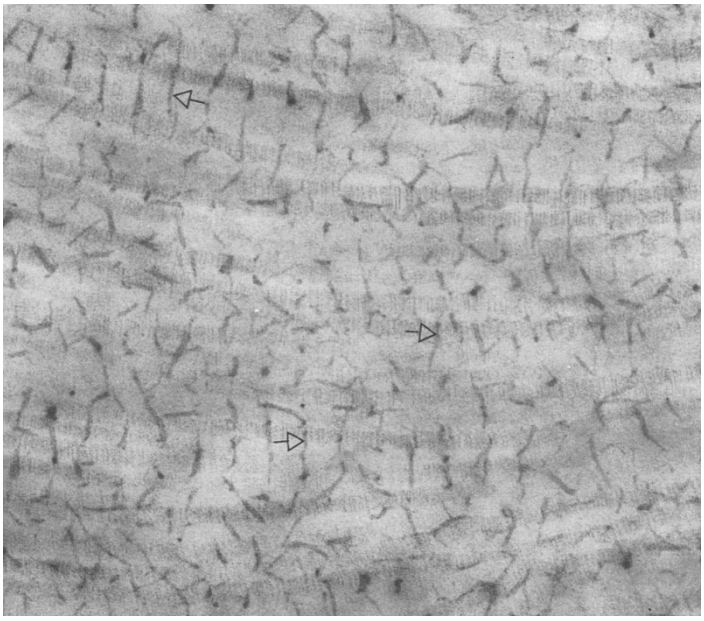

Figure 1.12. Image of the electron microscope in bovine corneal stroma. Arrows show fine proteoglycan filaments, which are frequently regularly spaced and orthogonal to the collagen fibrils. Collagen fibrils are banded structues running approximately horizontally (picture after Scott and Haigh, 1988).

1.6.1 Decorin

Decorin is a dermatan sulphate proteoglycan of Class I small leucine-rich proteoglycans (SLRPs). Its main role is to keep the surface of the collagen fibrils apart by participating in collagen fibril formation (Hulmes, 2008). There are two glycosaminoglycans (GAGs) appearing in decorin: chondroitin sulphate and dermatan sulphate. In the structure of decorin the central domain has three attachment sites for N-linked oligosaccharides and the amino- termini consist of a chondroitin or dermatan single attachment site.

Decorin has high affinity binding sites in the central domain for collagen Type I, II, III, and VI. The main feature of decorin is that it comprises 10 LRRs flanked by cysteine-rich domains. According to Iozzo (1998) and Weber et al. (1996) the model structure of decorin is composed of an arch shape molecule with the α-helices on the outer surface and the inner concave β-sheet surface where the triple helix of collagen would be bound (Fig. 1.13).

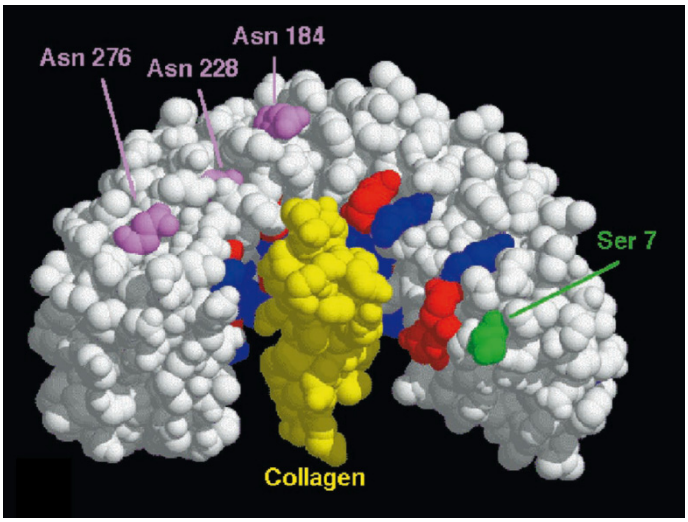

Figure 1.13. Three dimensional organization of decorin (*white*) interacting with a triple helix of collagen (*yellow*). The concave surface of decorin consists of charged residues with basic (*blue*) and acidic amino acid residues (*red*). In this model the glycosaminoglycan attachment site on asparagine (N-linked oligosaccharide) and serine domains are seen as *purple* and *green* residues, respectively (picture adapted from Iozzo, 1999).

Class I is the only member of the SLRP family (Fig. 1.11) that contains a pro-peptide. And this pro-peptide is a signal for xylosyltransferase – the first enzyme that takes part in the synthesis of glycosaminoglycan (GAG) domains. Class I SLRPs have a unique pattern which is completely different from the other classes and it is expressed as follows: CX_3CXCX_6C. Class I is encoded by genes composed of eight exons in highly conserved positions and these10 LRRs are encoded only by six exons: exons III-VIII (Iozzo, 1999).

1.6.2 Lumican

Lumican is a keratan sulphate proteoglycan, one of the Class II small leucine-rich proteoglycans (SLRPs). It is the major keratan sulphate proteoglycan of the corneal stroma. Lumican is known to be one of the factors contributing to corneal transparency by influencing collagen fibril formation and hence collagen assembly (Chakravarti et al., 2000). It has a weight of ~40 kDa and is composed of four main components: (1) a signal peptide of 16 residues, (2) N-terminal peptide with negative charges comprising a disulfide bond and sulphated tyrosine, (3) tandem leucine-rich repeats that affect interactions e.g. with collagen, (4) the carboxyl terminal peptide of 50 amino acids with two cysteines 32 residues (Kao et al., 2006, Kao and Liu, 2003).

Lumican's role is to regulate stromal collagen matrix assembly which is very important for the cornea to maintain transparency. Lumican enables the keratocytes to migrate in an in vitro cell migration assay. Thus is involved in many biological functions e.g. cell migration, adhesion, proliferation, and wound healing (Kao et al., 2006). Lumican in normal corneas is produced by the keratocytes in stroma. Class II SLRPs, of which lumican (along with keratocan) is a member, possess a group of Tyr-sulphate residues which relate to the polyanionic nature of the proteoglycans. Class II is expressed by the typical pattern which is CX_3CXCX_9C and is encoded by three exons. One of these three is the large, central one exon that encodes almost all of the 10 LRRs (Iozzo, 1999).

1.6.3 Mimecan (osteoglycin)

Mimecan is a keratan sulphate proteoglycan, another small leucine-rich proteoglycan (SLRPs) occurring in the cornea and sclera and in other non-ocular connective tissues in the body. Mimecan is a member of Class III SLRPs. It is believed that its main role is to control cellular growth by regulating the expressions of keratocytes in the cornea as

well as providing transparency in the cornea. It has a weight of ~25 kDa and is highly sulphated (Funderburgh et al., 1997).

Mimecan is found as a linear polymer with N-acetylactosamine and asparagine residues linked to its core protein. Mimecan in the cornea is produced in a much larger amount compared to other tissues in the body in which it appears. It is believed that there is some special mechanism which can make the genes overexpress to produce proteins important for corneal transparency. This process is called gene sharing and also occurs in the lens of the eye (Funderburgh et al., 1997). Class III is characterized by the presence of only six LRRs and these LRRs are encoded by only three exons: exons V-VII, where at the same time these proteoglycans containing six LRRs are encoded by a gene of seven exons. Its unique pattern is CX_2CCX_6C (Iozzo, 1999).

1.6.4 Keratocan

Keratocan is a keratan sulphate proteoglycan, and is a member of Class II small leucine-rich proteoglycans (SLRPs), along with the lumican. It has 31% of its amino acid sequence identical to decorin. The keratocan core protein is built of 12 leucine-rich repeats (LRRs), four amino-residues and two endings with a carboxy group. These four amino (N) residues can be modified in N-glycosylation to keratan sulfate. The gene responsible for encoding keratocan is *KERA,* which occurs in embryonic mesenchyme (Chakravarti, 2006).

Keratocan is found only in corneal stroma, and it is believed that expression of the keratocan gene is modulated by the biological role of lumican by keratocytes. The lumican receptor could be present on the keratocyte. According to Carlson et al. (2005), a decrease in lumican expression carries with it a decrease in keratocan expression. These results showed that the corneal phenotypes such as: thin corneal stroma, opacity and disturbed fibrillogenesis in lumican knockout animals are not only the result of lack

of lumican expression but also the result of decrease of keratocan expression. This research suggests gene sharing, where expression of one member of SLRPs family can regulate the other members. This modulator can act as *matrikines* (e.g. lumican) – which means it is able to regulate either positively or negatively different cell activities.

1.7 Proteoglycan biosynthesis

The biosynthesis of proteoglycans (PGs) starts in the rough endoplasmic reticulum (RER) where N-linked mannose oligosaccharides are added to the core protein through a dolichol diphosphate intermediate which is moved to asparagine on the core protein. Hydroxylation of the core protein also occurs in the endoplasmic reticulum (with a glycol transferase). Addition of chondroitin sulphate (CS), keratan sulphate (KS), heparan sulphate (HS) and heparin (H) chains to the core protein and assembly of O-linked oligosaccharides takes place in the Golgi apparatus within glycosyl transferases, UDP-glucose and UDP-N-acetylglucosamine activities. Both UDP-glucose and UDP-N-acetylglucosamine can undergo epimerization at the C-4 position and form respectively, UDP-galactose and UDP-N-acetylgalactosamine. Synthesis of glycosaminoglycans (GAGs) is able to take place by adding single sugars. The simultaneous sulphation of GAGs also follows in the Golgi apparatus which is mediated by 3'-Phosphoadenosine-5'phosphosulphate (PAPS) and occurs along the chain of polymerization. After sulphation, the epimerization of glucuronic acid (GlAc) to iduronic acid (IdoA) occurs in DS, HS and H. The last step before secretion of PGs within the secretory vacuole into the extracellular matrix, is the conversion of high-mannose oligosaccharide to the sialic acid-containing-complex type oligosaccharide (Poole, 1986).

1.8 Proteoglycan/collagen interaction

Proteoglycans and collagen fibrils interact with each other forming a very well organized assembly within corneal stroma. In electron micrographs the collagen fibres show specific periodic features (electron dense sites) which are seen as a repeating pattern of dark bands named a, b, c, d, e within the D period of the collagen (the characteristic axial periodicity of collagen). The "gap zone" which is the gap between the ends of the collagen fibres (between the amino terminus of one molecule and the carboxy terminus of the next) contains the d and e bands, whereas band b appears in the "overlap zone". Bands a and c are located at the "step" between the "overlap zone" and the "gap zone" (Fig. 1.14).

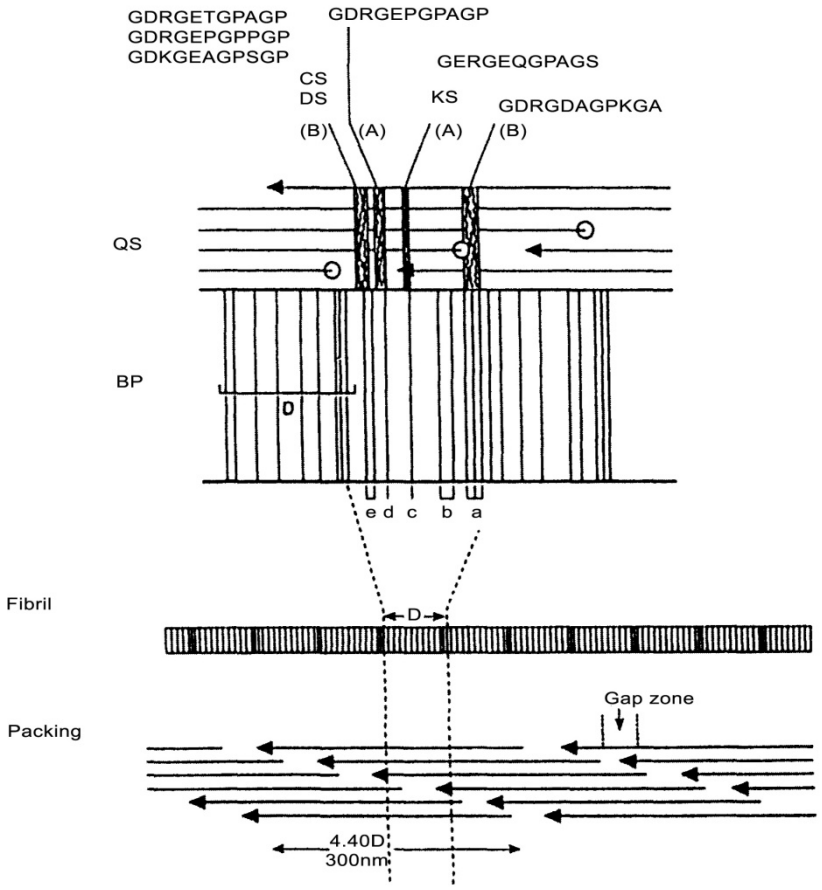

Figure 1.14. A schema showing proteoglycans binding sites (a, b, c, d, e) on collagen fibrils (diagram after Scott, 1995). The letters mean as follows: GDRGETGPAGP is an 11-amino acid sequence (at least one copy of each binding site); QS – ordered quarter-staggered array bands of polar amino acids; BP – bar-code pattern 'fibril', which is asymmetric and labelled with letters from a to e; CS – chondroitin sulphate; KS – keratan sulphate.

The individual collagen molecule shows quarter-stagger arrangement which means that they are located in an alternating pattern about one-quarter of their length. Two types of proteoglycans are associated regularly with the specific binding sites along the collagen fibres (within the D period of collagen). KSPGI and KSPGII are located at the a and c band, while CS/DSPG are located at the band d and e (Scott, 1995; Scott and Haigh, 1988; Scott and Haigh, 1985).

1.9 Corneal transparency

Corneal transparency depends on the very well organized extracellular matrix (ECM) in the corneal stroma. This results from interactions between collagen fibrils and proteoglycans around them, that leads to a consistent interfibrillar spacing (Chakravarti et al., 2000, Kao and Liu, 2003). According to Meek (2002) there are two main features for every substance to exhibit transparency: 1) it cannot absorb light, 2) it must not scatter light. The normal cornea does not contain any blood vessels, neither does it have pigments which would absorb any visible wavelengths.

The *Uniform Refractive Index Theory* is the simplest model for explaining the lack of scattering of the cornea. It assumes that each of the corneal components has the same refractive index. This model has not been accepted by many because it can not explain loss of corneal transparency when the tissue is deformed. Furthermore, it was proved (using X-ray diffraction) that collagen fibrils and extrafibrillar fluid have different refractive indexes (Meek et al., 2003).

Maurice (1957) suggested a theory (called a *Lattice Theory*) explaining corneal transparency which is grounded on the uniform diameter and regular spacing of the collagen fibrils in corneal stroma. According to his theory collagen fibrils are arranged in a regular lattice and each of them scatters light independently (Fig. 1.15). This scattered light then is eliminated by destructive interference and only the light going

forward is permitted to pass through the stromal layers in accordance with its regular direction. For this to occur, collagen fibril diameters have to be uniform, and this is considered to be controlled by interaction between collagen fibrils and proteoglycans (Meek and Leonard, 1993). Recent studies provide evidence that type V collagen and decorin regulate corneal stromal fibril formation and matrix assembly (Birk, 2009).

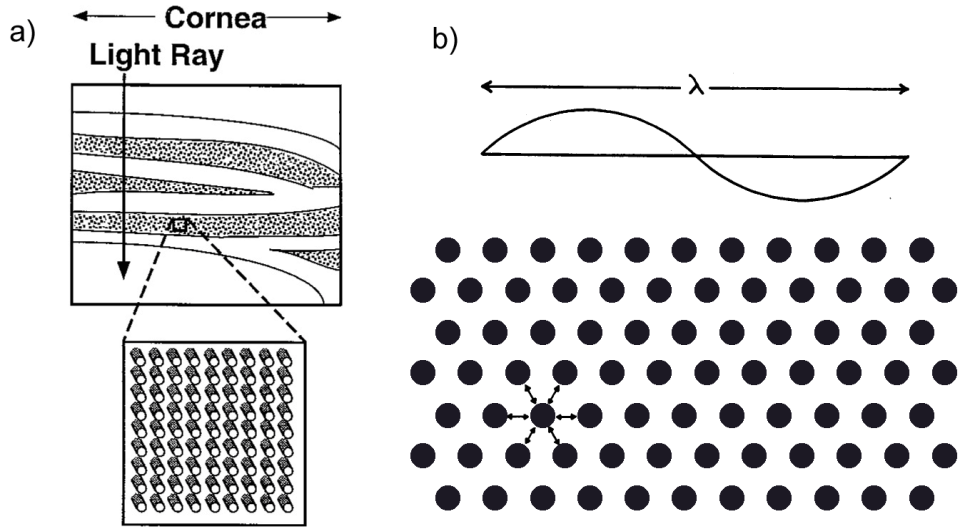

Figure 1.15. Two images presenting *Lattice Theory* of corneal transparency; **a)** section shows cornea as a lattice where collagen fibrils are arranged in a perfect order (after Ameen et al., 1998); **b)** picture shows hexagonal lattice where each of the fibrils scatter the light independently (picture adapted from Maurice, 1957).

Hart and Farrell (1969) proposed that, contrary to Maurice's hypothesis, the cornea does not need to be completely ordered in a special lattice. It requires only partial order in fibril arrangement to cause enough cancellation in scattered light. Their calculation gave an estimated value over 80 % of the light which is transmitted by the cornea. Benedek (1971) added that the tissue is transparent and the amount of scattered light is small as long as the spacing of the fibrils is less than a wavelength of light (Ameen et al., 1998).

Doutch et al. (2008) summarized parameters which are believed to be crucial in maintaining corneal transparency. These are: 1. density of collagen fibrils, 2. diameter of collagen fibrils, 3. refractive index differences between fibrils and interfibrillar or

ground substance, 4. thickness of stroma, 5. order in spacing of the fibrillar network. Thus every model trying to explain corneal transparency should consider the shape and size of corneal stroma and its elements such as collagen fibrils and proteoglycans, and their refractive indexes. These factors are essential because they influence the amount and direction of light which is scattered in going across the cornea. The average refractive index of the stroma has been calculated to be 1.375. It is based on the refractive index of collagen fibrils, interfibrilar fluid, volume of collagen fibrils and the volume of fluid (Ehlers et al., 2006, Meek et al., 2003).

An important requirement for maintaining corneal transparency is that the collagen fibrils do not touch each other. This can be achieved thanks to the negative charge of the proteoglycan-rich coating around collagen fibrils which prevents their aggregating (Meek, 2008). According to Chakravarti et al. (2000), lumican-deficient mice evolved cloudiness of the cornea because lack of this proteoglycan leads to a distorted structure and organization of the corneal fibrils.

The space between the collagen fibrils is occupied by GAGs and depends on the content of water in the matrix. The transparency has to be maintained by the balance between the proteoglycan matrix (which forms a hydrated gel) and the corneal collagen fibrils. Thus, the special structure of cornea and its collagen fibrils are the factors that keep the water level constant thus maintaining fibrillar order and transparency (Oyster, 1999, Kao and Liu, 2003). The physiological hydration in cornea is maintained at about 78 % in humans. When the cornea swells, the distance between collagen fibrils within the lamellae is increased and voids form within lamellae (Benedek, 1971). Thus the light scattering increases. This happens because the proteoglycans (with negative charges) absorb water in the corneal stroma (which is hydrophilic). To prevent corneal swelling it is important to maintain the balance between ions and fluid in cornea by its

dehydration which is possible thanks to the leaky barrier and ion transport in the endothelium (Mergler and Pleyer, 2007, Stiemke et al., 1995). Edelhauser (2006) listed the four most important factors which are necessary to maintain corneal transparency in the healthy normal human cornea, which are: peripheral endothelial cell density (ECD), tight junctions, many of the Na^+/K^+-ATPase pumps, and minimal apoptosis with age which enables the endothelial cell mosaic to be intact during its whole life (Fig. 1.16).

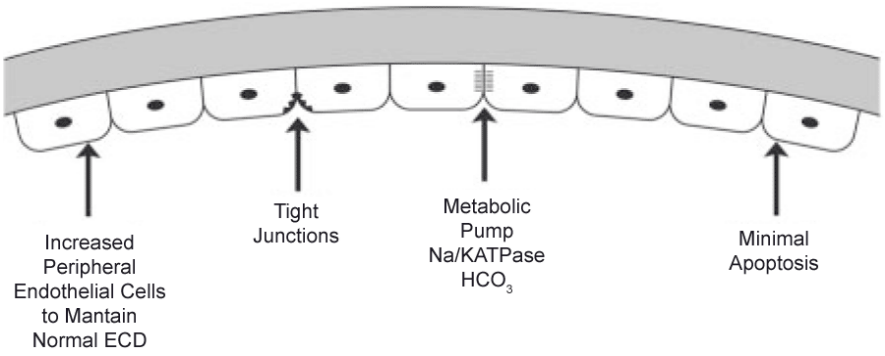

Figure 1.16. Diagram showing factors important in maintaining transparency of normal corneal endothelium (picture after Edelhauser, 2006).

1.10 Corneal metabolism

The epithelial cells of the cornea fulfil the same role as other outer layers in the whole organism which is mainly a protective barrier against the outside world and keeping the cells together as a layer as well as a creating a good passage for nutrients, solvents and other substances which are important in its biological function.

Transport of all the important constituents, such as: oxygen, glucose, vitamins and other proteins, is possible by three exchange routes in cornea: the anterior epithelial surface, the posterior endothelial surface and the peripheral limbus. Corneal metabolism occurs in a range 32-34 °C degrees, which is below body temperature. Oxygen is taken directly from the air by diffusion through the epithelium, while glucose gets endothelial barrier thanks to the ion pumps (Ehlers et al., 2006).

1.11 Specialist techniques used in this study

In this study we used several specialist methods. Chapter 3 uses the transmission electron microscope (TEM) in order to learn more about the three-dimensional relationship between collagen and the stromal proteoglycans. Previously, the dye cuprolinic blue has been used to show the two-dimensional organisation of proteoglycans with respect to the collagen (Figure 1.12) but, for the first time, we have attempted to use three-dimensional electron tomography to determine the full spatial relationship in the normal human cornea.

Certain pathological conditions lead to loss of corneal transparency. Climatic Droplet Dystrophy is one such condition and we were able to examine a guinea pig model of this disease to see if there were changes in the collagen, proteoglycans, or their spatial relationship. In Chapter 4 we used low angle X-ray diffraction combined with conventional electron microscopy to study these parameters. As described above, there is a relationship between collagen lamellar organisation and corneal shape. Fish have interesting corneas because they have to be very strong to withstand underwater pressures, but they have no refractive function, because their refractive index is close to that of water. Fish corneas, therefore, offer an interesting system to study the relationship between structure, transparency and shape. Accordingly, X-ray diffraction was used to examine fish corneas (hake, mackerel, salmon and seabass) in chapter 5.

1.11.1 Electron tomography

Electron tomography (ET) is a tomography technique based on transmission electron microscopy (TEM) for obtaining a 3-D model from any macromolecular specimen e.g. cell organelles, membranes, fibers (such as collagen), multi-enzyme complexes and viruses (usually around a few nanometers thick). Using the transmission electron microscope for collecting data, this method generates 3-D images (Fig. 1.17) of a

specimen as a series of 2-D projections taken at different tilt angles (McIntosh et al., 2005). This process involves creating a beam of electrons in the beam gun (of TEM) which passes through the sample at 1 degree intervals around the centre of the specimen. The final image is magnified, focused and displayed on a screen (as the electrons interact with the specimen) and recorded by a CCD camera.

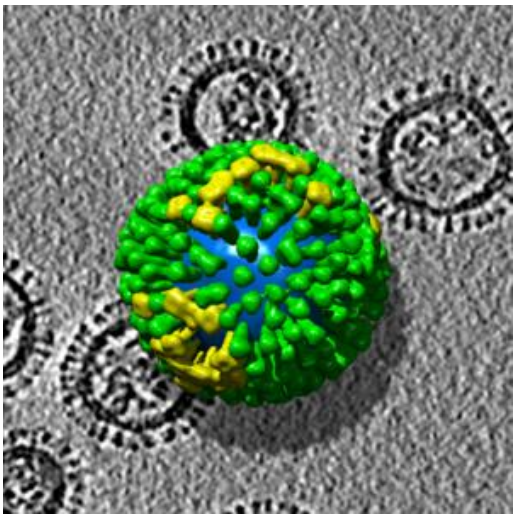

Figure 1.17. An example of the model generated using electron tomography: 3-D reconstruction of the virus based on 2-D projections (adapted from Harris et al., 2006).

A dedicated software package is then used to build a tomogram (an image which is produced as a 3-D model). This stage involves many steps of alignments, reconstruction, segmentation and rendering which helps to visualize and analyse the arrangement or structure of the specimen.

1.11.2 X-ray diffraction

As we have discussed, the orientation of corneal fibrils is important not only because it explains corneal transparency, but because mechanically it can affect the corneal curvature. Electron microscopy provides a lot of information about the ultrastructure of the cornea. However, because of the limitation connected with high magnification of electron microscopy, it is not possible to examine the fibril orientations using this technique quantitatively. Therefore, x-ray diffraction (XRD) is a good method to define

information about the structure and arrangement of collagen fibrils, both across and through the thickness of the whole tissue. Maurice (1957) was the first to register the x-ray pattern from the cornea but the reflections he obtained were poor and not clear compared to modern standards. The reason was that the recording time was many hours which could cause the specimen to deteriorate (Meek and Fullwood, 2001a). The current synchrotron x-ray sources produce a very intense beam of x-rays, which allows researchers to examine the specimen within a short exposure time and without using any invasive methods such as embedding and staining. The tissue remains close to its natural condition (Meek et al., 2009, Meek et al., 1987, Newton and Meek, 1998). The information obtained represents an average from the whole tissue through which the x-rays are passed and thus allows quantification of the structures being measured. Thus, x-ray diffraction has been established as a quantitative method for examining corneal structure.

There are two kinds of x-ray diffraction which are an important source of information about collagen: the low-angle x-ray pattern (also called: small-angle pattern) and the wide-angle x-ray pattern (also called: high-angle pattern). The first gives information at the fibrillar level. This pattern includes two elements: diffraction obtained from the interfibrillar arrangement of collagen fibrils (called equatorial) and the diffraction received from the axial structure of the collagen (meridional). In this thesis, the low-angle patterns are used to measure average fibril diameters and centre-to-centre fibril spacing.

The wide-angle x-ray pattern arises from smaller structures and gives information about each of the collagen molecules in the corneal stroma (molecular level), and about the organization of atoms and groups of atoms within the molecule (Meek et al., 2009, Meek et al., 1991). Both low- and wide-angle diffraction also give

quantitative information about the directions of the collagen fibril axes. In this thesis, wide-angle diffraction was used to quantify fibril orientation.

To obtain the x-ray pattern requires running a focused, monochromatic beam of x-rays through the specimen. Some of the x-rays passing directly through the specimen are absorbed by a lead "backstop". This is a small device behind the sample, protecting the detector from the very high intensity x-rays which are not diffracted. Some x-rays are absorbed by the specimen, and the rest of them are scattered and can be recorded by an x-ray detector placed a fixed distance from the sample (Fig. 1.18).

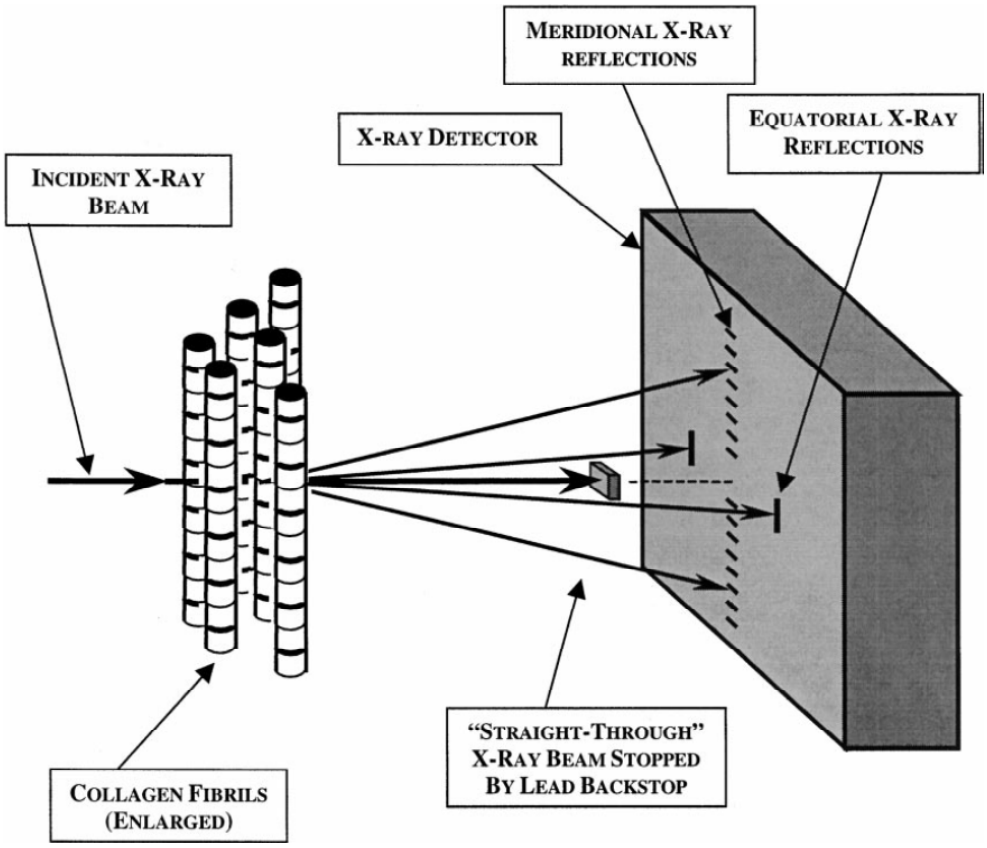

Figure 1.18. A diagram displaying the reflections of the cylindrical collagen fibrils placed in an X-ray beam (picture after Meek and Fullwood, 2001a).

Each of the vertical collagen fibrils in the x-ray beam scatters x-rays parallel to the fibril axis, giving a series of low-angle meridional reflections. This scatter arises from the 65nm D-periodicity along the collagen fibril axis due to the packing arrangement of the molecules within the fibrils. At the same time the lateral packing of

the molecules in each of the collagen fibrils gives a wide-angle equatorial pattern at right angles to the fibril axis. Also where there is a preferred lateral fibril arrangement (because of the fibrils with the uniform diameter and have certain order over a short range), cornea produces a low-angle equatorial pattern at right angles to the direction of the collagen fibril axis (Meek et al., 2009, Meek and Fullwood, 2001a).

1.12 Aims of the Thesis

The overall aim of this thesis is to use cutting edge methodologies to explore the ultrastructure of the corneal stroma:

1. To use electron tomography to determine the three-dimensional relationship between collagen and proteoglycans in the human cornea which is the basis of corneal transparency.
2. To investigate the the ultrastructural causes of light scattering in a guineapig model of Climatic Droplet Dystrophy
3. To carry out a study of fish corneal ultrastructure for comparison with that of mammals, and thus determine which ultrastructural properties are important for transparency and which may be more relevant to tissue shape.

2 General materials and methods

2.1 Transmission electron microscopy (TEM)

In this project we used staining with the dye Cuprolinic Blue (CB) which is a specific reagent for PGs. The samples were counterstained with uranyl acetate and phosphotungstic acid to stain the collagen fibrils. The cornea was embedded in resin and trimmed in the ultramicrotome to get gold sections (around 0.1 μm) of the tissue to examine in the transmission electron microscope (TEM).

2.1.1 Sample preparation – fixation and dehydration

The human specimen used for tomography was supplied by Dr Ahmed Elsheikh (Dundee University) and was stored in Optisol. Guinea pig corneas were supplied by Professor Horacio Serra from National University of Cordoba (Hayes et al., 2011). Fish corneas were obtained from a local market. The human tissue was cut into several-millimetre cubes and suffused with a solution of 0.05% Cuprolinic Blue (Quinolinic phthalocyanate) in 25mM sodium acetate buffer, pH 5.7, containing 0.1 M $MgCl_2$ and 2.5M glutaraldehyde overnight at room temperature. The Guinea pigs' corneas were treated in 2.5% glutaraldehyde and 2% paraformaldehyde in 0.1M Sörensen's phosphate buffer at pH 7.4. The tissue was then rinsed three times, each time for 5 minutes, in 25 mM sodium acetate buffer, pH 5.7. Afterwards the samples were washed three times in aq. 0.5% sodium tungstate, again each time for 5 minutes and with 0.5% sodium tungstate in 50% ethanol for 15 minutes as described by Scott and Orford (1981). The tissue then was dehydrated by passing it through of a series of increasing ethanol concentration (70%, 90%, 100%, v/v ddH_2O – for 15 minutes each session). Finally, they were incubated with three changes of 100% PO_2 (propylene oxide), and

then with 1:1 PO_2/Araldite resin mixture in small vials for 1 hour. These samples then were incubated with 100% Araldite resin for 1 hour.

The next step was the resin infiltration, which was the sequence of changes of the resin: early pm, mid pm, late pm. The tissue was incubated with fresh 100% resin overnight at RT in a fume hood. At this stage the vial tops were removed so any remaining PO_2 could evaporate. The next day resin was changed three times: early am, mid am, midday. At the end of this process the tissue was embedded in moulds with further resin in the oven at 60°C for 24 hours (minimum).

2.1.2 Sectioning procedures

- ***Support films***

Support films were used in grids with a large open space, such as slot grids (Fig. 2.1). They allowed us to examine the section without any unnecessary obstacles like grid bars obscuring the view, and are essential for 3-D tomographical studies because of the need to tilt the specimen in the TEM electron beam. Support films, as the name indicates, give the viewed section a stable support, helping to prevent the specimen from any destruction or drift under the electron microscope beam. The best known support films are made from Formvar, Butvar, collodion, or carbon. In this case we used PEI (polyether amide) solution. To make this solution it was necessary to dissolve PEI in ethylene dichloride (1,2-dichloroethane). This mixture had to stand at least 48 hours to dissolve before use. This was important for making consistent thin films, whereas PEI which is too fresh, consists of long strands of undissolved polymer which does not make good films.

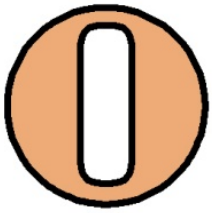

Figure 2.1. Slot grid, mainly used for tilting the specimen under TEM.

PEI was poured into an ethylene dichloride mixture just before making a film. Slides were prepared by cleaning them with flash cleaning spray or lens tissue. They were then placed in a slide grip. Each slide had to be dipped into the PEI solution for about 20 seconds, 2/3 up the slide. They were removed quickly and put back into the slide grip. Slides had to dry for at least 45 minutes before using to prevent the film from introducing additional moisture.

When the slides with the film on them were dry, the edges were scored using razor blades (about 2 mm from the edges) so the film could be stripped off easily. Some distilled water was dropped onto a dish. The surface of the water had to be almost at the top of the dish. The film was fogged by breathing on it. Then the slide was placed at about a 10 degree angle to the water surface (so, as the slide went deeper into the water, the film remained smoothly on the surface). The slide was lowered down until the film floats free on the water.

To make the grid covered with the film we prepared the slides as above and the floating film on the water surface. Then we used a special plastic holder (plastic bridge) with small holes (Fig. 2.2) to pick up the film from the water surface. In this case the film was with no grids on, so it sticks directly to this plastic holder. During sectioning the grids with the tissue were placed on the film within the holes.

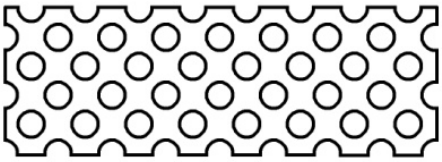

Figure 2.2. Special plastic bridge used for storing the grids on the film unfolded within the holes.

- ***Ultramicrotomy***

The ultramicrotome is a device used for sectioning ultrathin (10-100 nm) and semithin (0.25-0.5 μm) sections of the specimen which in turn are used in microscopic analysis. In our study we used only 100 nm sections as thinner ones were too easy torn out. Every modern ultramicrotome is typically built out of the following elements: movable specimen-holding arm, a chuck for holding the specimen block, a knife holding stage assembly, stereomicroscope, hand wheel, and the lamp (Fig. 2.3).

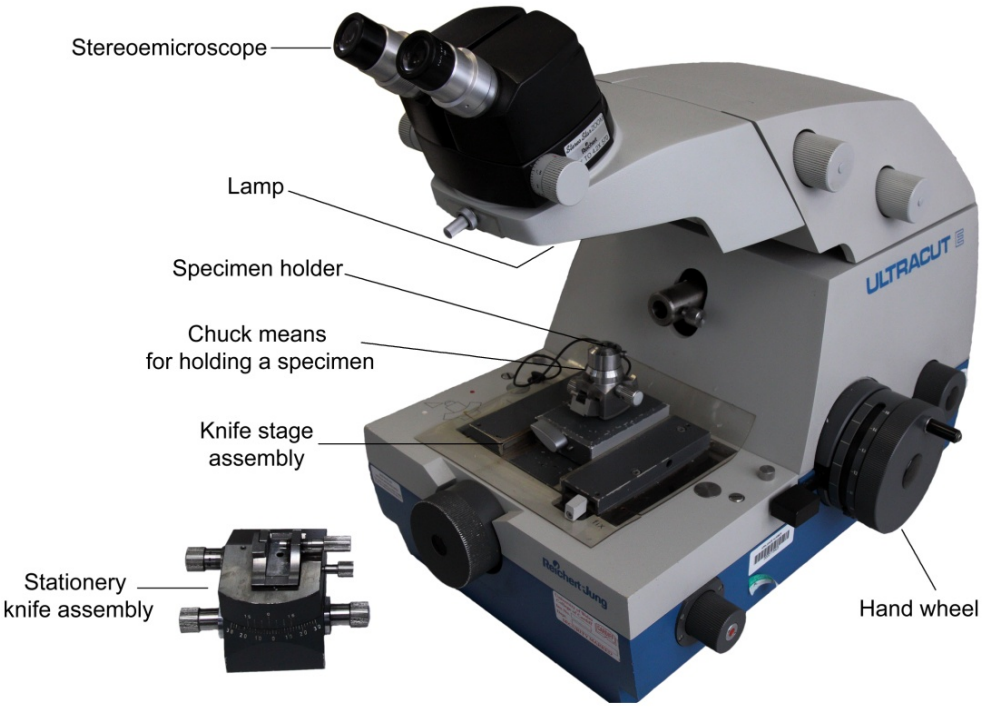

Figure 2.3. Reichert-Jung 'Ultracut E' Ultramicrotome station.

The specimen-holding arm served as the part which moves the chuck holding the specimen. This permitted a single-pass cut every time when the block touched the knife.

The knife-holding stage assembly let the knife boat approach the block with the tissue to cut sections as required. The lamp above the knife holding stage assembly provided the light which was needed to estimate the section thickness. This was possible because of the fact that each section floating on the water produced a different interference colour. When a ribbon of sections was cut, it floated off onto the water in the boat. A toothpick with an attached eyelash was used to place the gold sections so that they were easy to pick up with the slot grids. The grids were then left to dry for several hours before staining and viewing under the electron microscope

2.1.3 Staining of ultrathin sections

The grids were stained in uranyl acetate and phosphotungstic acid for routine examination of ultrastructure. For the tomography study, the grids were placed on a suspension of colloidal gold particles (10nm in diameter) prior to analysis in the transmission electron microscope.

Uranyl acetate (UA) and phosphotungstic acid (PTA) were prepared the day before staining. Vials containing 25ml of each were centrifuged at 14000 for 5 minutes at RT. When the stains were ready, grids were placed on a drop of 1% PTA for 1 minute at RT. Then they went through 3 washes with ddH_2O, for 1 minute each. The next step was to move the grids from water to 2% UA. They were placed on the top of UA for 13-15 minutes at RT, then washed 3 times with ddH_2O as described before, and rinsed out carefully again in ddH_2O in two different dishes to get rid of any additional stain. Grids were left to dry at RT.

Grids stained before with PTA and UA were placed on the drop of colloidal gold suspension which was stored in fridge at 4°C. Such prepared grids were left to dry before analysing them under the electron microscope.

2.2 X-ray diffraction study

2.2.1 Introduction

The work on wide-angle XRD was done at the Daresbury Synchrotron Radiation Source, Warrington, UK. All the rest of the x-ray diffraction data (low-angle x-ray diffraction of the fish and Guinea pigs) was performed at the Diamond Light Source, Oxfordshire, UK (Fig. 2.4).

Figure 2.4. Diamond Light Source (picture adapted from the Diamond web page:http://www.diamond.ac.uk/Home/About.html)

2.2.2 Sample preparation

Corneas were fixed in 2.5% formalin or 4% paraformaldehyde, or frozen at – 80°C (and kept wrapped in cling film). Before doing the experiment the fixed samples were removed from their fixative and wrapped tightly in cling film. This protected the tissue against dehydration in the x-ray beam. The samples were also marked at the 12 o'clock position to recognize top and the bottom.

2.3 Low-angle x-ray diffraction

2.3.1 Data collection

Low-angle x-ray diffraction patterns were taken at Station I22 at the Diamond Light Source Ltd, Diamond House, Oxfordshire, UK using a focussed monochromatic x-ray

beam with a wavelength of 0.9796nm. The patterns were recorded on a RAPID2 detector. The distance from the specimen to the detector was about 6 metres.

The corneas were placed into an air-tight sample holder. The CCD detector recorded the x-ray pattern which was created by the sample through which the x-rays passed. Between the corneal sample and the detector was placed a lead backstop to protect the detector from the high intensity non-diffracted x-rays. At the beginning of each experiment, a rat tail tendon was used for calibration. It has a know D-periodicity which is 67nm so it is a good reference material.

2.3.2 Data analysis

To analyse the x-ray diffraction patterns collected at the Diamond Light Source we used the Unix based image analysis software Fit2d (produced by Dr. A. Hamersley, ESRF, Grenoble, France). The other programs which helped to analyse the data were: Statsoft Statistica (based on Windows system) and Microsoft Excel spreadsheet packages to calculate the values for the interfibrillar spacing (IFS) and the fibril diameter as well as to create the graphs and diagrams showing relationships between different values.

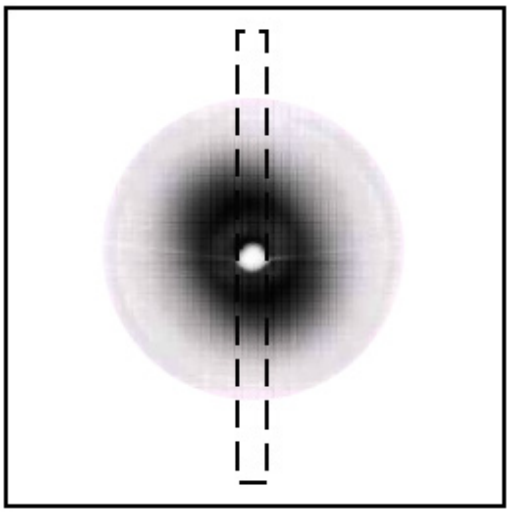

Figure 2.5. Low-angle x-ray pattern from the centre of a normal fish cornea (a vertical transect selected thorough the centre of the pattern was chosen to create an intensity profile – shown as dashed black rectangle).

Each file with data was normalized against appropriate ion chamber readings (1 or 2). To produce an intensity profile of the x-ray pattern, a vertical transect was selected from the centre of the pattern and integrated horizontally (Fig. 2.5). To increase the signal and make an average of the intensity profile of the two halves from the x-ray pattern (which is symmetrical), the pattern was folded around the centre (Fig. 2.6). The centre point was calibrated against the rat tail tendon file.

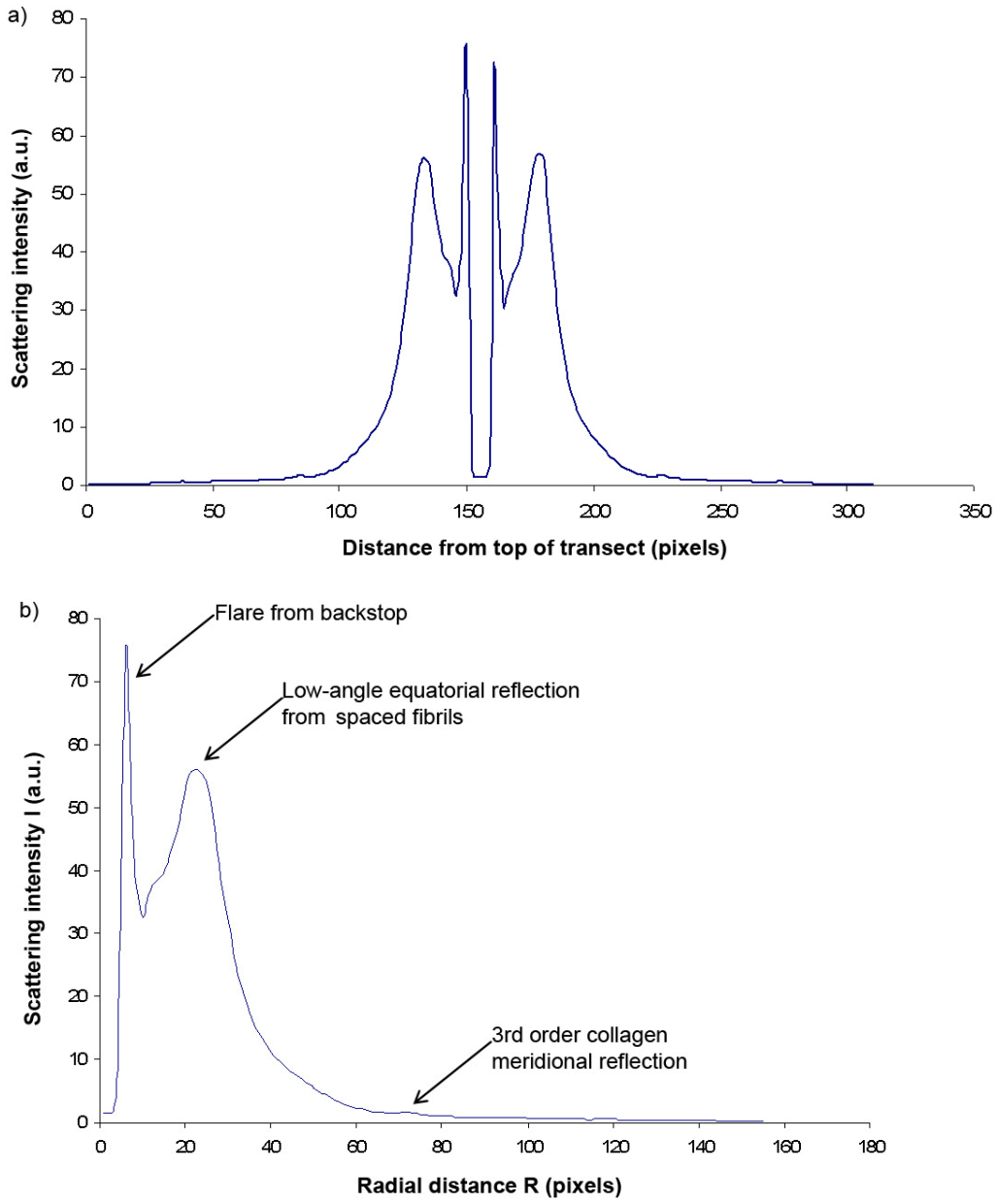

Figure 2.6. a) An intensity profile of the x-ray pattern; **b)** the same pattern folded around the centre producing average intensity profile of the two halves.

As only a small section of the whole circular x-ray pattern was used, the correction for the linear scan across this pattern was done by multiplying the scatter intensity (I) and radial position (R). There is a contribution to the scatter from non-collagenous components of the cornea. This background was removed by fitting a power series to the data. A log IR vs. log R graph was generated to allow a linear background to be fitted (Fig. 2.7). This linear background was then anti-logged. The next step was to subtract the background from the image profile. After this removal only the peaks connected to the low-angle x-ray pattern of the cornea remained.

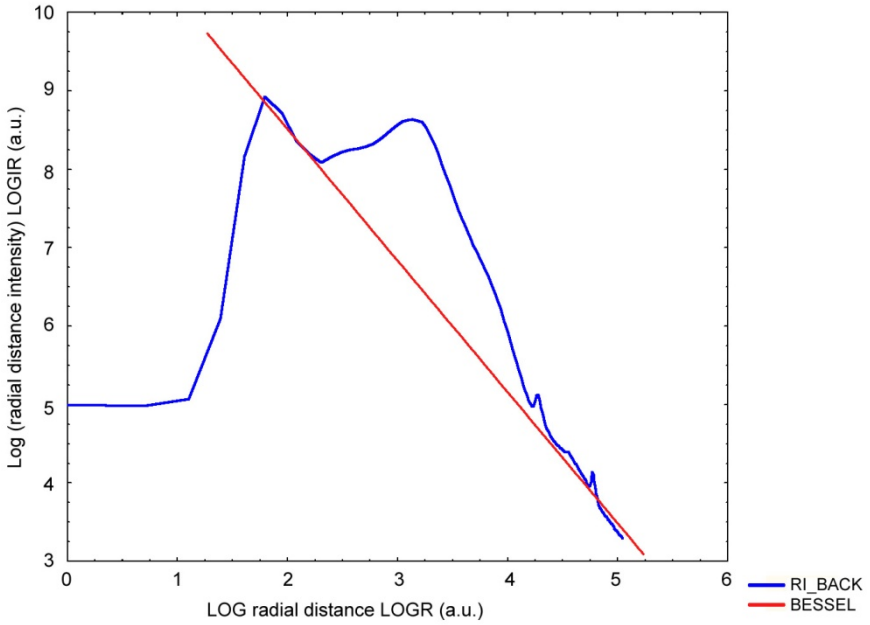

Figure 2.7. A linear background was removed from image profile of scattering intensity. This action left only the low-angle reflection of the cornea.

The first subsidiary maximum of the equatorial pattern is produced by the fibril transform which takes the form of a 1st order Bessel function (Meek and Fullwood, 2001a). A Bessel function was fitted to this peak as shown in Figure 2.8.

To calculate the Bragg interfibrillar spacing of corneal collagen the position of the 1st order reflection of rat tail tendon was used as a calibrant. The position of this reflection was divided by the position of the low-angle equatorial reflection of the corneal

collagen after the removal of the background scatter. This ratio was then multiplied by 67nm, the D-periodicity of the rat tail tendon that gives rise to the 1st order meridional reflection. To obtain the interfibrillar spacing (IFS) the Bragg spacing was converted with the use of the multiplication factor of 1.12 which is based on the assertion of a liquid-like packing of the corneal collagen arrangement (Worthington and Inouye, 1985).

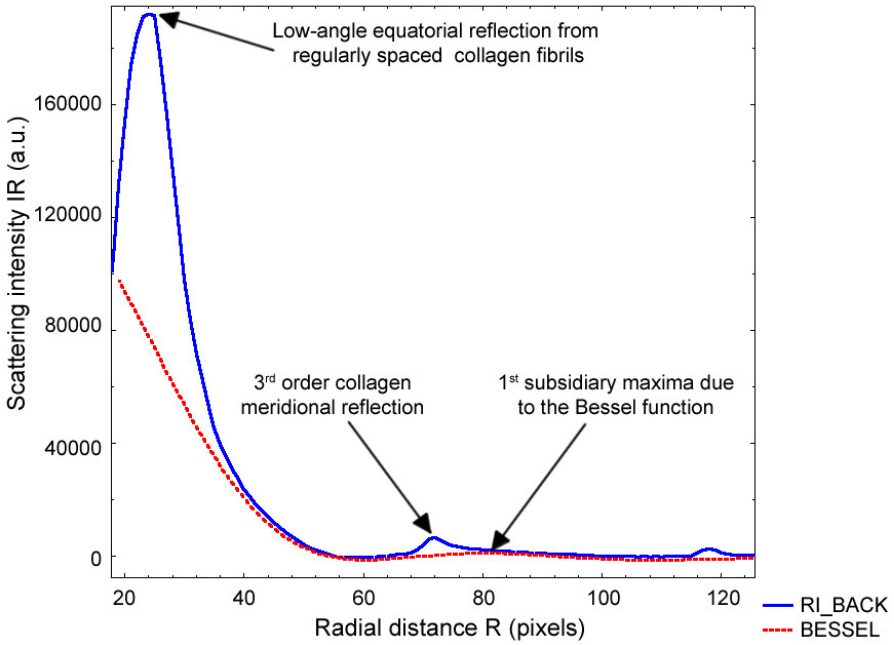

Figure 2.8. The Bessel function fitted to the 3rd order of collagen in the profile of scattering intensity.

To calculate the collagen fibril diameter we used following equation (Meek and Fullwood, 2001a):

$$D = 2 \times \frac{5.14M}{2\pi}$$

Where:

D – fibril diameter

M – Bragg spacing of the subsidiary maximum

As the collagen fibres may be regarded as long cylinders, the scattering from them takes the mathematical form of a 1st order Bessel function. The fibril diameter

(diameter of the cylinder – D) is inversely related to the distance which occurs as the first maxima in the Bessel function (1/M).

2.4 High angle x-ray diffraction

2.4.1 Data collection

High-angle x-ray patterns (often known as wide angle diffraction patterns or WAXS) resulting from a 15 seconds exposure were collected at 1mm intervals from pairs of fish corneas on Station I02 at the Daresbury Synchrotron Radiation Source, Warrington, UK by Dr Craig Boote (Optometry and Vision Sciences, Cardiff University). A 0.2x0.2mm beam with a wavelength of 0.1488nm was used. The images were recorded on a Quantum 4R CCD detector (ADSC, Poway, CA), placed 150mm behind the sample.

The corneas were placed in the sample holder. An ion chamber positioned between the specimen and the incident x-ray beam recorded the average intensity of the x-rays during each exposure. A typical WAXS pattern from corneal collagen is shown on Fig. 2.9.

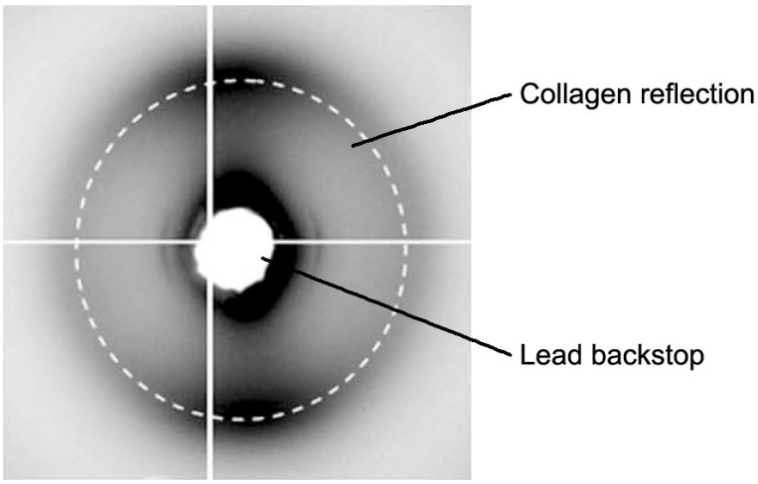

Figure 2.9. Typical WAXS pattern from corneal collagen (picture adapted from Boote et al., 2004).

2.4.2 Data analysis

To analyse the high-angle x-ray scatter pattern we used Unix based software (Fit2d), image analysis (Optimus 6.5, Media Cyberanetics), and Microsoft Excel spreadsheet (Windows based) packages.

The high-angle x-ray data were normalized by multiplying the average ion chamber reading recorded during each exposure by the exposure time in seconds. This provided the x-ray intensity value so we could normalize the corneal x-ray scatter pattern against this value.

To locate the centre of the scatter pattern the programme Optimus 6.5 was used. This was done by measuring the intensity around the circumference of 150 concentric circles. The Optimus 6.5 program formed a series of concentric rings from the centre of the pattern to just beyond the ring of the collagen scatter so it comprised the whole information about the x-ray scatter pattern. Subsequently we divided the circumference of each concentric circle into 256 sectors. The intensity of each segment was plotted against radial distance. To remove the background (obtained by flare from the lead backstop and the scattering from non-fibrillar material of the cornea) a power law curve was fitted to every segment.

Each of 256 profiles was integrated radially across the collagen reflection, and the area under this plot was calculated, giving a single intensity value for every point around the collagen reflection. This profile which was relative to radial position (0-256) was converted then into the profile relative to angular position (0-360) (Figure 2.10a).

The total scattering (which is the intensity of x-ray scatter around the intermolecular reflection and is expressed as a function of angular position) is composed of isotropic collagen (the scatter from collagen that lies in all directions, equally within the surface of the cornea) and aligned collagen (the scatter from collagen

fibrils which are aligned in preferred orientation) (Fig. 2.10a). Thus the area under each graph gave a single value for either the total scatter (Figure 2.10a) or the preferentially aligned collagen scatter (Figure 2.10b) for the tissue volume through which the x-rays pass. These scatter values, under normal circumstances, are related to the total amount of fibrillar collagen, or the amount of preferentially aligned collagen respectively. When mapping whole corneas, the values of either total scatter or aligned scatter from each point in the tissue could be displayed as contour plots using Excel software. In some cases, the ratio of preferentially aligned scatter to total scatter was also plotted. This value is known as the β value (Daxer and Fratzl, 1997) and represents the percentage of lamellae that take up a preferred orientation at that point in the tissue.

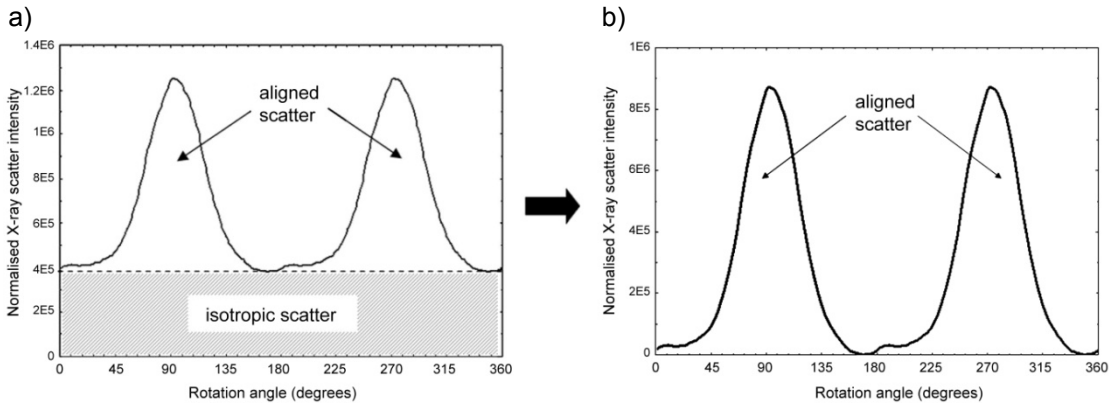

Figure 2.10. a) Normalized X-ray scatter intensity around the intermolecular collagen reflection: isotropic scatter (collagen) and aligned scatter (collagen); **b)** only the aligned scatter (collagen) displayed without background (picture after Boote et al., 2004).

The aligned collagen could also be displayed as a vector plot. This was done by removing the uniform background (from the isotropic collagen) and leaving only the collagen (Fig. 2.10.b). The vector plots were obtained by shifting the intensity profile by 90 degrees (using Statistica software), as it is known that high-angle x-ray equatorial reflections occur at right angles to the fibril axis. The distance from the centre of the vector plot to any direction (given at any angle to the edge) represents the amount of collagen fibrils which are preferentially orientated in that particular direction and it is

shown as a polar plot (Fig. 2.11). For mapping whole corneas, vector plots from each position across the cornea were transferred onto a grid corresponding to preferred orientation of aligned collagen as a function of corneal position.

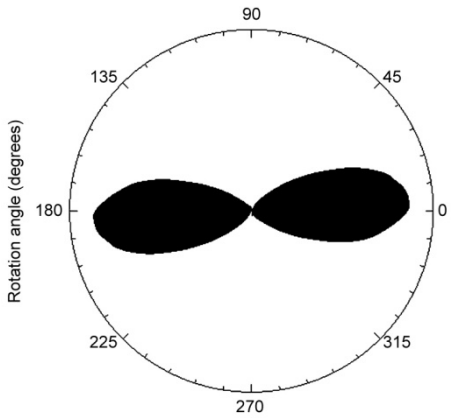

Figure 2.11. Sample of polar coordinates created by conversion of the aligned collagen by shifting the intensity profile by 90 degrees (taking into consideration the fact that collagen fibrils scatter X-rays at right angles to the fibril axis (picture after Boote, et al., 2004).

2.5 Histology

Histology is one of the most essential methods for studying the anatomy of the tissue under the light or electron microscope. The tissue has to be preserved and undergoes the following treatments: chemical fixation, dehydration, clearing and infiltration, embedding, sectioning and staining. The last one is very important to give the contrast of the tissue as well as to highlight the particular features of the tissue which are of interest. In this work, histology was carried out to examine the structure of fish corneas (chapter four).

2.5.1 Sample preparation

Dissection was carried out on the fish corneas. We worked on fresh eyes as the collection was made on the same day. The corneas were marked with a scalpel to recognize the top and the bottom of the tissue. Then they were placed in the fixative

formalin (a solution of 37% formaldehyde dissolved in water) for histologic examination.

2.5.2 Processing the tissue for wax embedding

The fish corneas from the fixative then went through different gradients of alcohol to dehydrate them. The corneas were placed in 50% alcohol (vol/vol with distilled water) for 30 minutes, in 70% alcohol for 1 hour, and in 90% alcohol the specimen was left overnight. On the next day the corneas were transferred into 100% alcohol for 1 hour. Then we put them again into 100% alcohol, only for 30 minutes. The next step was several changes of chloroform: the tissue was placed first in 50% vol/vol mixture of absolute alcohol and chloroform for 30 minutes, and the two times in 100% chloroform, each for 30 minutes. After this we poured off most of the chloroform and warmed the vials containing the tissue by placing them on top of a wax oven for 10 minutes. The tissues were blotted on filter paper and placed into clean wax pots in the wax oven for 1 hour until all the chloroform had evaporated. The corneas were then transferred to clean wax pots and left for 30 minutes to ensure the wax had impregnated the tissue. The specimens were embedded in wax using suitable sized moulds on a refrigerated base. They were left in such condition for 30 minutes and then transferred to the fridge overnight.

2.5.3 Sectioning the tissue

The wax blocks with the tissue were sectioned using a Microm HM 325 Microtome (Fig. 2.12). The thickness of the sections we used in this study was 10μm. The sections were transferred first to the water bath (which was kept at around 47°C) and then placed on slides with an adhesive coating for mounting tissue sections. The water bath was used to stretch the wax sections over the surface which helped to catch them using the

slides. The slides then were placed on the top of hot plate for about 10 minutes and left overnight in the oven at 56°C.

Figure 2.12. The Microtome (Leica, Microm HM 325).

2.5.4 Clearing (de-waxing) and rehydration of the tissue

The slides with the specimen were cleared and rehydrated in xylene and a decreasing gradient of alcohol in a special staining rack in a fume hood as follows: 1st xylene for 5 minutes, 2nd xylene for 5 minutes, 100% alcohol (dish 1) for 20 seconds, 100% alcohol (dish 2) for 20 seconds, 90% alcohol for 20 seconds, 70% alcohol for 20 seconds, 50% alcohol for 20 seconds, and washed in running tap water for 5 minutes (Fig. 2.13).

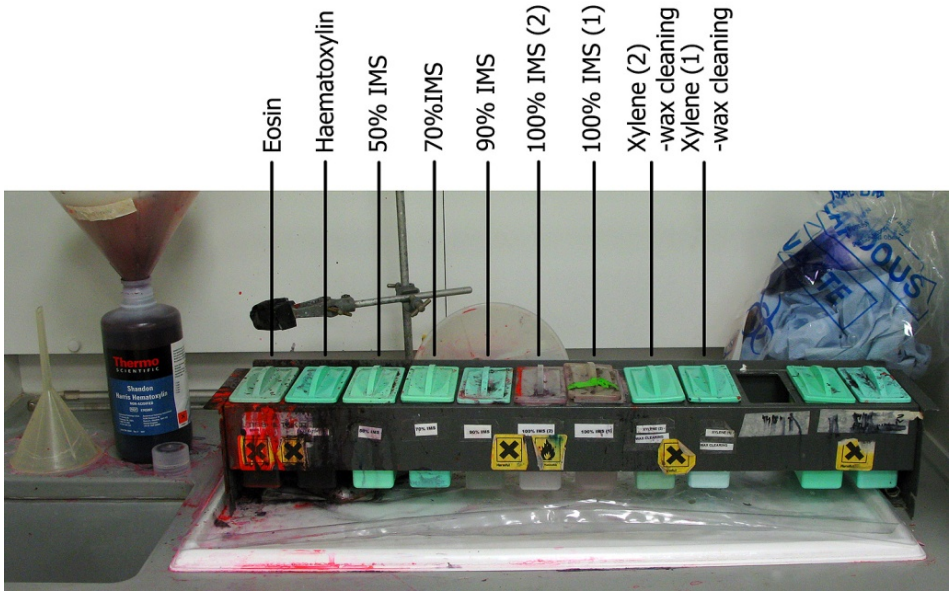

Figure 2.13. Fume hood with all the stains ready for staining procedure.

2.5.5 Haematoxylin and eosin staining

Haematoxylin was filtered, using 'Harris Filters' filter paper, into a staining pot. The slides with the sections then were immersed into this stain and left for 5 minutes. The slick was removed and rinsed in running tap water until the water ran clear (about 20 seconds). The next step was to immerse the slides in 1% eosin for 3 minutes. The slides then were dipped briefly in running tap water and an increasing gradient of alcohol: in 50% alcohol, 70% alcohol, 90% alcohol, and 2 x 100% alcohol for 20 seconds each. The last stage was placing the slides with the tissue in xylene for a couple of seconds. Such prepared slides then were mounted with a clean coverslip using mounting medium, which is miscible with xylene e.g. DPX – a mixture of distyrene (a polystyrene), a plasticizer (dibutylphthalate - butyl, phthalate, styrene - BPS), and xylene. This medium helped to preserve the stain and dry quickly. Slides with the coverslips were left overnight at room temperature in order for the mountant to harden.

2.6 Spectrophotometry

2.6.1 Sample preparation

The spectrophotometry study was carried out on fresh fish corneas as they were collected on the same day. Each cornea was marked so it was known where the top and the bottom was. The measurements were collected from the following fishes: hake, mackerel and salmon as they are species popular on the British market.

2.6.2 Data collection

The data needed in this study were collected using the Pye Unicam SP8-100 double beam spectrophotometer which produces a light source with the beam size adjusted to 1mm (Fig. 2.14).

Figure 2.14. Pye Unicam SP8-100 Spectrophotometer.

The photon beam is sent from the light source and goes to the monochromator which diffracts the light giving the appropriate wavelength. This particular diffracted spectrum is transmitted through the sample. In our case, the sample (fish cornea) was placed in a custom built sample holder (chamber) that was designed so as to produce a trans corneal pressure similar to the intraocular pressure. This ensured that the cornea was under tension and that there were no lamellar undulations which may scatter the light. The cornea does not absorb in the visible region, so any loss of light is caused by

scatter by the collagen fibrils within the lamellae. Thus some of the light was scattered by the tissue but the rest of it was transmitted through the tissue and collected finally by the detector (Fig. 2.15). As expected, the intensity of light that leaves the light source is higher than the intensity of light that reaches the detector.

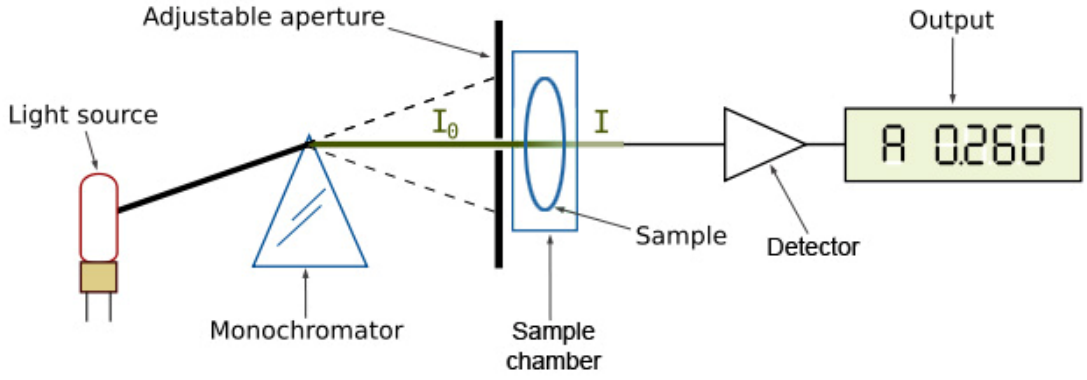

Figure 2.15. Schematic picture showing the process of the light transmission through the sample inside the spectrophotometer (adapted from http://en.wikipedia.org/wiki/Spectrophotometry).

The sample (fish cornea) was placed in the sample chamber filled with silicon oil (Dow Corning 200/5cS) using a syringe. The silicon oil has a refractive index similar to that of the cornea and thus eliminates surface reflection. The chamber was built of two parts with glass and caps, and the basis (on the part the whole instrument was settled) (Fig. 2.16). After filling the chamber with the oil, the caps were screwed on to maintain the intraocular pressure. To avoid air bubbles inside the chamber, it was checked and refilled with the oil if necessary. The prepared chamber was then placed into the spectrophotometer such that the anterior cornea was always facing the light source. The chamber with the sample was centred using a ruler so that the beam passed through the centre of the cornea.

Figure 2.16. The sample chamber designed for spectrophotometry study.

The readings were recorded at wavelength intervals of 10 nm for each position on a given cornea. The measurements were repeated at 1mm intervals across diameters of corneas for each of the fish species.

2.6.3 Data analysis

The spectrophotometer had to be calibrated before the measurements were taken. This procedure is known as "zeroing". This is measured using the blank value which is only the solution (in this case the silicon oil) without the sample. The intensity of the light passing through the blank (I_0) is the first value. The other measurements of absorbency of light are recorded with reference to the initial blank (zeroed) substance. The second value is the intensity of light that passes through the solution and the sample (I). The experimental data then is used to calculate two values: the transmittance (T) and the absorbance (in our case the scattering) (A_λ).

$$T = I/I_0$$

$$\text{and } A_\lambda = -\log_{10} T$$

Transmittance (T) is a value that describes a fraction of light from the original photon beam which passes through the sample and reaches the detector. A_λ, (also called optical density) on the other hand is the ratio which measures an amount of light (at a

specified wavelength λ) which is absorbed as the light passes through the sample. For example: if there is no light absorbed or scattered by the sample, *T* equals 100% (whereas A_λ is zero).

The blank measurement was obtained by calibrating the spectrophotometer at 400nm. The concentration was recorded at each step of increased wavelength value (increased by the intervals of 10nm) until it reached 700nm.

3 A study of proteoglycans/collagen interaction in the human cornea based on electron microscopy

3.1 Introduction

Corneal transparency is a feature that can be explained by the regular arrangement of collagen fibrils and proteoglycans within the corneal stroma. This special assembly promotes destructive interference of scattered light and allows only the light going forward to pass through the corneal stromal layers. There are four proteoglycans (PGs) occurring in corneal stroma: decorin, lumican, mimecan, and keratocan. Thanks to the negative charges on their associated glycosaminoglycans, they make a hydrated interfibrillar gel around collagen fibrils so that the fibrils do not touch each other. However, the way the proteoglycans interact with collagen to promote this spacial arrangement is not known. By staining with the proteoglycan-specific dye Cuprolinic Blue and preparing samples for analysis under the transmission electron microscope (TEM), it is possible to get a set of images at different angles. These images can then be used to create a tomogram a model generated using electron tomography tools (ET). The model described in this report represents a 3-D reconstruction of the tissue, which is based on multiple projections taken as 2-D images. This kind of data collected using tomography techniques can provide much information to help our understanding of the organization of macromolecular assemblies such as occur within the human cornea.

3.2 Aims and Objectives

Electron tomography (ET) uses three-dimensional reconstruction techniques to determine the organization of macromolecular assemblies such as occur in proteoglycan/collagen interactions (Fig. 3.1). Using this method we are attempting to generate the three-dimensional organization of collagen and proteoglycans in normal

human cornea. This 3D model is obtained from a set of images, collected at different tilt angles. Using computational tools such as dedicated software packages (involving many steps of alignments) we are able to build a tomographic reconstruction of the corneal extracellular matrix. The aim of this project is to visualise the arrangement of collagen fibres and proteoglycans at different positions across the human cornea.

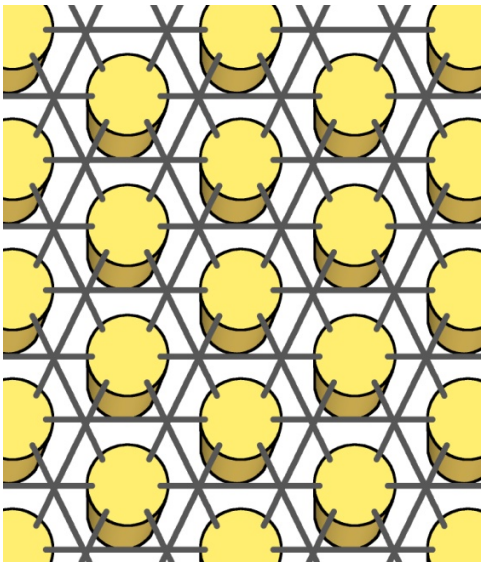

Figure 3.1. Schematic representation of the components from a model of proteoglycan/collagen interaction. This picture shows collagen fibrils as yellow cylinders arranged in regular lattice. Proteoglycans (seen as grey lines) are connected to the next nearest collagen fibril creating the hexagonal pattern around each of them (adapted from Müller et al., 2004).

3.3 Materials and methods

3.3.1 Sample preparation: human corneas

In our study we used normal human corneas from a woman aged 86 years. At the time of her death the transpareny of the cornea was good and the thickness of the tissue was also normal. The tissue came from the Monza Eye Bank (Banca degli Occhi di Monza) in Italy. The corneas were transported to Cardiff University (Wales, UK) in Optisol.

The cornea we had for our study was 8.5mm in diameter with a 2mm scleral rim. We divided it for futher processing into several-millimetre cubes: central, peripheral,

limbus and scleral parts (Fig. 3.2). The tissue was then kept in 4% paraformaldehyde buffer in a fridge until processing for electron microscopy.

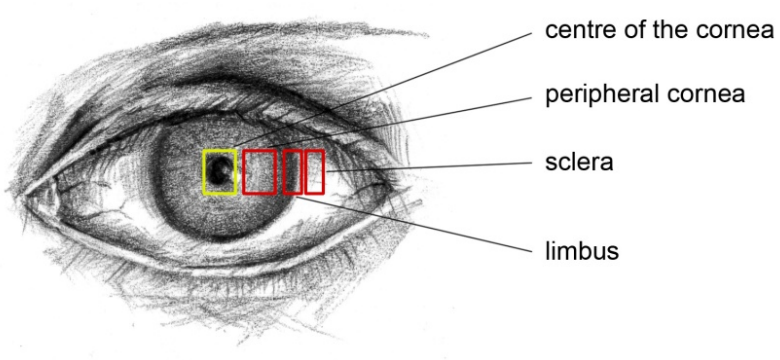

Figure 3.2. Picture presenting the parts of the cornea where the sections were taken: central part of the cornea, peripheral cornea, sclera and limbus.

3.3.2 Sectioning of corneas

The human corneal cubes were suffused with a solution of 0.05% Cuprolinic Blue (Quinolinic phthalocyanate) in 25 mM sodium acetate buffer, pH 5.7, containing 0.1M $MgCl_2$ and 2.5M glutaraldehyde overnight at RT. The tissue was then rinsed three times in 25mM sodium acetate buffer as described in subsection 2.1.1. The samples went through 0.5% sodium tungstate washing process, with ethanol dehydration and finally with incubation in different mixtures of PO_2 and Araldite resin. The whole process is explained in detail in subsection 2.1.1.

The resin was then infiltrated and the tissue was embedded in moulds and left at 60°C for a day. Such prepared blocks were cut on the ultramicrotome to prepare ultrathin sections ready to use under TEM. To collect all the data needed for this study we used a Jeol 1010 transmission electron microscope (Fig. 3.3).

3.3.3 TEM data collection

To make the 3D reconstruction of the human cornea it is very important to take a set of images at tilt angles in TEM. Each TEM image is a 2D projection but the images may be combined to provide information about the objects' characteristics in 3D (Fig. 3.3).

This requires preparing the specimen, and using colloidal gold particles placed on the surface of the specimen as fiducial markers. These markers are used as implements to make the alignment in the eTomo program (with the IMOD software package, Boulder Laboratory for 3-Dimensional Electron Microscopy of Cells and the Regents of the University of Colorado).

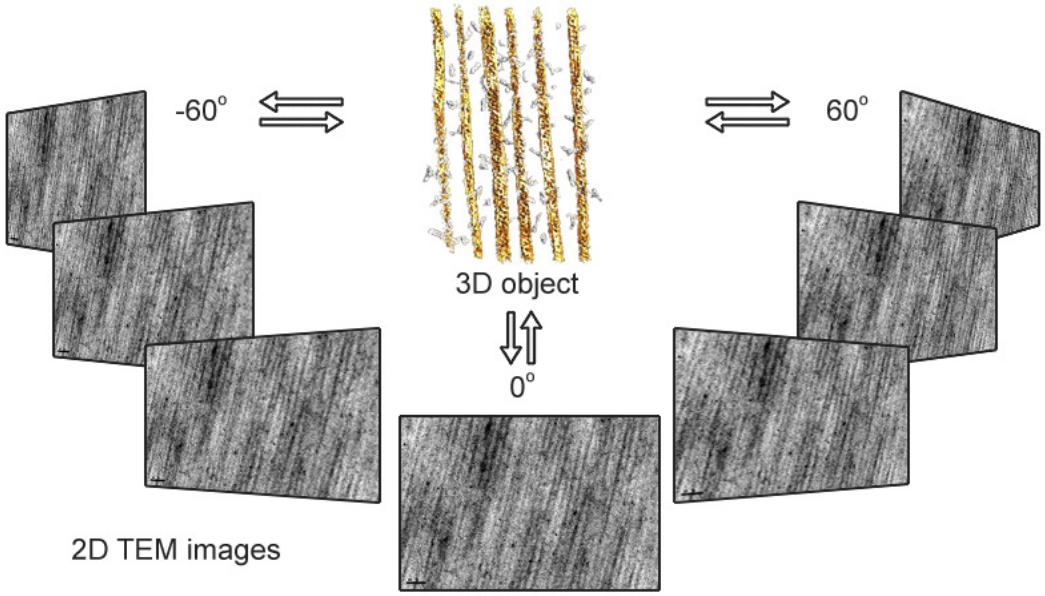

Figure 3.3. Image showing relationship between series of 2D images obtained from TEM and 3D objects made in special software package IMOD.

A single axis tilt series was obtained under a transmission electron microscope (TEM) at nominal magnification of 20 000. Pictures were recorded by automatic correction of image shift and focus variation using a 1.4/digital cooled Gatan CCD camera. The microscope was also equipped with a goniometer which allows an object (in this case it was the specimen holder with the human tissue) to be rotated to a precise angular position. The electron tomographic data set was collected by tilting the specimen manually over a tilt range of ± 60° with 1° increments in a high tilt holder (Koster et al., 1997). Tilt series started at 0° and proceeded towards positive angles at a range of + 60°, and the second part was carried out from 0° towards the negative angles

at a range of – 60°. The astigmatism was corrected every five degrees. The specimen was rotated around a single fixed axis which is perpendicular to the optical axis in the electron microscope (Midgley and Weyland, 2003). A suitable area (from the centre of the cornea, in longitudinal section) containing very well preserved collagen fibres and proteoglycans with good deposition of gold particles was chosen in the electron microscope to collect a tilt series shown on Figure 3.4.

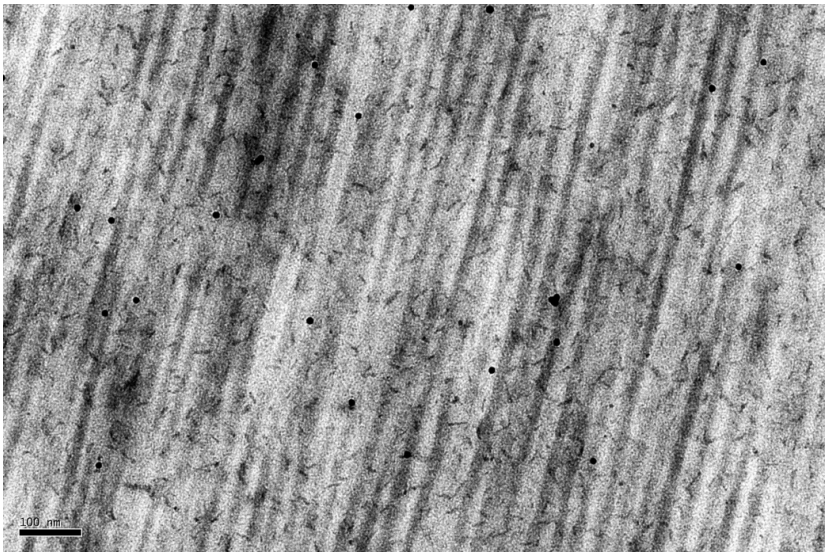

Figure 3.4. Picture taken at tilt 0° under transmission electron microscope (first picture from the whole tilt series).

It was only possible to obtain images from longitudinal cross sections because of problems with burning tissue. Further analyses were based on this particular arrangement between collagen fibrils and proteoglycans (PGs) within central human cornea.

3.4 Results

3.4.1 Data analysis using eTomo programme (with IMOD software package)

The eTomo (with the IMOD software package) program involves a large number of steps. It implements alignment by means of fiducial markers which are in this case colloidal gold particles placed on both surfaces of the specimen (Fig. 3.5). It is possible

to obtain the tomogram (set of images reconstructed in three dimensions) by tracking these fiducial markers. They can be easily located on the image because of their inability to move and their high contrast compared to the specimen structure (Winkler and Taylor, 2006).

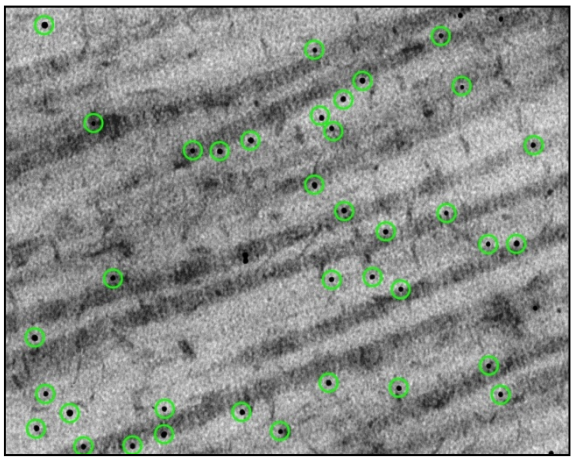

Figure 3.5. Image showing colloidal gold particles (surrounded by the green circles) act as fiducial markers placed on the surface of the specimen.

The alignment of tilt series was carried out in several stages. The first one was the coarse alignment where the pictures were aligned to each other by cross-correlation. This was done by the fact that neighbouring images in the tilt series determine the x and y shifts. The alignment proceeds in a sequential order. The first image was a point of reference to which the rest of the images were aligned by tracking the fiducial markers. This was the second stage of alignment which is called fiducial model generation. On this level, a set of fiducial points were chosen from the first image. In this case it was the picture taken at tilt 0° (Fig. 3.6). The program then found the rest of the fiducials on the subsequent pictures so they were related to each other. The essential condition to get through to the next stage was to fill all of the gaps in fiducial markers within all pictures where it was required. At the next stage which was the fine alignment, the program provided some tools to correct any supplementary errors in the fiducials' positions such

as finding a middle ground for them. This substantially improved the quality of the alignment (as described by Mastronarde, 2006).

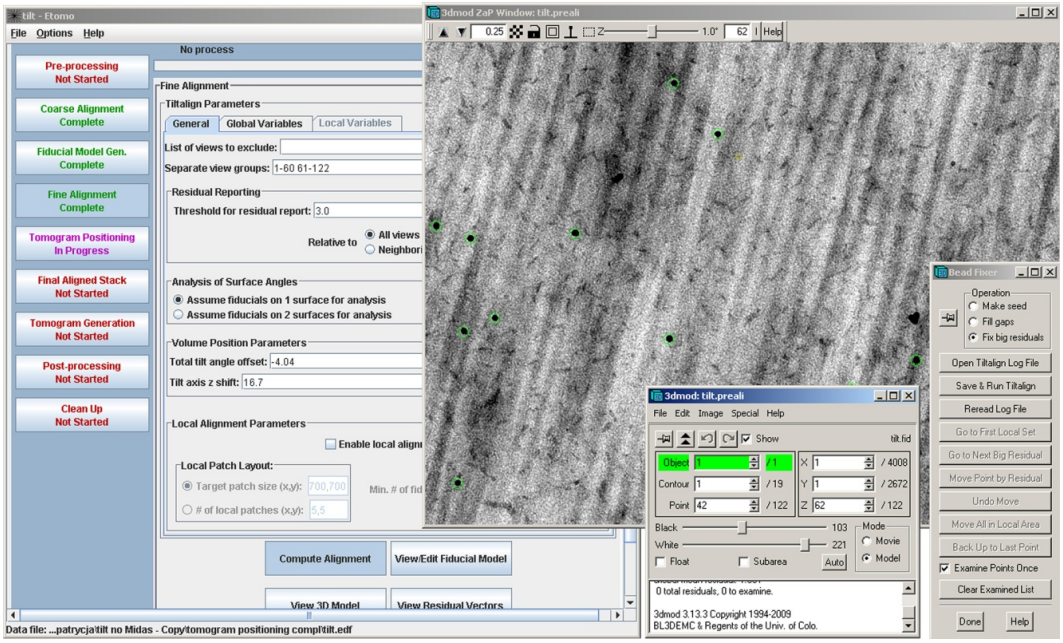

Figure 3.6. Screenshot showing the interface of the eTomo program which is used for making the initial alignment.

The last important stage was the tomogram positioning. At this point it was possible to create boundaries of the existing specimen within the whole tomogram (Fig. 3.7). This helped the specimen to be placed in the centre of the reconstructed volume and make adjustments in horizontal position. The file saved was in MRC format and from this stage taken to the EM3D to make the final alignment. This format is very useful because it can store the 3-D image or stack of pictures in 2-D as one file (after Kremer et al., 1996).

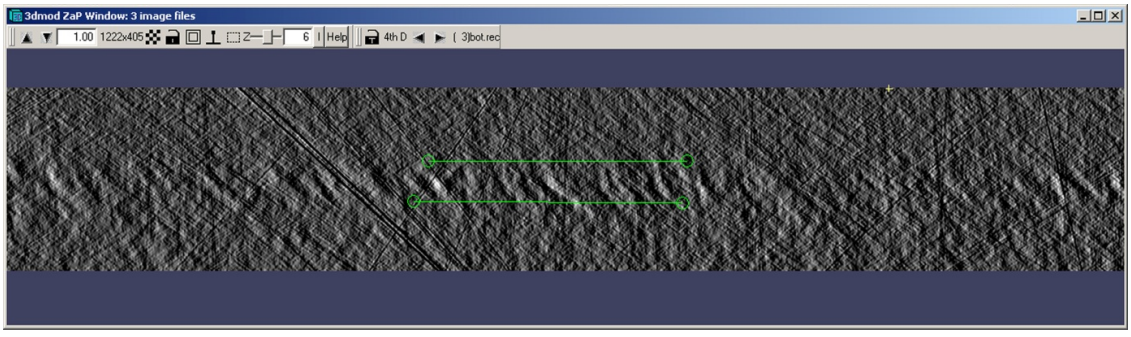

Figure 3.7. Screenshot from the tomogram positioning stage of eTomo program.

3.4.2 Creating tomography reconstruction (a model of human cornea) in EM3D

The EM3D application was used to make the final alignment, reconstruction, segmentation and rendering of the achieved model so it could be analyzed in terms of collagen/proteoglycans arrangement in human corneal stroma.

The software provided all necessary tools to create the model from the tomogram made in eTomo. After the final alignment in EM3D the projections (stack of pictures in 2-D) were converted into a volume mode from which the reconstruction could proceed. At this point it was important to determine the lower and upper slice limits for reconstruction so the dataset was adjusted exactly in the centre. This means that it contained only the information of interest. The next stage was the segmentation where using special tools in the EM3D panel (EM3D visualization window), individual structures like collagen fibres and proteoglycans, were drawn. This process created volumes-of-interests (VOIs) which were isolated from the data set volume based on their structural components (Ress et al., 2004). That was obtained thanks to their greyscale density (Fig. 3.8). The model of created structures could be visualized in the subsequent stage of this EM3D application which was the rendering stage. It was possible to give them different opacities and colours so that they could be easily displayed and analyzed.

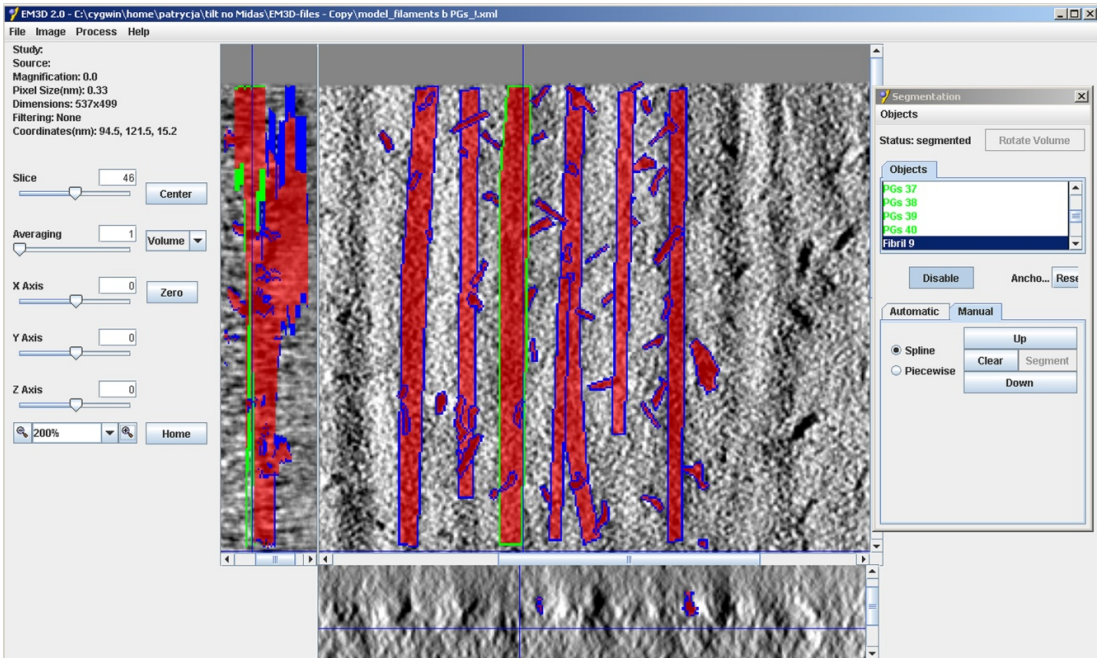

Figure 3.8. Screenshot showing the interface of EM3D programme (longitudinal collagen fibres and small proteoglycans between them which were drawn using this tool as red elements).

3.4.3 Analyzing proteoglycan/collagen interactions in the model

The uniform diameter and characteristic spatial organization of collagen fibrils are assumed to be fundamental requirements for tissue transparency, and thus affect the internal and well organized structure of the cornea. Along with the proteoglycans, collagen fibrils build this regular association where collagen fibrils are regularly spaced within the lamellar structure of the corneal stroma. Negatively charged GAGs have sufficient swelling pressure (from osmotic forces attracting cationic ions from water) to inflate the extracellular matrix.

Meek and Leonard (1993) suggested that collagen molecules and GAGs are synthesized in a fixed numerical ratio. The more collagen molecules (which build the collagen fibril), the bigger number of GAGs spaced in the interfibrillar collagen matrix. Thus, the distance between collagen fibrils becomes larger. Species with smaller fibrils (such as human) would therefore have fewer proteoglycans than those with larger fibrils (such as cow).

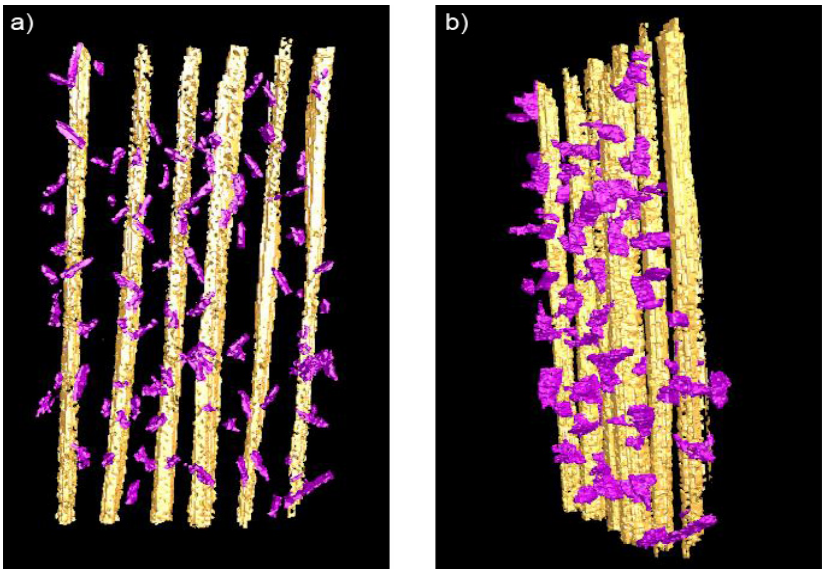

Figure 3.9. Model of normal human cornea arranged in longitudinal section. Collagen fibrils are shown as long cylindrical strings, whereas small proteoglycans concentrate along their axis are marked with claret and purple colour, **a)** face view of the model, **b)** side view of the same model.

In our studies, the model obtained from EM3D applications shows the organization between collagen fibres and proteoglycans in normal human cornea (corneal stroma) in longitudinal arrangement. As shown on Figure 3.9, at first glance the collagen fibres go parallel to each other and proteoglycans are organized in an undetermined distribution around them. Closer inspection shows that many proteoglycans appear to be attached at specific locations (but they are radiating out at different angles). Some fibrils are bridging directly to the neighbouring ones, but most are not. There is clearly no regular organisation of proteoglycans as has been shown in the literature (Scott and Haigh, 1985). Proteoglycans visible in our model do not seem to have regular diameter or shape. However, they are not easily separated into large CS/DS proteoglycans and small KS proteoglycans which are found in other species, i.e. mouse cornea. Proteoglycans in figure 3.9 are shown as attaching to only neighbouring collagen fibrils. Some of them appear to be located along the axis but not closely packed together or adhered to fibrils' surface. Although the proteoglycans of collagen fibrils are not arranged in any systematic way, they seem to be attached to each of these

fibrils in connection with collagen binding sites (after Funderburgh et al, 1997; Ihanamäki et al., 2004; Iozzo, 1999).

3.5 Discussion

Previous studies based on electron histochemistry (especially involving staining with Cupromeronic Blue in 'critical electrolyte concentration' (CEC), described by Scott, 1995) provide some information about collagen/proteoglycans interactions in corneal stroma. Fibrils appear to have almost identical diameters (around 26 nm) and are spaced by a constant distance which is around 66nm. This combination of PGs/collagen fibrils was termed a 'shape module' after Scott (2001). The proteoglycans usually go perpendicular to the collagen fibres, which are linked to two or more of these molecules (Fig. 3.10). The PGs can also aggregate one to another making a bigger conglomeration. Altogether, these make a very well organized extracellular matrix (ECM), so that the cornea remains transparent.

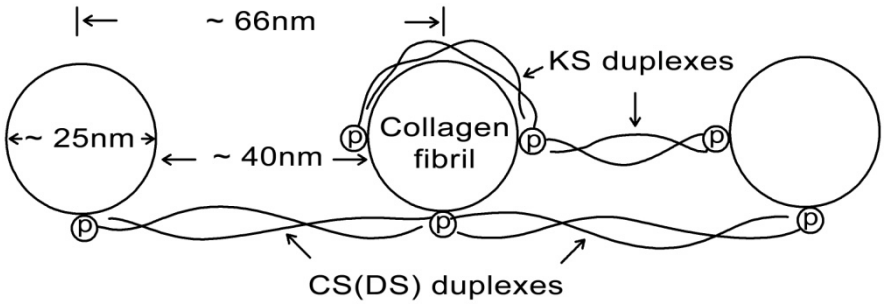

Figure 3.10. A diagram showing interaction between collagen fibrils and proteoglycans in corneal stroma (p means protein core of PGs). KS and CS/DS proteoglycans occur as duplexes which means they have at least two glycan chains. CS/DS GAG chains are longer than KS GAG chains (picture adapted from Scott, 1992a).

Scott (1992b) described collagen fibrils as cylindrical forms which are in contact with neighbouring molecules, ahead and behind. In that position they can create a regular array which helps to enhance their cooperative interactions. The pattern of amino acids along the collagen fibril gives the proteoglycans (PGs) many interactive sites, so they can bind to the fibril at specific sites along its repeating D period.

Proteoglycans appear as molecules with well-defined shapes, where the globular protein head is attached to one or two glycosaminoglycans (GAGs).

It is known that in human corneal stroma there are proteoglycans with two different kinds of glycosaminoglycan: keratan suphate and chondroitin sulphate. Using the same CEC method Scott (1992a) noticed that the CS/DS proteoglycans' were significantly longer then KS proteoglycans. He suggested that shorter KSPGs could make bridges which join neighbouring collagen fibrils (which were seen on longitudinal sections), while CS/DSPGs could form a tangent shared with two or more of these molecules. The proteoglycans bind to the collagen fibrils thanks to their protein core. As long as CS/DSPGs have similar length within different species, KSPGs could be varied in this parameter.

Scott (1993) suggested that there are different patterns of the shape and distribution of collagen fibrils and the proteoglycans interacting with them. One of them is that GAGs filaments bridge one fibril to another or more in direct lines (interfibrillar); another one shows GAGs, oriented along the fibril axis (intrafibrillar); and the last one is that GAGs are orthogonal to the fibril axis and they are annular, focused around one fibril. These arrangements could appear thanks to cooperative electrostatic bindings between the acid group of the GAGs and the amino groups of collagen fibrils. More specifically amino groups are located in the side chains of lysyl and arginyl residues of collagen (Junqueira and Montes, 1983).

Comparing these studies to our results we can say that proteoglycans (PGs) in our model are not arranged in any specific way, but are definitely arranged along the longitudinal axis of the collagen fibrils. There is no difference in size and shape of PGs but we can assume that there are two kinds of proteoglycans: CS/DS and KS as in every

normal human cornea. Collagen fibrils shown in our model are more or less evenly distributed and they seem to have constant diameter.

Knupp et al. (2009) and Lewis et al. (2010) also proposed a mechanism explaining how the distance between two adjacent collagen fibrils in the cornea can be maintained. This new mechanism develops the previous model presented by Müller et al. (2004) which described collagen/proteoglycans interactions as a six-fold hexagonal lattice (see above in Section 3.2, Fig. 3.1). The new theory giving us a different view on corneal transparency is based on two balanced interacting forces in the corneal stroma. One of them is an attractive force which tries to bring the fibrils and PGs together. This one is based on the thermal motion of the PG/GAG complex and glycosaminoglycans themselves. The second one is a repulsive force which tries to push the collagen and PGs apart. This one is based on positive charged ions being attracted by negative charged GAGs. Thus water molecules are drawn to this area by osmosis (because of the creation of local concentration gradients) leading to a Donnon pressure between the collagen fibrils (Fig. 3.11).

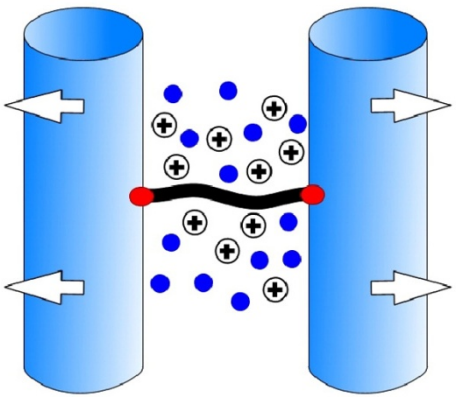

Figure 3.11. A diagram showing the relationship between two neighbouring collagen fibres and proteoglycans acting as a bridge (see full description in text), the pluses on the picture are the positive charged ions and the blue dots are the water molecules (after Lewis et al., 2010).

Maybe this mechanism can give us an additional glimpse into the structure of the cornea as the model of human cornea does not give us a precise view of the

collagen/PGs interaction. Lewis et al. (2010) created a model of bovine cornea in 3D that could be compared to our human one. Both corneas are similar physiologically but bovine is about three times thicker. However, the bovine model did not give the researchers evidence of any systematic arrangement within corneal collagens and proteoglycans around them (Fig. 3.12).

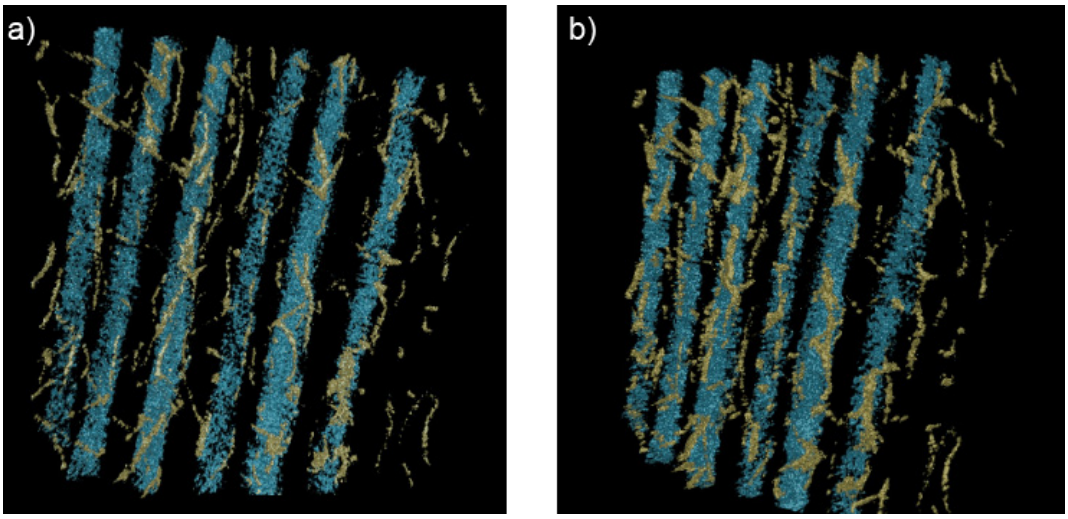

Figure 3.12. A longitudinal view of 3D reconstruction of bovine cornea, the collagen fibrils are marked with blue and proteoglycans are coloured with yellowish, thin threads around them; **a)** face view of the model; **b)** side view of the same model (adapted from Lewis et al., 2010).

As seen on the picture the larger proteoglycans - chondroitin sulphate/dermatan sulphate occupy the space within one or two collagen fibrils and lie mainly along the fibril axis and shorter proteoglycans - keratan sulphate are placed between two adjacent collagen fibrils. The mouse cornea also shows a different collagen PG arrangement. Chondroitin sulphate/dermatan sulphate proteoglycans connect neighbours and next neighbouring collagen fibrils, whereas the keratan sulphate proteoglycans are located in regular orthogonal intervals between these neighbours (Parfitt et al., 2010). The authors suggested that the CS/DS proteoglycans can also form tetramers or polymers. Above all, they found that the most frequent in mouse cornea were links between only three fibrils (Fig. 3.13). Thus to sum up the structure of the cornea is a dynamic and constantly changing environment where collagen fibres remain in a regular order and

proteoglycans, because of the contradicting forces acting around them, can let the whole arrangement of the corneal stroma keep this special array (with limited opportunity to change their position) which gives the cornea transparency.

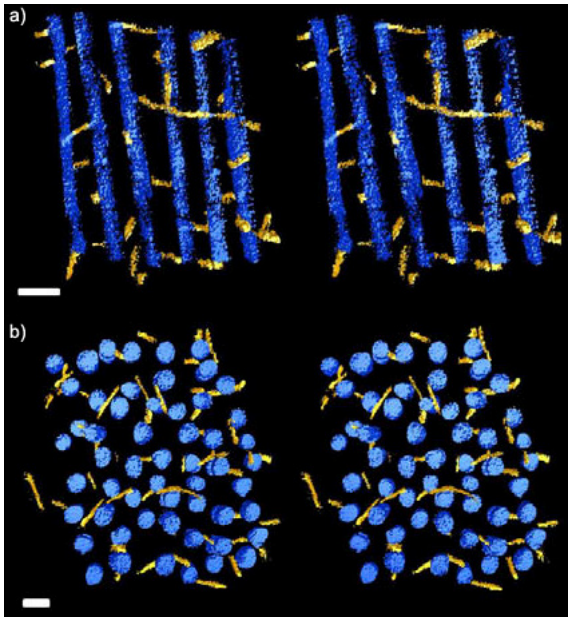

Figure 3.13. Picture showing three-dimensional reconstruction of collagen/proteoglycans arrangement in the mid stroma of the mouse cornea: **a)** longitudinal section; **b)** transverse section. The collagen fibrils are marked with blue colour and the proteoglycans are coloured yellow. Scale bar = 50nm (adapted from Parfitt et al., 2010).

3.6 Conclusion

The corneal stroma owes its remarkable transparency to the precise arrangement of the constituent collagen fibrils, which in turn are thought to be controlled by proteoglycans between them.

Our model obtained using tomography reconstruction shows normal human cornea in longitudinal sections. Collagen fibrils are distributed regularly (with almost constant diameter), whereas the proteoglycans are located along their axis. PGs do not differ from one another but presumably there are two different kinds of them: KS and CS/DS proteoglycans. There is no regular arrangement of the PGs along the collagen axis in the human cornea. The same tendency was found in bovine cornea (Lewis et al, 2010). What is more, comparing these three models: the human cornea, the bovine

cornea, and the mouse cornea, we have observed that the first one has more shorter proteoglycans than bovine, which are aligned in the collagen axis. The mouse cornea does not show any specific order in the proteoglycans, while the collagen fibrils demonstrate the regular arrangement of pseudo-hexagonal order (Parfitt et al., 2010).

Due to time limitations and the difficulty of obtaining appropriate tissue, it was only possible to examine a single human cornea. However, the results showed significant differences compared to the mouse and the bovine, suggesting important species differences in the collagen/proteoglycan organisation. It is, therefore, necessary to gain more details about collagen/proteoglycans arrangement in human and other animals' corneas to confirm these differences.

3.7 Future work

This was very much a preliminary study, the first to attempt to use tomography to visualise the 3-D arrangement of proteoglycans in the human cornea. Tomographic techniques require collecting images of the specimen from different directions which is possible using transmission electron microscopy. However, taking a set of images manually is very time consuming and demands many adjustments. First of all, the goniometer has its own mechanical imperfections, so the tilt axis is not completely stable (Koster, 1997). Thus tilting has to be done very carefully. Secondly, even if the axis is well aligned, the image shift is still noticeable. Because of that fact it is so important to correct the focus and astigmatism almost at every single degree. Every action contributes to the exposure of the specimen to the beam. This causes frequently structural degradation of the tissue (as is shown on Figure 3.14).

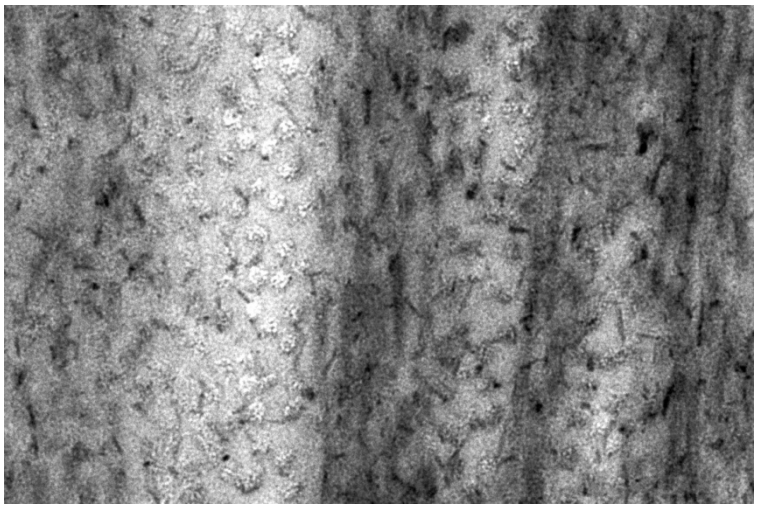

Figure 3.14. A human corneal stroma exposed to exceeding critical electron dose (there are visible distinct pattern of burning tissue – seen as white bubbles, mostly on the left hand side of the picture).

In this connection (described above) the future work should mainly focus on improving the microscope methods and preparing the specimen. Improving the specimen preservation could also be achieved by using new high-pressure freezing methods. Initially, the aim was to determine the arrangement at different positions across the cornea and approaching the limbus. This was not achieved due to time constraints, so could be pursued in future. Furthermore, the technique could also be applied to pathological human corneas (where an alteration in the proteoglycans is expected), in particular: keratoconus and corneal oedema.

4 A study of corneal structure and collagen orientation in sea fish corneas (hake, mackerel, salmon, seabass)

4.1 Introduction

Vision in the deep sea requires special adaptations which allow the animal to see clearly in the environment where light transmission changes are noticeable with depth. Because of the fact that water absorbs light, the increased depth reduces dramatically its intensity. As described by Warrant and Locket (2004) there are two kinds of light sources in the water: (1) natural light originating from the sun and moon (this light occurs closer to the surface of the water), and (2) bioluminescence light, which comes from other aquatic animals (the light in water is organized as the flash coming to the eye from different points – its sources are in the deep depths of the sea where natural light cannot penetrate).

In the clearest oceanic waters, natural light (solar light in the middle of the day) can penetrate to the depth of 1100m and still be visible to deep sea fishes, while for the human it will be visible only to a depth of around 800m. The limit for the light from the moon is at around 600m for the fish eye (Bone and Marshall, 1982). The water molecules attenuate effectively the other wavelengths of light e.g. ultraviolet and long wavelengths, and because of that the maximum transmission remains between 400nm and 500nm. Below a depth of 1100m, fishes can use point-source bioluminescence light from the other animals and they have usually big and complex eyes (Bone and Marshall, 1982, Guthrie and Muntz, 1993).

4.1.1 The structure of the fish cornea

The aquatic animal's cornea has to keep the balance between transparency (maximising light transmission from water surface while maintaining the ion balance, especially in a hypertonic environment such as sea water) and strength (resisting the force of water

pressure and temperature changes). In most of the fish eyes the cornea consists of two distinct layers: an outer, dermal layer (which is also called the spectacle), which is continuous with the skin and contains external epithelium, stroma and posterior epithelium; and an inner, scleral layer, which is a continuation of the sclera and could be built of the same 5 layers as any other terrestrial cornea (with some exceptions), but mainly of the stroma, Descemet's membrane and endothelium.

The spectacle can be attached (fused) to the scleral cornea and make a uniform structure (e.g. in the hake) or be detached and separate from the scleral cornea by the connective tissue (e,g, in the mackerel). The transparent spectacle can act as the protective goggle for the eye and allows it to move underneath it easily (Collin and Collin, 2001). The cornea is flattened while the lens is almost spherical in shape (Fig. 4.1), whereas in human these two are completely opposite. This is because the cornea has very little refractive power in water, so all focusing is performed by the lens. The outer cells of the external epithelium possess microprojections which are suggested to help in oxygen movement and nutrients as the tear film in water is not necessary (Collin and Collin, 2001, Nicol and Somiya, 1989).

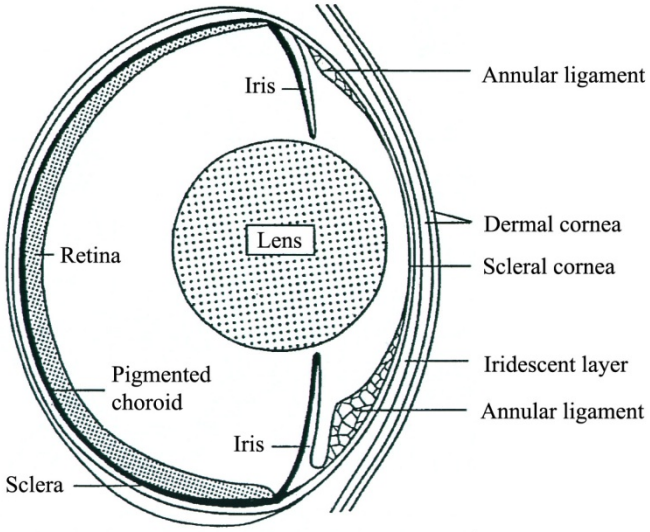

Figure 4.1. Image presenting the structure of the fish eye in cross-section (Collin and Collin, 2001). Individual elements are described in the text.

In a number of bony fishes was also found a so-called iridescent layer, which is a separate layer of coarse fibres and is situated between the scleral stroma and Descemet's membrane. Its main function is to increase the visual range under the water whilst not sacrificing the sensitivity (Nicol and Somiya, 1989). Another frequent but not universal element between the cornea and iris was described as the annular ligament (meshwork). This group of cells in the iris angle is not strictly a ligament but the name was given because of their supportive feature to the anterior segment.

There are some corneas which have yellow colouring and their cut-off points are at around 400nm; they absorb light strongly between 400 and 500nm. The colour of these corneas is obtained thanks to the presence of the yellow cells which contain coloured carotenoids. This prevents the ultraviolet light (short wavelength) from reaching the retina and they can play the role of eyeshades which reduce the amount of light that goes to retina from above (Nicol and Somiya, 1989).

4.1.2 The function of the fish cornea

The main feature of the fish cornea is to be transparent. The deep sea is very poorly illuminated and therefore demands of this outer layer of the eye is the ability to maximize the amount of light reaching the fish retina, so that the animal can behave in a special way, for example while feeding, hiding from predators, or signalling to the other individuals of danger or changes in the immediate area. As is known, swollen corneas become opaque, so maintaining the right level of hydration is essential for the cornea to stay transparent.

In teleost fish, the cornea is impermeable to salt and water which means that the fish cornea is not a leaky barrier as it is in terrestrial animals (Fischer and Zadunaisky, 1977). It is believed that in fish corneas the ion balance is mainly regulated by the electrical resistance of the epithelium and the ciliary body which is responsible for

maintaining the balance of swelling forces in hypotonic environment produced by the epithelium (aqueous humour). Along with the endothelium the hydration is regulated so the cornea remains transparent (Nicol and Somiya, 1989). Thanks to this feature the intraocular humour has half of the osmotic concentration compared to the surrounding sea water. This does not mean that the fish cornea cannot swell or imbibe water. It means that the fish cornea remains impermeable to salt water or large molecules coming from the aqueous humour which is responsible for the osmotic balance (Smelser, 1962).

In fish the refractive index of the cornea is similar to that of the surrounding aquatic environment (sea water) and can vary from 1.335 to 1.382. In this situation the refraction takes place only in the lens of the eye which is very dense and has a short focal length. Because of this, focusing requires the lens to move backwards and forwards along the optical axis towards the retina using the lens muscle (Bone and Marshall, 1982, Guthrie and Muntz, 1993, Hawryshyn, 1998). The human lens is not as dense as that of the fish, and while focusing, it can change its shape. It is very elastic and uses the ciliary body to change the form (Fig. 4.2).

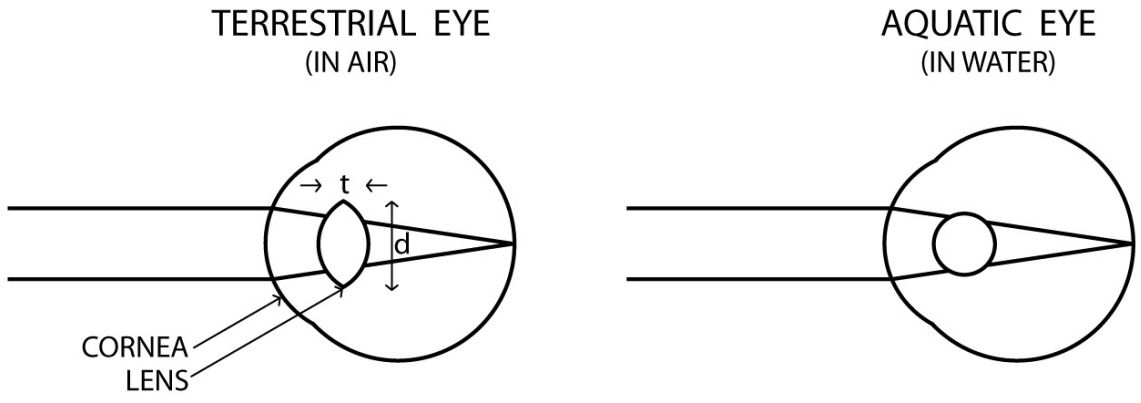

Figure 4.2. Two diagrams comparing the accommodation in human and fish cornea. These two pictures show the difference in shape of the cornea in different environment (picture adapted from Hawryshyn, 1998). The letters in the diagram refer to the following: *t* is the thickness of the lens, *d* is the lens diameter.

The teleost lens can be moved by a complex of four or more muscles: backwards (towards the tail of the fish), forward, obliquely downwards, and obliquely upwards. As Nicol and Somiya (1989) described, the system of accommodation in teleosts' eyes is built of three elements: (1) the lens and the closest ligaments, (2) the lens muscle and its pigmented covering, and (3) the ciliary nerve which is responsible for innervating the lens muscle (Fig. 4.3).

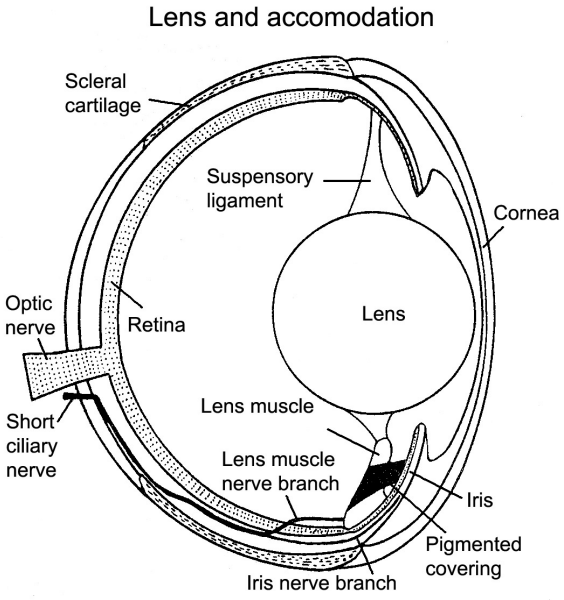

Figure 4.3. Picture showing the location of the lens muscle (Nicol and Somiya, 1989).

4.1.3 Aquatic environment of four selected species (hake, mackerel, salmon, seabass)

In our study we used four of the most commonly occurring market fish species: hake, mackerel, salmon, and seabass. As they are very popular in Great Britain, they are easy to collect from any fish markets.

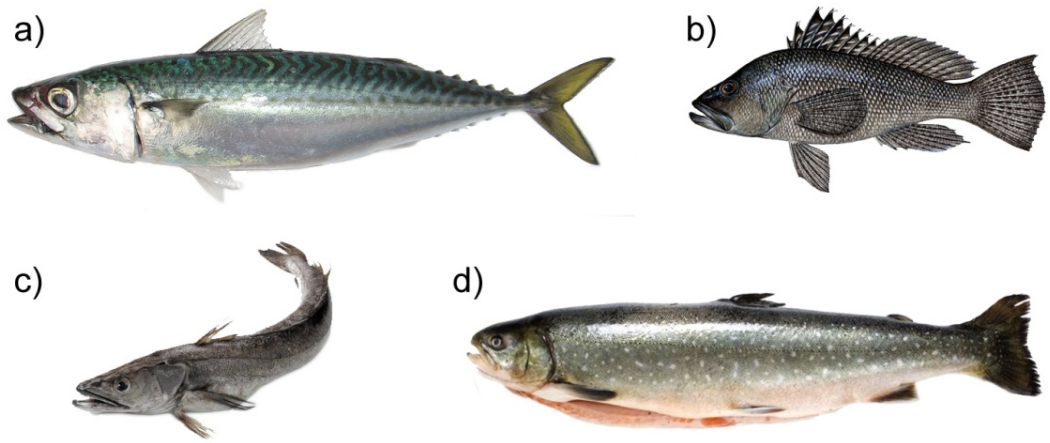

Figure 4.4. Picture showing four of the fish species used in our study: **a)** mackerel; **b)** seabass; **c)** hake; and **d)** salmon (pictures not to scale).

The European hake, *Merluccius merluccius* from the family Merluccidae, is an active predator and plays an important role in the marine food chain, transferring the energy between species (Fig. 4.4c). The range of this species in the sea water is represented between 50m and 750m. Adult individuals feed mostly on other fishes, relocating in the water column during their lives. They look for food not only near to the bottom but also close to the top. The juveniles occur between 100m and 200m and feed on small crustaceans. Because of such a wide range of appearance in the water depths, hake is exposed to different light levels. Its visual system must be able to adapt to different environmental requirements regarding types of predators, prey and other factors in its water habitat (Bozzano and Catalán, 2002).

The Atlantic mackerel, *Scomber scombrus* from the family Scombridae, is a highly commercial species, along with the tuna from the same family. Mackerel is a fast-swimming fish and it has to swim all the time as its gills require constant flow of water for good ventilation (Fig. 4.4a). This species creates a column of adult individuals (of many thousands) in the water surface and swim actively, mainly during the day and close to the surface in the open ocean – pelagic zone (from spring to autumn). It

migrates to the deep sea for the winter and stops feeding until spring. Mackerel feeds mainly on other fishes and small crustaceans which it can filter from the water.

The Scottish farmed Atlantic salmon, *Salmo salar*, from the family Salmonidae, in the wild is born in fresh water, then migrates to the ocean and stays there until its returns to the fresh water (where it was born) for reproducing (Fig. 4.4d). The adult individuals stay their whole life in the open ocean (sea water), between the depths from 2m and 10m. They group together in small numbers and look for food which is mainly squids, shrimps, and small fish. They are mainly active during the day. This species is able to adapt to two different environments: fresh and sea water and thus its visual system is also well adapted to such different habitats.

The European Sea bass, *Dicentrarchus labrax*, from the family Moronidae, is a major fisheries and significant marine species in European aquaculture (Fig. 4.4b). It is not only a sea water fish but also a fresh water species. In the ocean its depth range is between 10m and 100m but it is mostly found in the bottoms of lagoons and occasionally in rivers. They migrate to rivers and coastal waters in summer but return to deep sea waters during winter. The adults do not form a school as much as the juveniles. Their main food as they are predators is molluscs, prawns, crabs and other fishes.

4.2 Aims and Objectives

Fish is an excellent animal for any study because it is common and easy to get as a material. As was shown in the introduction to this chapter, the fish cornea is fundamentally similar to the human and other land animal's corneas. However, due to light restriction and visual problems in water (as it is a dense medium through which the light has to pass getting to the fish eye), some of the elements in the fish eye demonstrate different changes in response to the available level of light reaching it. To

perform this study we have chosen four different sea fishes: hake, mackerel, seabass (deep sea fishes) and salmon (from two different habitats: sea and fresh waters).

The aim of this study is to compare the main structure of the four corneas and find the similarities or the difference between the species and between the fish and the terrestrial cornea in order to relate structural features to functional differences. Beginning with histological studies we describe the general structure of the fish cornea and its basic properties. Then using x-ray diffraction we investigate the factors responsible for corneal strength and transparency: collagen fibril diameter and interfibrillar spacing as well as the local order of collagen and the distribution of collagen within the fish cornea. Spectrophotometry data was used to provide information about the transmission of light that can pass through the cornea of these four species.

4.3 Materials and methods

4.3.1 Sample preparation: fish corneas

In this study we used normal fish corneas collected from Cardiff Central Market. Corneas were dissected from the fish and kept in formalin (a solution of 4% formaldehyde dissolved in water). This fixative was used to preserve the tissue for histologic and x-ray examination. In our study we used the following sea species: hake of the family – Merluccidae, mackerel of the family – Scombridae, salmon of the family – Salmonidae, and seabass of the family – Moronidae. All can be found in salt water, salmon also in fresh water where it returns to reproduce. Only for the spectrophotometric study did we used fresh fish (not fixed) as the data had to be collected on the same day.

4.3.2 Histology

As outlined in chapter 2, the tissue was processed for wax embedding before pictures under the light microscope were taken. All corneas were cut in half (across the centre), subsequently went through different gradient of alcohol for dehydration and chloroform and then embedded in wax moulds. Such prepared blocks were sectioned at a thickness of about 10μm and placed on slides with adhesive coating. The sectioning was done from the centre of the cornea going towards the perimeter (Fig. 4.5). The tissue was cleared (de-waxed) then rehydrated in xylene and a decreasing gradient of alcohol. Next, the fish corneas were stained with the haematoxylin and eosin staining in the fume cupboard. The sections placed on the slides were used under light microscope for further analysis.

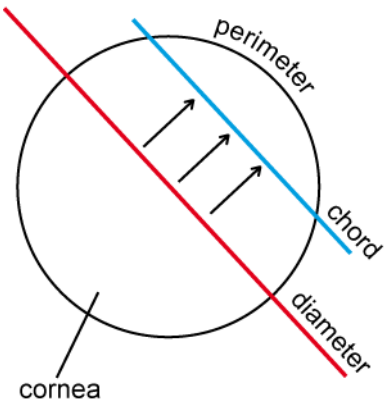

Figure 4.5. A diagram showing the way the cornea was cut for the histology study

The histological pictures of the four fish corneas were taken using a Leica DM RA2 microscope and Image Processing and Analysis Software – Leica QWin (Fig. 4.6).

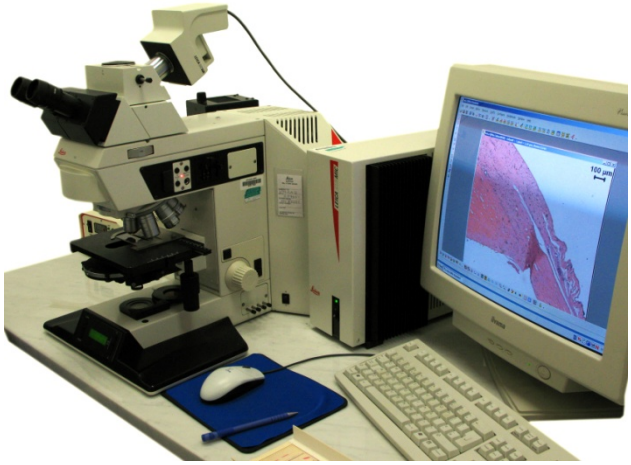

Figure 4.6. Leica DM RA2 microscope.

4.3.3 High angle x-ray data collection and analysis

As outlined in section 2.4.1, the wide-angle x-ray patterns were collected at Station I02 at the Diamond Light Source (Oxfordshire, UK). The beam size used in that study was 200µm x 200µm. The data was recorded using 0.9796nm wavelength and the detector distance of 550mm.

In this study we used three species: hake, salmon and seabass. Data was collected horizontally going from the top of the cornea to the bottom at 1mm intervals: hake data was recorded with 10 seconds exposure, salmon with 15 seconds exposure and seabass with 10 seconds exposure (Fig. 4.7). All the data was analysed in the manner described in Section 2.4.2.

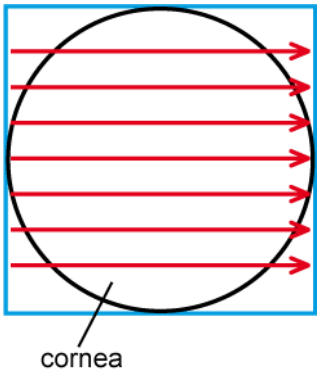

Figure 4.7. A diagram showing the way the cornea was scanned for collection of the high-angle x-ray patterns. The arrows show the direction of the monochromatic x-ray beam.

4.3.4 Low-angle x-ray data collection and analysis

As described in Section 2.3.1, the low-angle x-ray patterns were collected at Station I22 at the Diamond Light Source. The study was carried out using the evacuated camera of length 6m and the beam size 250x300µm. The current used for normalization was 240µÅ and the wavelength of the light used was 0.9796nm.

Only two species were used in this study: mackerel and salmon. The scan taken from the mackerel was recorded horizontally across the centre of the cornea at 0.5mm intervals with the exposure time of 5 seconds (Fig. 4.8). The salmon data was also recorded across horizontal (only through the centre of the cornea) at 1mm intervals with the exposure time of 5 seconds. The data was analysed as it is outlined in Section 2.3.2.

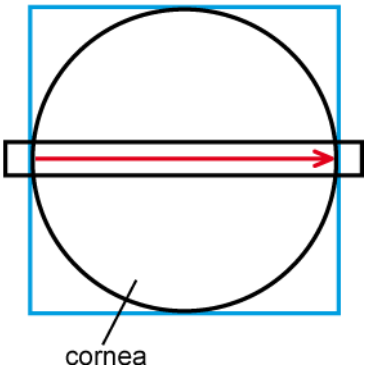

Figure 4.8. A diagram showing the transect scan across the centre of the cornea collected for low-angle x-ray pattern. The arrow shows the direction of monochromatic x-ray beam.

4.3.5 Spectrophotometry

As outlined in chapter 2 the samples (fish corneas) were collected on the same day from the Cardiff Central Market. The spectrophotometer was calibrated each time (before taking the measurement from each fish cornea) with the reference to blank measurements (in our study: silicon oil). Subsequently, the measurements of each cornea were taken at the range between 400nm and 700nm wavelength and recorded as the absorption value. This value was explained in more details in second chapter,

subdivision 2.6.3. The data was collected from the following species: hake, mackerel, and salmon.

4.4 Results

4.4.1 Histology

On dissection of the fish eyes some of the features described in subsection 4.1.1 were noticed. The hake eye is relatively large (around 15mm in diameter). The cornea is a soft tissue, where the spectacle (dermal cornea) is attached to the scleral cornea (almost unnoticeable as a separate layer with the naked eye). The mackerel cornea is a hard tissue; the spectacle is not attached to the basic cornea. It is easy to separate these two layers. The size of the cornea is around 10mm. The salmon cornea is again a hard tissue, especially the scleral part. The spectacle is also detached and the size of the whole cornea is between 10-12mm. The seabass cornea is another soft tissue with a diameter around 12mm. The spectacle is fused with the scleral cornea and hardly seen with the naked eye during dissection.

The cornea of most of the fishes is divided into two different layers: dermal cornea (spectacle) – outer layer and scleral cornea – inner layer, as was described in subsection 4.1.1. In our histological study we found that two of our species: hake and seabass have the spectacle visible under the light microscope shown in Figure 4.9 – 4.11 and 4.15 – 4.17. The remaining species: mackerel and salmon have the spectacle detached as it was easy to separate it from the tissue while doing dissection. The pictures of the mackerel species are missing as the tissue was too hard to cut it with the wax embedding method described in subsection 2.5. The structure of the last species – salmon is shown in Figures 4.12 to 4.14.

In our histological sections, the outer layer is not very dense, while the inner layer is more compact and uniform. At the edge of the cornea there is a well seen

cartilaginous sclera. What is more, on our pictures there is also an internal fibrous part of the cornea, which is called the annular ligament. This element is the third layer of the cornea and it is thin in the centre part of the tissue.

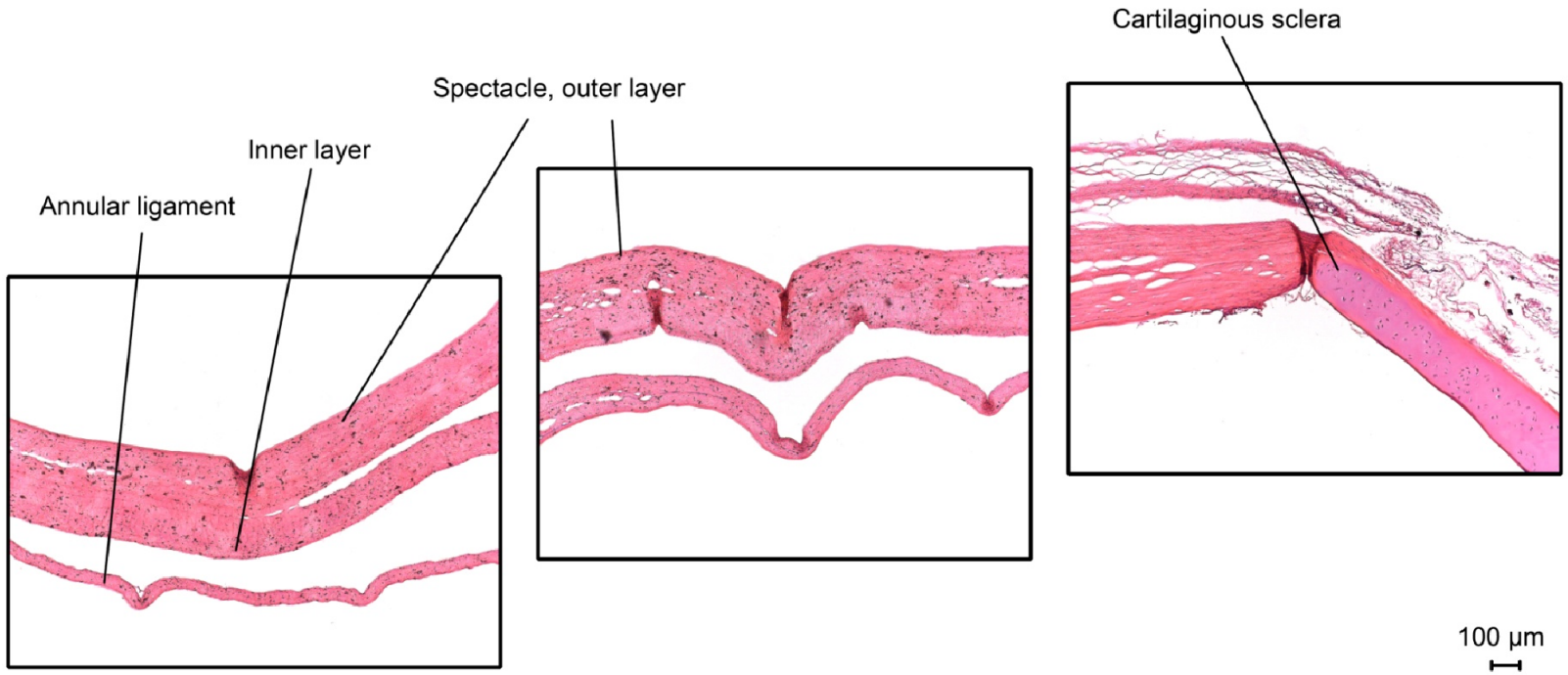

Figure 4.9. The hake cornea. Cornea is divided into two layers: outer layer (dermal cornea) and inner layer (scleral cornea) – both are visible in the picture. The outer layer – spectacle is attached to the scleral cornea. The picture shows also the cartilaginous sclera at the edge of the cornea, and the annular ligament appearing as a third layer of the cornea.

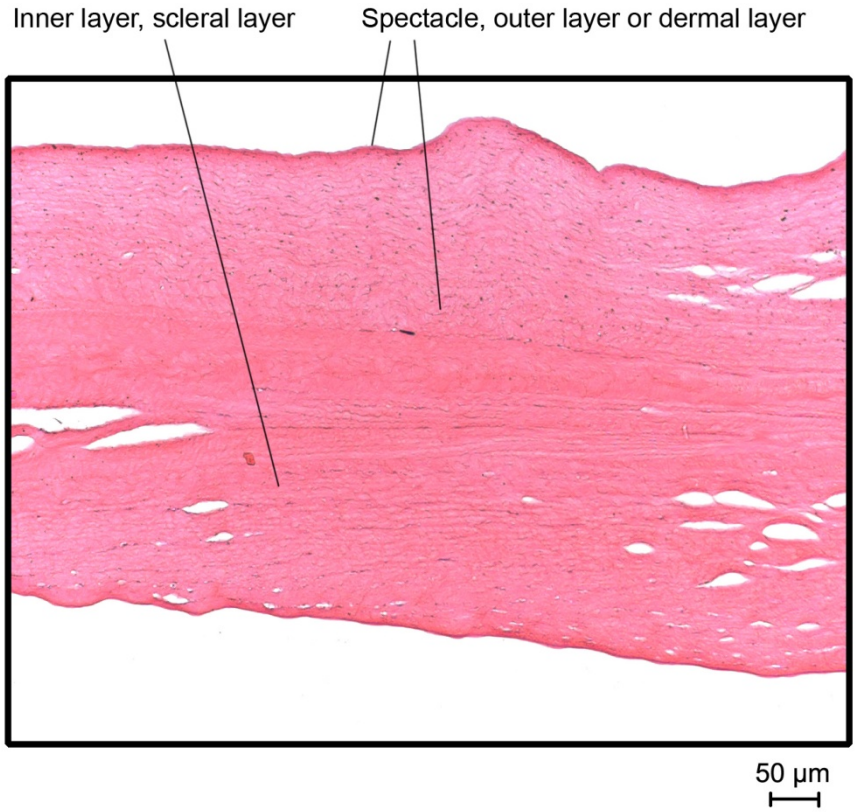

Figure 4.10. The hake cornea (the close-up). In the picture there is well seen the division between two corneal layers: outer and internal layer.

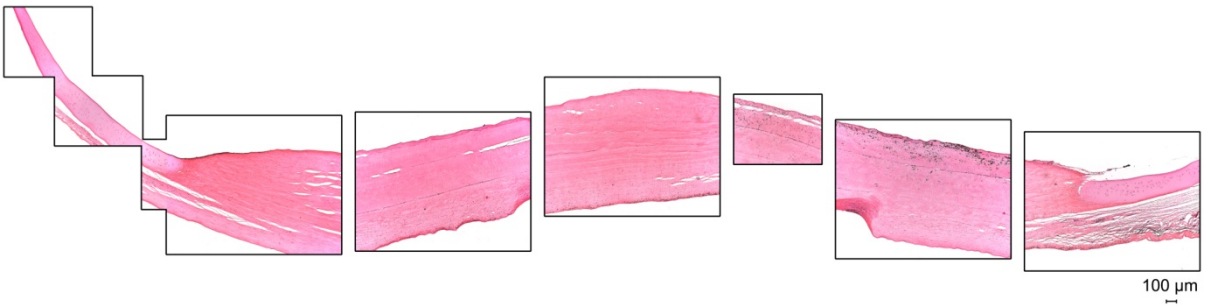

Figure 4.11. The hake cornea. The general view showing the basis cross section through the whole tissue.

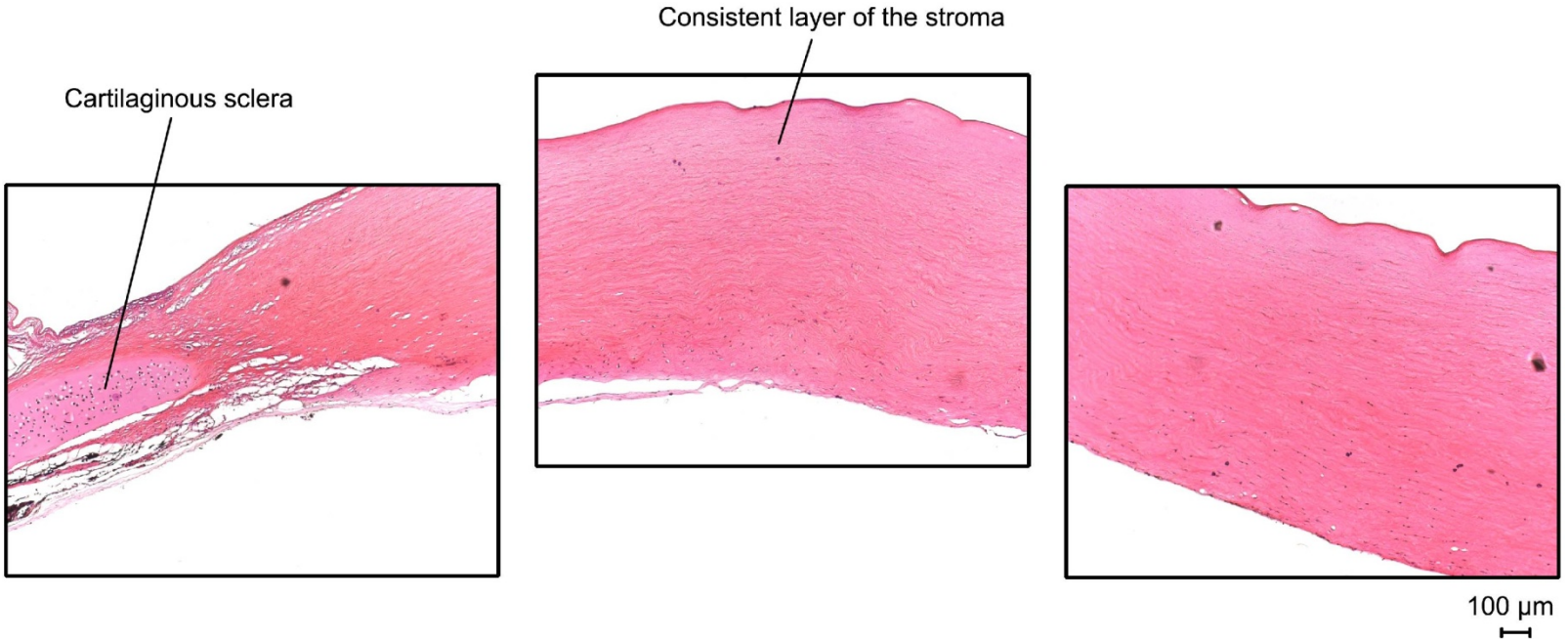

Figure 4.12. The salmon cornea. The tissue is consistent with no distinguished separate layers, the spectacle is detached from the cornea (it is not visible under microscope). The picture shows the cartilaginous sclera at the edge of the cornea.

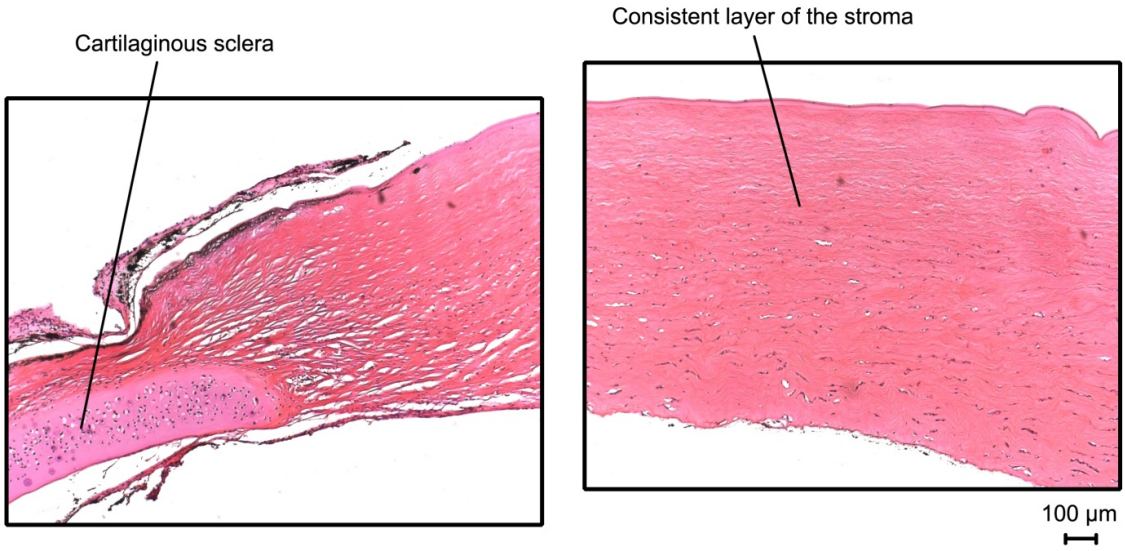

Figure 4.13. The salmon cornea. On the picture there is very well seen the homogenous structure of the tissue and the cartilaginous sclera at the edge of the cornea.

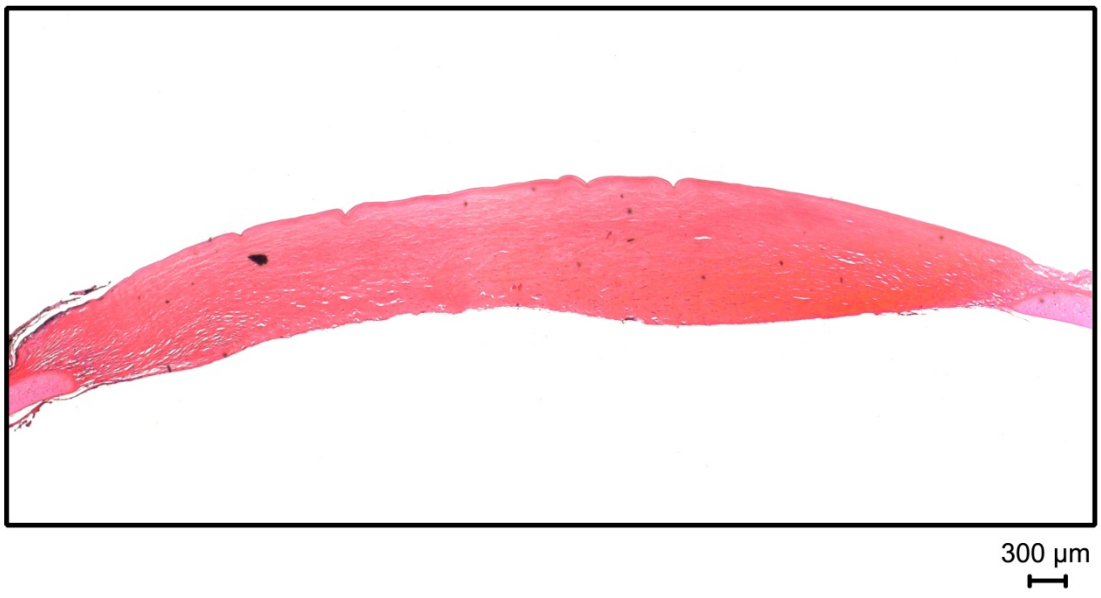

Figure 4.14. The general view of the salmon cornea.

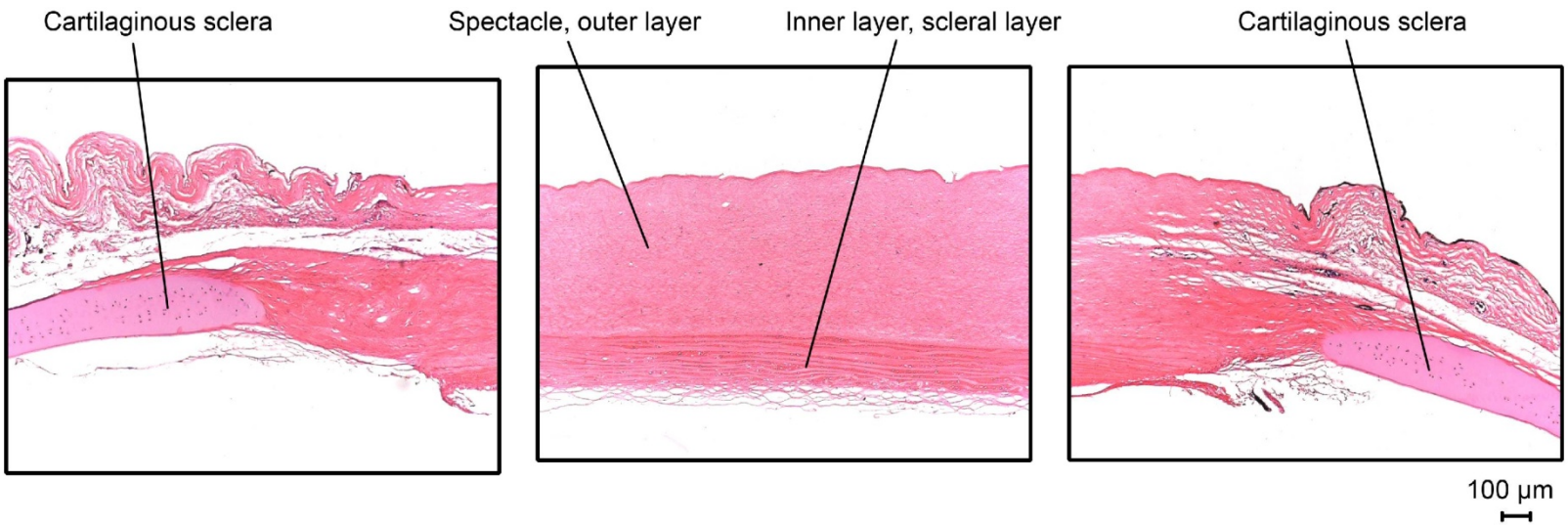

Figure 4.15. The picture showing the seabass cornea with two distinguished separate layers: the outer layer – spectacle and the inner layer. The spectacle is fused (attached) to the sclera cornea hence there are two clearly visible separate layers.On both sides is visible cartilaginous sclera.

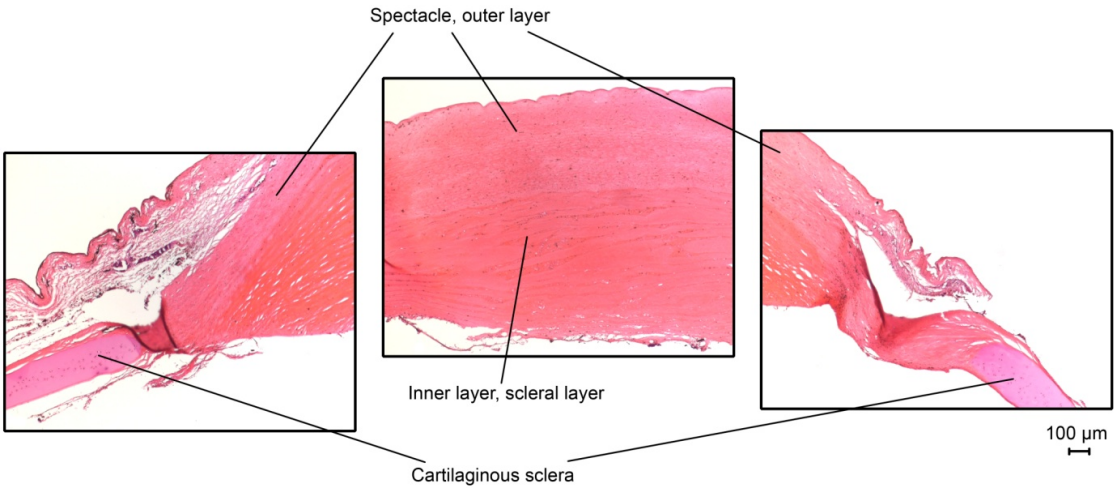

Figure 4.16. The seabass cornea with all the structures described in the picture.

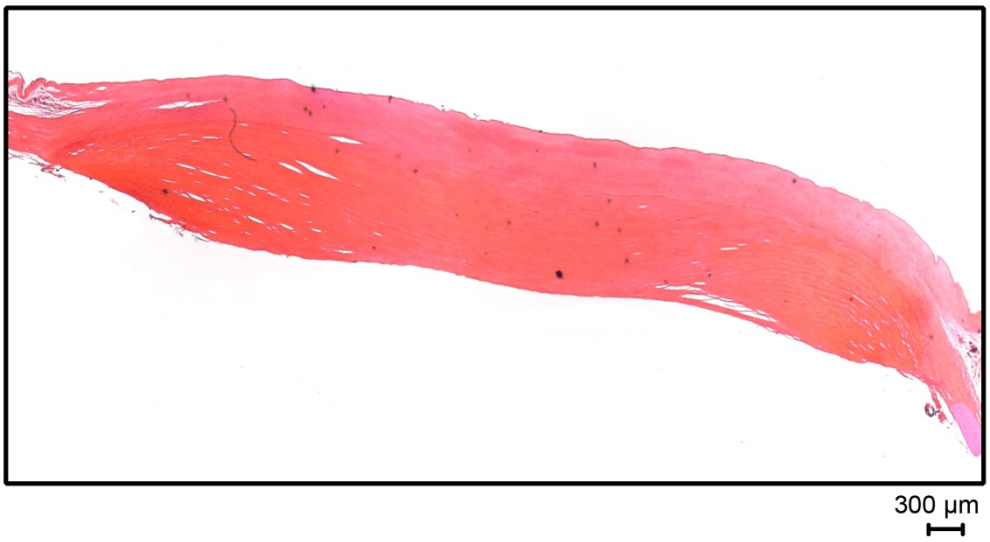

Figure 4.17. The general view of the seabass cornea.

In most of the tissues there is no epithelium which could be explained by the fact that this outer layer of the whole cornea is usually lost before the fish is bought at the market. Furthermore the epithelium of deep sea fishes is usually lost during formalin processing (Munk, 1965). Bowman's membrane is seen as the first part of the whole fish cornea. The outer layer, when visible (attached to the scleral cornea), is not very dense, compared to the inner layer which is more tight. Its fibres are compact and easy to dissociate. Fig. 4.10 shows many places where fibres are falling apart. The other difference between those two layers is that in the outer part many of the nuclei are seen, indicating that this layer consists of keratocytes that produce collagen fibres. It is known that the inner layer is continuous with the sclera; it joins the sclera in the scleral cartilage. On some of the pictures taken from the chord of the cornea (e.g. Fig. 4.9), remains of the annular ligament are still present. The annular ligament is thin in the centre and gets thicker by the edge of the scleral cornea. The posterior cell monolayer of cornea is well shown on Fig. 4.10.

4.4.2 High-angle results

Because of the lack of the beam time at the Diamond Light Source, the high-angle data was taken only for three of the fish species: hake, salmon and seabass. X-ray patterns were collected from the left and right eye of each species. During dissection the cornea was marked to indicate the nasal and temporal side of the tissue (as shown in Fig. 4.18).

For each of the corneas (right eye – R, left eye – L) the total, aligned and beta graphs were created, as well as the polar plot maps and these are shown in Figures 4.19 to 4.21. As outlined in chapter 2: the total scattering shows the integrated scatter around the intermolecular reflection; the aligned scattering means the scatter was only from collagen fibrils which are aligned in preferred orientation; and the beta scattering shows the ratio of scattering (aligned scatter/total scatter), and indicates what fraction of the

collagen is aligned in predominant directions (the higher the number, the more highly is collagen aligned).

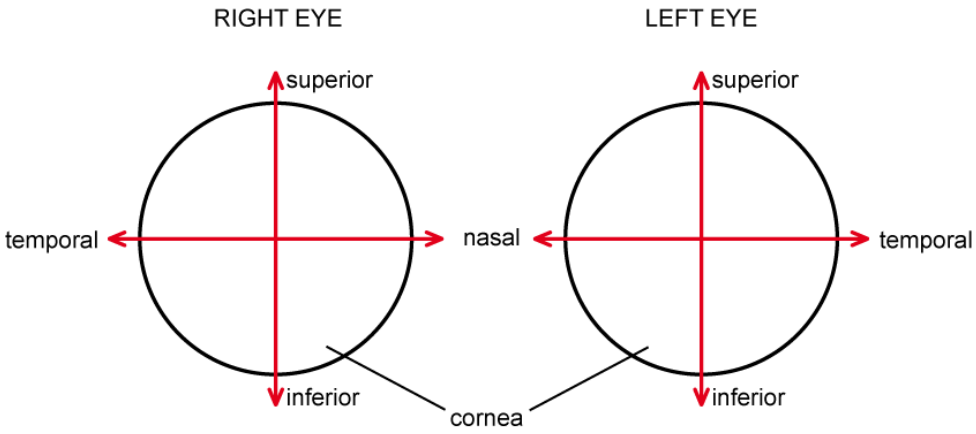

Figure 4.18. A diagram displaying how the features on the graphs from the high-angle x-ray pattern correspond to the position in the fish cornea.

Figure 4.19 shows the high-angle x-ray results from the hake cornea. The feature seen in the middle of the cornea on all of the graphs for hake seems to be only a fold in the tissue. Looking at the graphs it is clear that the tissue is relatively uniform until the limbus. In this area the collagen fibres create something like the annulus in human cornea. This is expressed by the blue ring going in some distance in circumference of the cornea on Fig 4.19a and b and the red/black ring on Fig. 4.19c. According to Fig. 4.19c over 80% of the collagen is going in the same direction in parts of this structure. Notice the abrupt change in orientation from predominantly vertical lamella orientation in the cornea to a circumferential orientation at the limbus (Fig 4.19d). This suggests that the patterns arise from two separate structures.

The salmon high-angle x-ray pattern displayed on Fig. 4.20 shows a very symmetrical collagen profile, especially well seen on Fig. 4.20c (beta scattering). These two graphs coming from the left and the right eye are like mirror images, displaying the collagen density on the opposite sites of cornea of each of the eye. The graphs from total scattering and aligned scattering of the salmon (Fig. 4.20a, b) demonstrate

considerably less scattering, and therefore less collagen in the centre of the cornea which is related to the thickness of this part of the tissue. Less collagen density means thinner cornea in the centre. Collagen fibres are going equally in different directions, getting thicker towards the end. Collagen orientation in the salmon (Fig. 4.20d) appears to be more circular except at the very centre of the cornea. The limbal annulus is narrow and well defined. In the peripheral tissue studied, the lamellae take on an almost radial arrangement.

Seabass displays the least distinct features compared to the hake and the salmon corneas. Figures 4.21a and b show that the annulus in this species in not as well distinguished and strong as it is in hake cornea. The annulus is seen at the top and the bottom of the cornea and not on both sides as it is in hake. The centre of the cornea is thin, getting thicker towards the limbus and the sclera. The vector polar plots show that the orientation of the collagen fibrils is circular through the cornea and adjacent sclera.

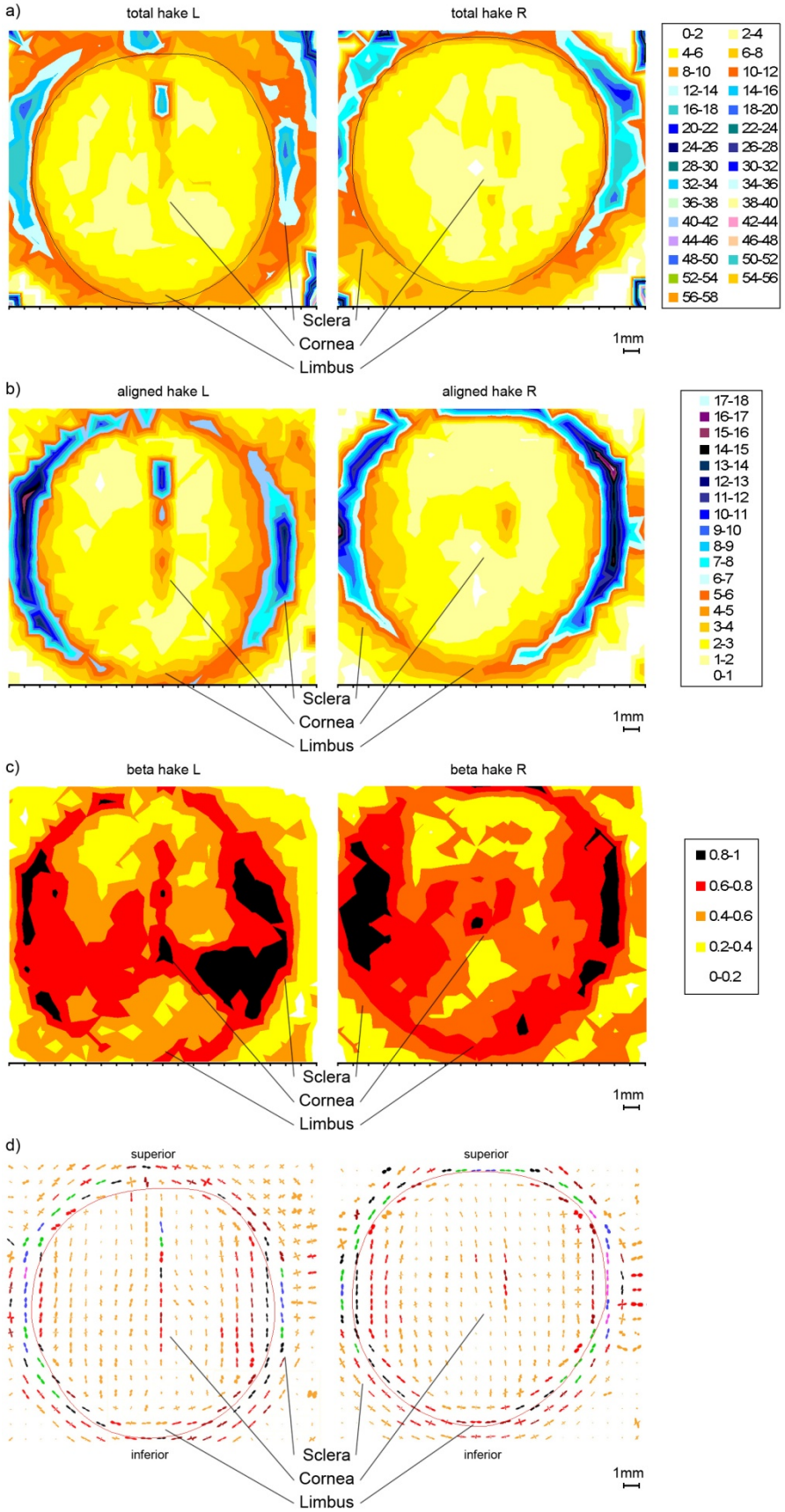

Figure 4.19. The graphs showing: **a)** total, **b)** aligned, and **c)** beta scatter, **d)** vector polar plot of the hake cornea (the annulus is marked as the red line around the cornea). Picture: a, b and c has also the scale of density shown in the key.

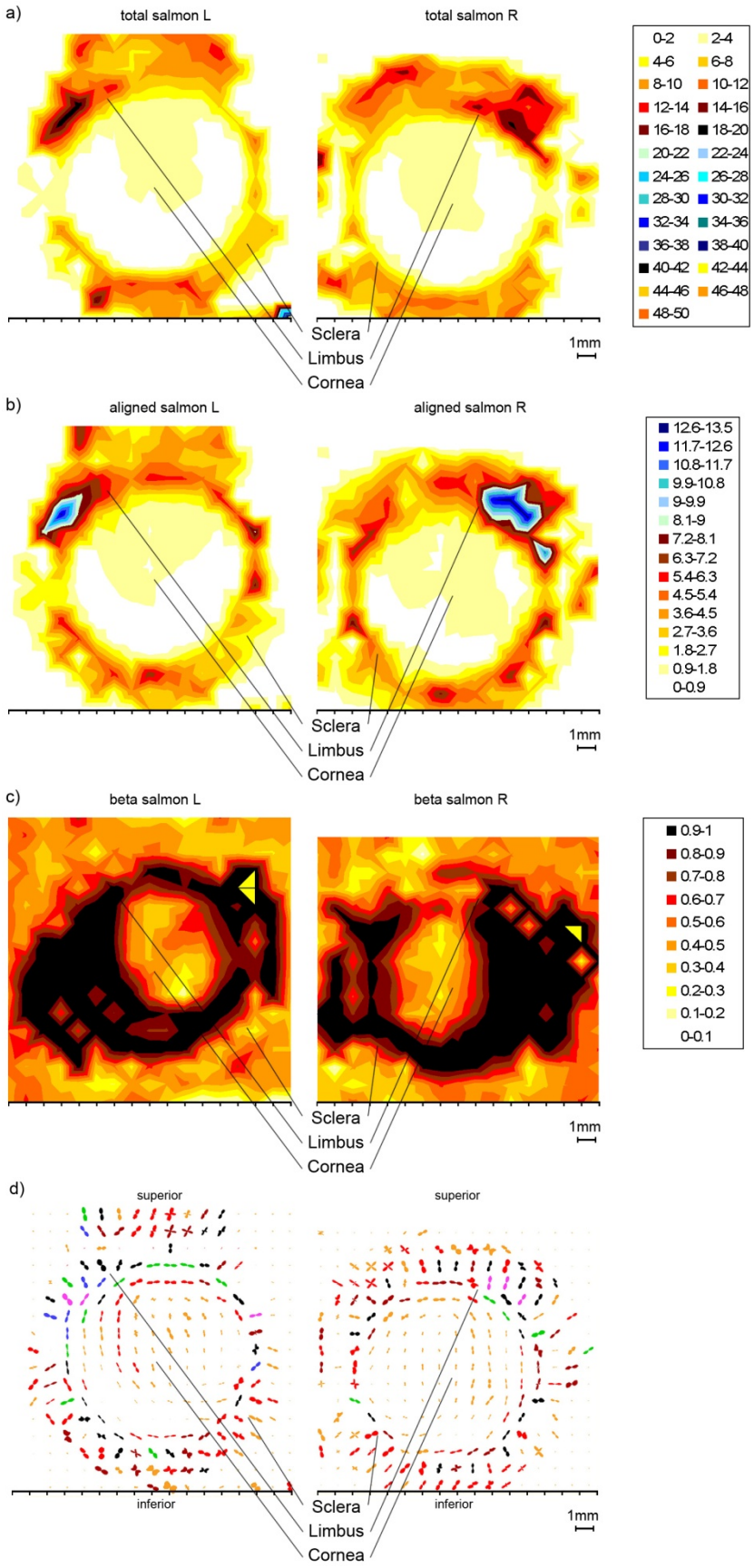

Figure 4.20. The graphs showing: **a)** total; **b)** aligned; and **c)** beta scatter; **d)** vector polar plot of the salmon cornea. Picture: a, b and c has also the scale of density shown in the key.

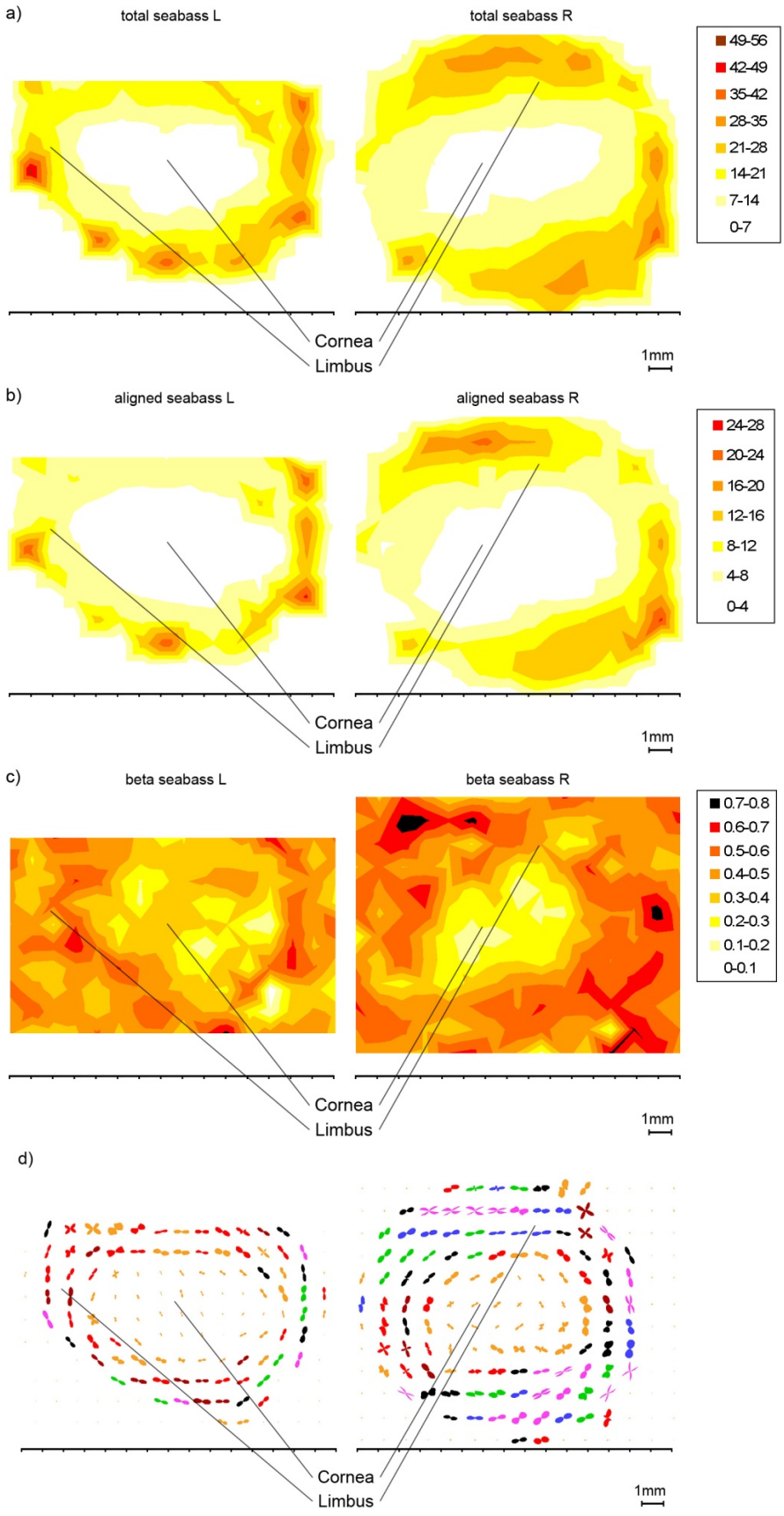

Figure 4.21. The graphs showing: **a)** total; **b)** aligned; and **c)** beta scatter, **d)** vector polar plot of the seabass cornea. Picture: a, b and c has also the scale of density shown in the key.

4.4.3. Low-angle results

The low-angle x-ray pattern was obtained only for two of the four species: mackerel and salmon. This was because of the lack of available beam time as was the case with the high-angle x-ray data. Figures: 4.22 to 4.23 show collagen fibril diameter and interfibrillar spacing of the left and the right cornea of these two species.

Data collected for mackerel and salmon indicate that left and right eyes seem to be mirror images of one another. This is obvious for the mackerel fibril diameters and interfibrillar spacings (Fig. 4.22a, b). The interfibrillar spacing (4.22a) is high at the beginning (in the nasal part), goes almost regularly across the centre and increases sharply towards the other end (the temporal part). The same tendency is seen in Fig. 4.22b which shows the collagen fibril diameters. The salmon displays similar features, but only with reference to the fibril diameter (Fig. 4.23a). The interfibrillar spacing does not have very strong position dependence going from one edge to the other (along the nasal-temporal transect). It is more regular and remains more or less constant across the whole cornea. It increases marginally but only slightly towards both ends: nasal and temporal.

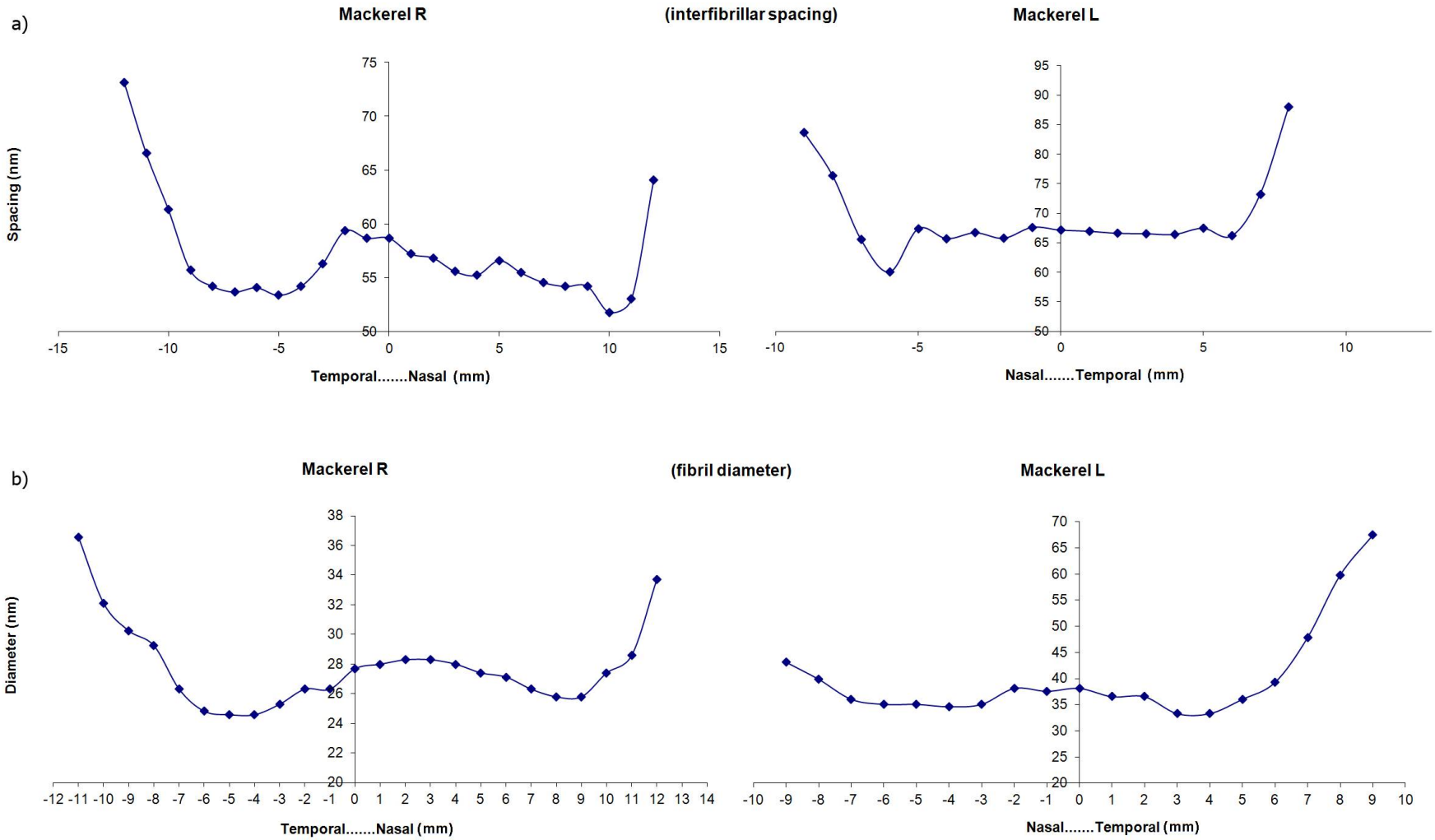

Figure 4.22. Two graphs showing results from low-angle x-ray scatter: a) interfibrillar spacing, b) fibril diameter of mackerel cornea. Pictures indicate the results for left and right eye.

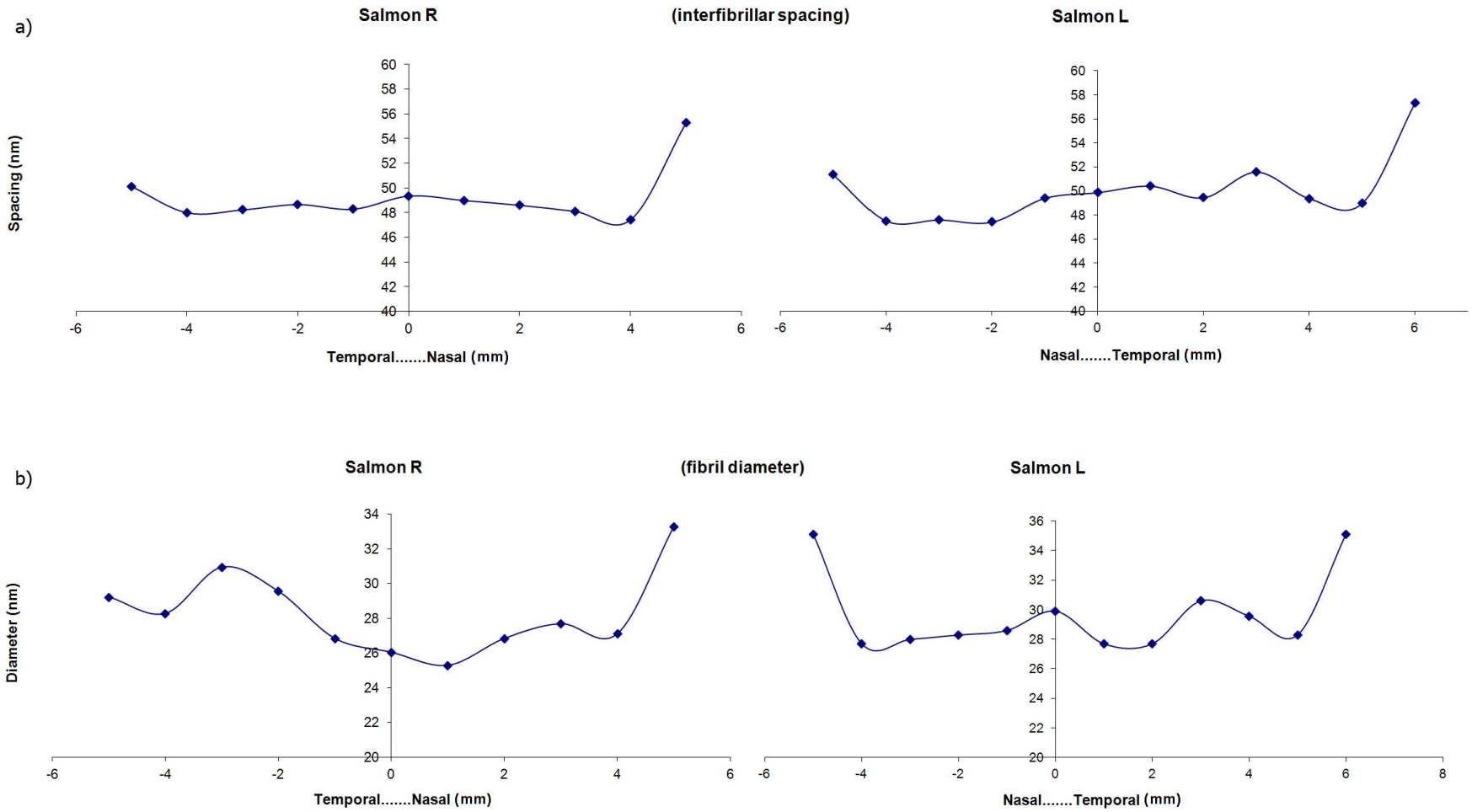

Figure 4.23. Two graphs showing results from low-angle x-ray scatter: a) interfibrillar spacing, b) fibril diameter of salmon cornea. Pictures indicate the results for left and right eye.

4.4.3 Spectrophotometry

Figures: 4.24a, 4.24b, and 4.24c show variation in transmission as a function of wavelength at different positions across three different species of fish corneas. The data was collected only from the left eyes and each plot is the average of several corneas: hake – 3 corneas, mackerel – 4 corneas, and salmon – 3 corneas. These graphs demonstrate that, in general, transmission increases as a function of wavelength at most points in the fish cornea, except, interestingly near one side (the nasal side). This trend is seen for each of the three fish species.

The apparently asymmetrical behaviour of transmission as a function of position can be seen more clearly by plotting transmission as a function of position for a given wavelength (550nm was chosen as it is near the centre of the visible spectrum). The results are presented in Figures: 4.25a, 4.25b, and 4.25c. Because the optical centre of the cornea could not always be made to coincide exactly with the geometrical centre of the cell, each set of data was shifted laterally by up to 2mm, using a least squares procedure to optimise the superposition of data from each sample within a species. This allowed the zero displacement points to be aligned more accurately in the graphs.

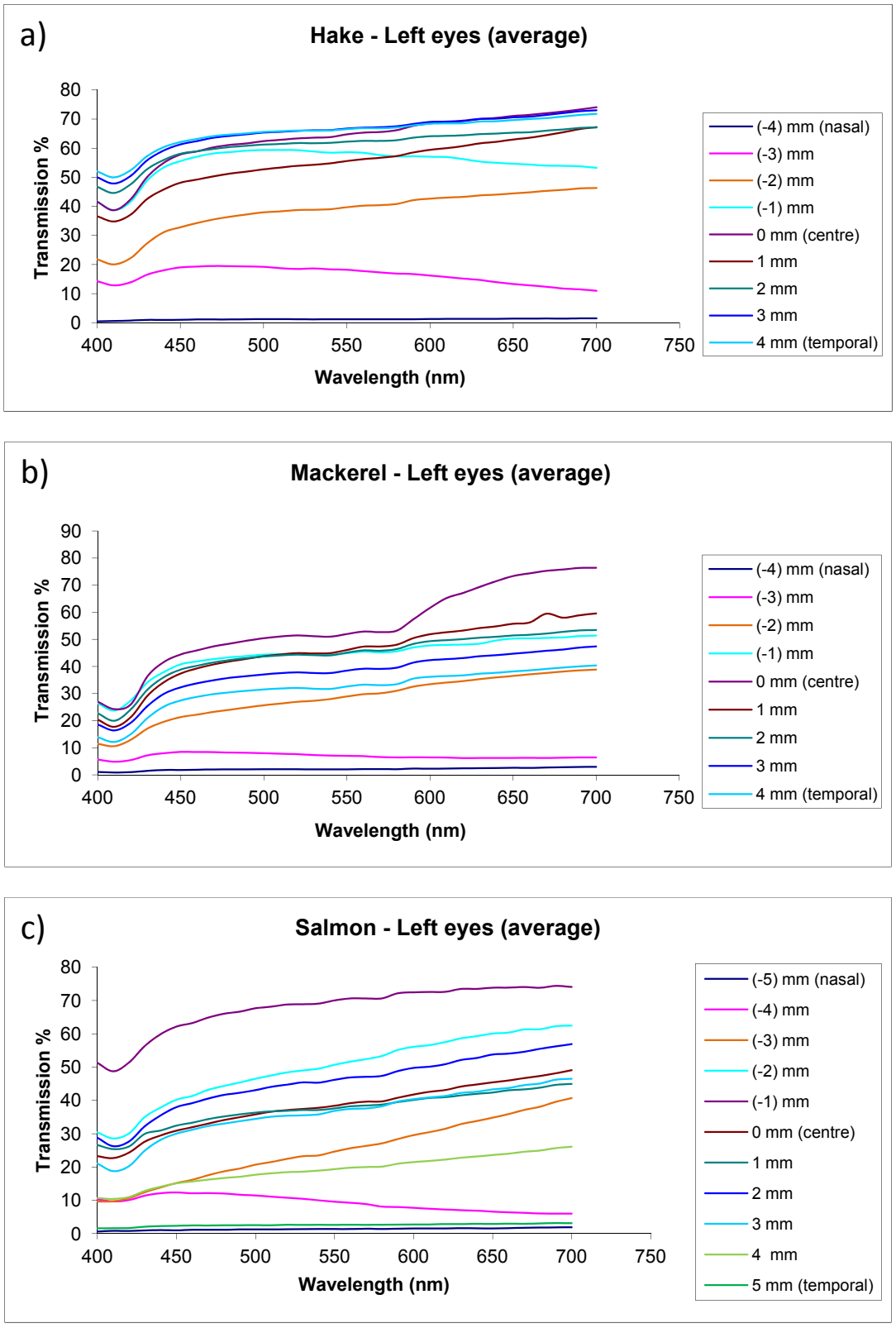

Figure 4.24. The graphs showing the average variation in transmission as a function of the wavelength, at different positions across the fish corneas from the left eye in: **a)** hake; **b)** mackerel; and **c)** salmon. The key presents the position of collected data from the: nasal, centre, and the temporal part of the cornea.

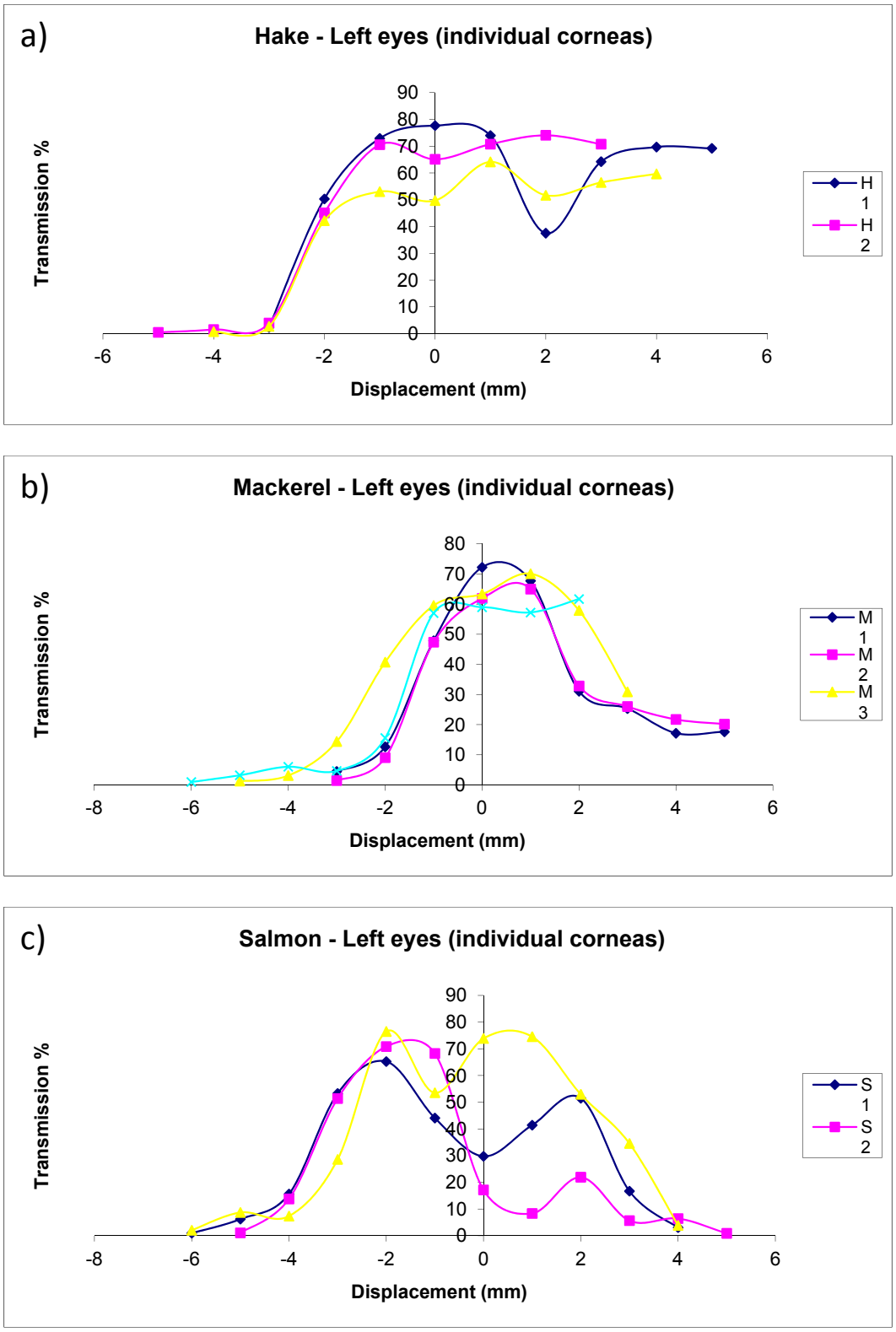

Figure 4.25. The graphs showing the variation in transmission by plotting it as a function of position for a given wavelength (550nm was chosen as it is near the centre of the visible spectrum) across the fish corneas from the left eye in: **a)** hake; **b)** mackerel; and **c)** salmon. The key presents individual corneas: 3 hake's specimens, 4 mackerel's, and 3 salmon's. The values on the horizontal axis mean as follows: minus – nasal, 0 – around centre, and plus – temporal side of the cornea.

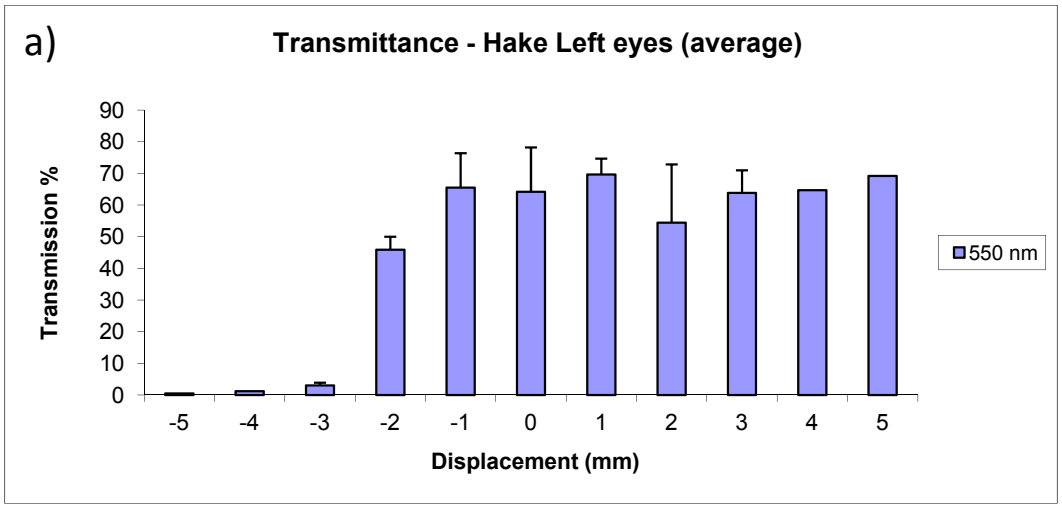

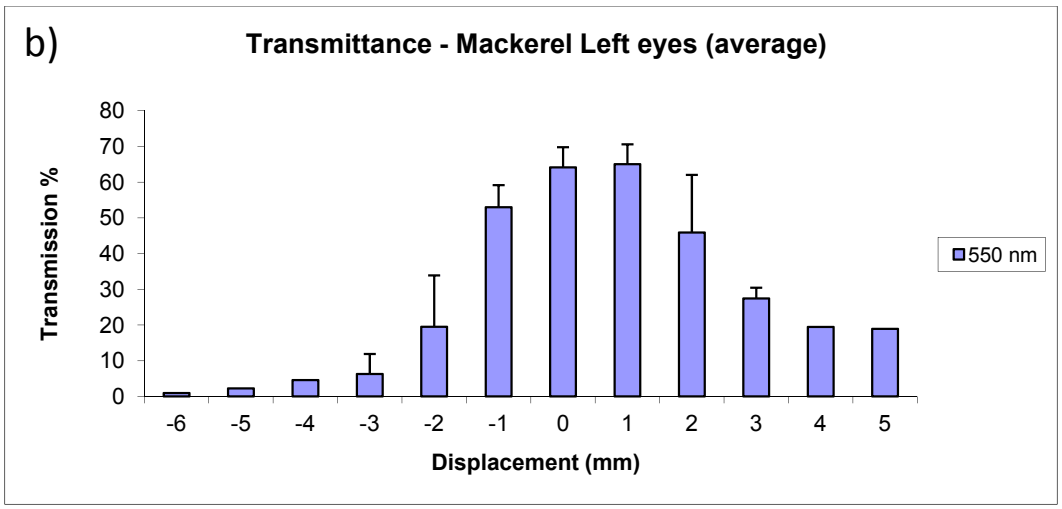

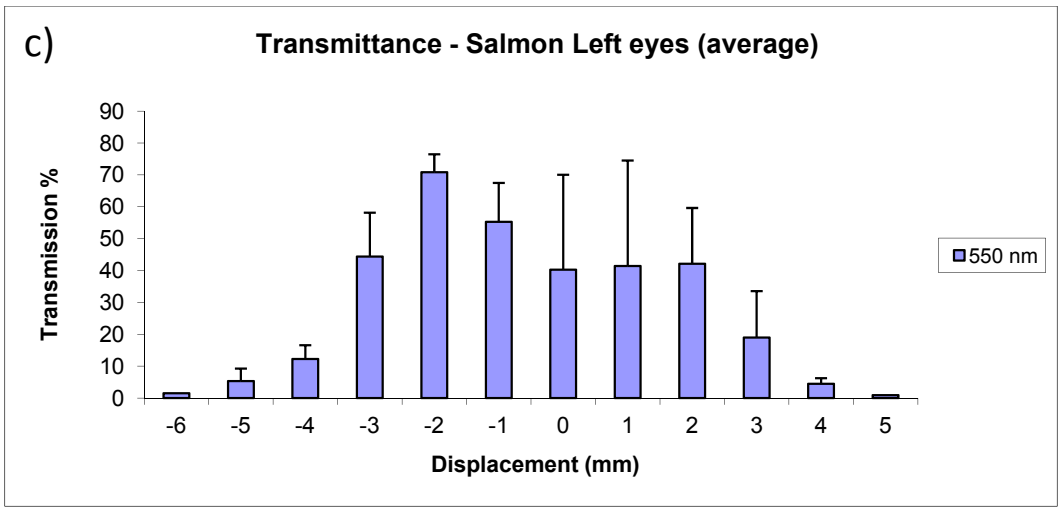

Figure 4.26. The graphs showing the average variations in transmittance as a function of distance from the centre of the cornea and the transmission of light (as a percentage). The wavelength chosen to calculate these variations is seen in the key (550nm was chosen as it is near the centre of the visible spectrum). The values on the horizontal axis mean as follows: minus – nasal, 0 – around centre, and plus – temporal side of the cornea.

The final results are shown on figure 4.26a, 4.26b, and 4.26c. These are the variations in transmittance as a function of distance from the centre of the cornea and the transmission of light (as a percentage). The hake data seen on Fig. 4.26a shows that the exact position of the optical centre of the cornea can be shifted slightly to the right as the transmission increases gradually from the left to the right on this graph. The lowest transmission appears to be between -5 and -3 and there is no similar tendency on the other side of the graph, as it is clear on the graphs presenting mackerel and salmon data: 4.26b and 4.26c. It means that the optical centre of the hake data can be expected to appear just between 2 and 5 position of displacement. This could be consequent upon the size of the hake cornea and the size of the chamber. As the hake cornea is bigger than the mackerel and salmon, the exact optical centre could be moved slightly in relation to the geometric centre of the cell, giving above results. Figure 4.26b and 4.26c show that the biggest transmission (higher transparency) is almost in the optical centre as we could assume from the structure of the cornea. The cornea is mostly transparent in the centre giving enough light for the animal to see, and gets less transparent as it reaches the sclera.

4.5 Discussion

The study of the fish cornea and comparison of this knowledge with the human cornea (which has been extensively studied) should help us learn about the relationship between corneal structure and function. Taking into consideration two different animals' tissues we have discovered as many similarities as differences. These differences mainly arise from the fact that the fish cornea is in direct contact with water and the human cornea is in touch with air. Hence there are different demands on the cornea. In aerial vertebrates, among them human, cornea is mostly responsible for the refractive power of the eye. In water vertebrates like fish, however, this task is moved to

the other elements in the eye, as the refractive indexes of their corneas and the water are similar (more details are described by Collin and Collin, 2006).

The main function of the human cornea is to transmit light to the retina (to be transparent). This is achieved thanks to the collagen fibrils which are uniformly narrow and regularly spaced within the corneal stroma (Gyi et al., 1988). The other feature of the cornea is to be strong in order to protect the eye contents from damage from the outside world. That is achieved by the large amounts of collagen stacked within packed lamellae. Finally the cornea should be precisely curved for refraction, and the stable shape of the cornea must be maintained during eye movement. Curvature of the cornea is achieved by the collagen alignment in all directions and there is also a preferential orientation toward the direction of the major rectus muscles (Hayes et al., 2007). These features of the tissue which characterise the human cornea are also common to the fish cornea but differ in the ways of reaching each goal. The cornea of the fish eye is transparent for the same reason as the human one and the structure of them demand the optimization between transparency and strength.

The fish cornea is thin in the centre (about half that of the human cornea) and getting thicker by the edge of the scleral part (Smelser, 1962). The differences between human and fish cornea from our experiments is that in the fish cornea apart from the original epithelium there is another layer of corneal collagen called the spectacle. This element helps the cornea to protect the eye especially in the aquatic environment.

The first obvious difference between the human and the fish cornea appeared at the beginning of our studies as we prepared the tissue for the experiment. The three basic properties that are distinctive from each other are: size, thickness and shape. The adult human cornea is about 11mm in diameter and in fish this parameter could be very different. As we describe above it varies in fish from our experiment between 10-12mm

in mackerel, salmon, seabass and around 15mm in hake. The thickness of the human cornea is about 0.5mm in the centre and its shape is spherical near the visual axis. The fish cornea is about half that of the human one. The fish cornea is more flat and the eye in general has a streamlined shape.

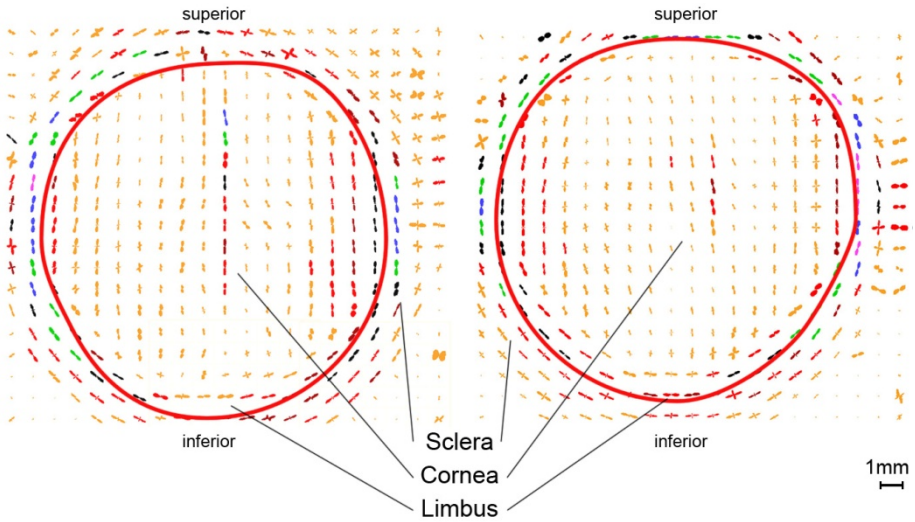

Figure 4.27. Vector polar plot of the hake cornea (the annulus is marked as the red line around the cornea).

The wide-angle x-ray pattern confirmed the observation from the light microscope. More specifically, the thin cornea in the centre of the tissue was also observed in the x-ray examination. As was mentioned above, the lower collagen density in the central part of the cornea relates to the thinning of this region. What is more, our results from wide-angle x-ray scatter showed that the fish cornea also possesses the annulus like the human cornea (Fig. 4.27). In the human, the annulus was supposed to be related to maintaining the change in curvature between the cornea and the sclera (Aghamohammadzadeh et al., 2004; Boote et al., 2004; Hayes et al., 2007; Newton and Meek, 1998). However, this change in curvature does not occur in the fish that we have examined, casting some doubt on this speculation. It could be that the annulus acts as an anchor for collagen fibres from the extraocular muscles, helping to prevent the tension exerted by these muscles from distorting the central cornea during eye movements.

The arrangement of the collagen lamellae in the central cornea in the human is preferentially inferior-superior and nasal-temporal. This preferentially aligned collagen is considered to give the eye additional mechanical reinforcement during eye movements (Daxer and Fratzl, 1997). As Hayes et al. (2007) stated the appearance of four extraocular rectus muscles is a common feature to all mammalian species, among them: human, marmosets, horses, pigs, cows, mice and rabbits. They could obviously vary in terms of their position, width and length. The position mentioned above of four rectus muscles is the same in the fish eye (Nicol and Somiya, 1989). However, there was variation in the arrangement of the lamellae; animals with high visual acuity showed the orthogonal orientation as in the human, animals with lower acuity such as pigs, tended to show a uniaxial orientation, and animals with low visual acuity (like mice) had a more circular arrangement. In the present study, the fish species also showed some variation; the hake (Fig. 4.19 and Fig. 4.28) showed a uniaxial (vertical) arrangement whereas the seabass and the salmon (Fig. 4.20 and Fig. 4.21) showed a more circular arrangement. The hake, as an active predator, would require a higher visual acuity, with more precise eye movements, than the other two species, which may explain the different collagen organisation in this species (Fig. 4.28).

In the human cornea, Boote et al., (2003) observered that fibril spacing and diameter increased in the peripheral cornea. Larger fibrils would strengthen the tissue at the expense of transparency. We have obtained the same results from our small-angle x-ray scatter for fish cornea. Fibrils in the central cornea are narrower and more closely spaced than those in the periphery. The combination of a thin cornea and narrow fibrils would lead to higher transparency. In the two species studied (mackerel and salmon) the collagen diameter curves display an inverse correlation with the transparency from spectrophotometry data (described in section 4.4.4). Combining these results with the

histology, which showed a thinner central cornea, explains why the central fish cornea allows the light a good passage into the fish eye. This is true except for the hake eye where the transparency does not drop off on one side. It is because the hake is bigger than the others and the measurements did not get to the edge of the cornea.

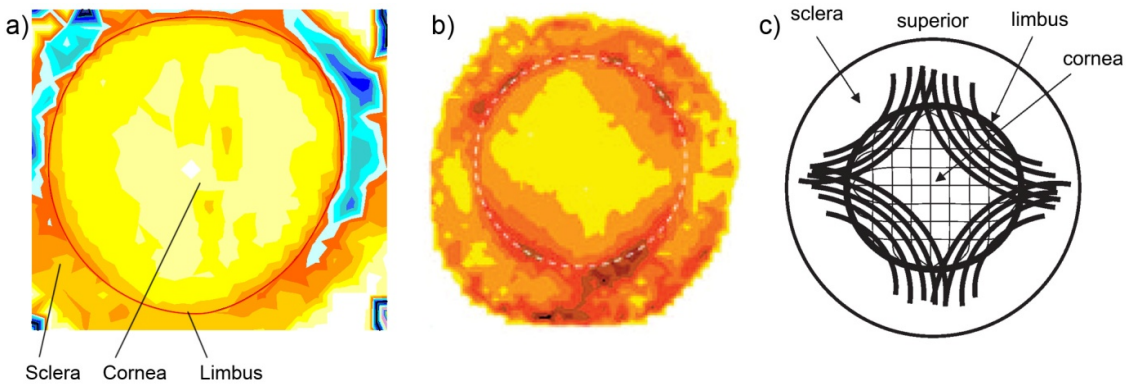

Figure 4.28. Diagrams showing the right eye of: **a)** fish – aligned vector polar plot of hake; **b)** aligned vector polar plot of human (after Boote et al., 2006).; and **c)** a model of theoretical arrangement of collagen aligned in predominant directions in human cornea (after Boote et al., 2006). The rhombic shape does not occur in the fish eye as it does not need as high visual acuity as terrestrial eyes (this shape seems to be a feature of the terrestrial eyes). They have also the suturing lamellae which are thought to help flatten the peripheral cornea to make a smoother transition with the sclera (Aghamohammadzadeh et al., 2004). This act is not necessary in the fish cornea.

4.6 Conclusion

Comparing these two species: human and fish we have discovered many similarities. To begin with the most distinct feature from our results, we have found that both human and fish have the annulus. This feature arises from the specific lamellar directions in the central cornea: in human it is inferior-superior and nasal-temporal (Daxer and Fratzl, 1997). In human this component of the eye helps to maintain the proper curvature in the place where cornea meets the sclera (Aghamohammadzadeh et al., 2004; Boote et al., 2004; Hayes et al., 2007; Newton and Meek, 1998). What is more, the cornea is thin in the centre and getting thicker towards the periphery in human as well as in the fish cornea. The other thing which changes towards the edge of the cornea is increase in diameter and spacing between fibrils (the main feature that affects the transparency).

This is observed in the cornea of human and fish. Following on from this both species demonstrate a decrease in transparency going peripherally. There is also distinct left/right symmetry in the structure of corneal tissue in the human and also in the fish.

Searching for the similarities which confirmed that the structure of the fish and the human cornea are alike, we have found some differences as well. The most important and most distinctive feature distinguishes these two species is the spectacle which is typical only in the fish cornea as it helps to protect the eye from the outer environment. What we have said before, the annulus is responsible for corneal curvature, while there is distinct difference in curvature between human and fish. The fish cornea is more flat and human cornea is more spherical in shape. The other difference that we have observed is that there are no suturing lamellae in the fish eye. They are responsible for the flattening of the peripheral cornea (Aghamohammadzadeh et al., 2004) and are not important in the fish. What is more, the variation in the arrangement of the lamellae in both species is different: in human is orthogonal, and in the fish is more circular (seabass, salmon). The hake cornea (as it is a predator and requires higher visual acuity) is unaxial (which is something between orthogonal and circular). The fish cornea also possesses more microprojections which are responsible for the flow of the nutrients and oxygen.

Both corneas (human and fish) require the special structure to maintain transparency. The right thickness and fibril diameters are responsible for that fact. The shape of the cornea should answer the demands of the environment to remain stable during the eye movements. It is spherical in human as they are terrestrial animals. The lamellar directions is the central cornea is inferior-superior and nasal-temporal. Human cornea also possesses the suturing lamellae which additionally flatten the cornea making a good transition with the sclera (Aghamohammadzadeh et al., 2004). The fish cornea is

flat anyway as it is immersed in the water environment and demands different shape that is opposed to the water flow.

4.7 Future study

As we examined only small group of the fish corneas (and collected small amount of data), there is definitely need to obtain a lot more to look closely at the relationship between transparency and strength in this particular tissue. There is also need to collect more specimens from which we could understand more clearly the structure and function of the fish cornea and then compare them to human. The interfibrillar spacing (and consequently the corneal transparency) depends on water and the glycosaminoglycans in surrounding matrix. The future study would base on the experiments geared towards collagen/glycosaminogycans interaction. And then in the more distant future our study could include an electron microscope study of the fish stroma.

5 A study of Climatic Droplet Keratopathy in guinea pigs corneas as a model of human disease

5.1 Introduction

Climatic Droplet Keratopathy (CDK) is an acquired degenerative disease of the cornea which is diagnosed as opalescence and haziness in the superficial corneal layers. It is characterised by the presence of homogenous translucent yellow globular droplets (deposits) of different sizes. This condition was found mainly in some rural communities around the world such as: Patagonia, Argentina, North Africa, India (Punjab) and the Red Sea region. The effect of living in constantly extreme conditions may lead to problems involving serious visual deterioration.

Climatic Droplet Keratopathy is considered a corneal disorder which is related to environmental factors found in hot and cold climates. These factors are mostly: constant winds, high solar ultraviolet exposure (especially UVB) and reflection, lack of shade and clouds, and low humidity (Menegay et al., 2008, Urrets-Zavalia et al., 2007). Small injuries of the cornea caused by particles of dust and sand brought by the wind can be a significant part of CDK (Menegay, et al., 2008). But the most relevant factor in these conditions seems to be ultraviolet radiations, especially UVB (Wu et al., 2004). As described by Gray et al., (1992) the shorter the wavelength the more dramatic effects occur in the cornea and the skin, as they are directly exposed to the sunlight. It is known that the wavelength range of UVB radiation is 315nm-280nm. The wavelength of light absorbed by the human cornea is approximately 295nm but the highest absorption is observed at 288nm. Thus the UVB radiation is the most destructive wavelength to the eye. A high dose of UV can be received by the eye when the light is reflected from sand or snow covering the ground. It has been suggested that lowering the risk of UV exposure by up to 50% was obtained by protecting the eye with a shade such as a

peaked cap (Gray et al., 1992). The state of disease naturally depends on several factors such as: intensity and duration of exposure to radiation, size of exposed area, and the wavelength. CDK is found mainly in men over 40 years old who live in specific rural communities in many countries mentioned above (Urrets-Zavalia et al., 2006).

In the literature (Gray et al., 1992, Menegay et al., 2008, Urrets-Zavalia et al., 2006, 2007, Shidar et al., 2000) this disease is characterised by three different stages. Grade 1 (the initial stage or primary CDK) is described as small, almost transparent and multiple deposits located in subepithelial and peripheral cornea, placed close to the temporal and nasal limbus. At this stage there is no other visible corneal pathology. Along with progression of disease (grade 2, secondary CDK), these tiny deposits spread across the eye (along the visual axis) and makes the eye dull. The last stage (grade 3 or conjunctival form) is seen as homogenous, yellow and globular droplets (clusters) of variable sizes, some of them reaching 1mm in diameter (Fig. 5.1).

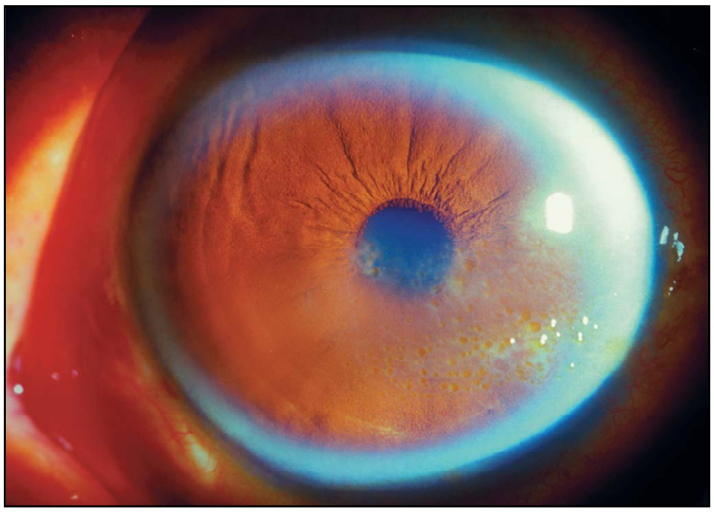

Figure 5.1. Picture showing the last stage (grade 3) of Climatic Droplet Keratopathy with clearly visible haziness in the lower part of the cornea and small yellow droplets spread within the eye (after Urrets-Zavalia et al., 2007).

These golden droplets, typical for the last stage of CDK, were studied and found to contain proteins incorporating: tyrosine, cysteine, cystine and tryptophan (Gray et al. 1992, Shidar et al. 2000). Electron microscopy studies showed that the droplets vary in

size, are approximately circular in shape, are electron-dense and are always smooth and sharp at the edges. The clusters were seen surrounded by basement membrane material with disorganized collagen fibrils around them (Fig. 5.2). As they are found in the anterior stromal cornea, the droplets can cause some changes in the corneal epithelium and Bowman's membrane: disruption and thinning.

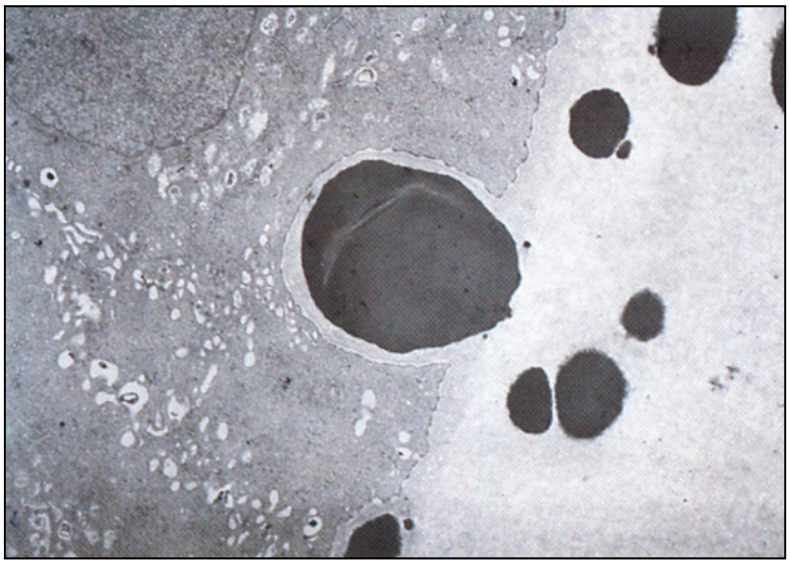

Figure 5.2. Image showing typical droplets found in CDK (3rd grade) surrounded by Bowman's membrane under EM (after Gray et al. 1992).

5.2 Aims and Objectives

A very good model to study Climatic Droplet Keratopathy (and other human ocular disorders: cataracts, retinal disease, and myopia) is the guinea pig cornea because of the similar structure and the same requirements for ascorbic acid as in human (Cafaro et al., 2009). The domestic guinea pig *Cavia porcellus* (also known as the cavy) has no enzyme gulono-lactone oxidase and the animals are unable to synthesize ascorbic acid (ascorbate) or AA), also known as Vitamin C, which is an excellent absorber of UV radiation, especially UVB. Like humans, these animals have to receive their daily intake of ascorbate from diet. Thus guinea pigs have become a more and more popular species to use as experimental animals, especially to search for ocular disorders.

In our study we used four different groups of guinea pigs, with and without ascorbate in the diet, and with and without ultraviolet exposure, to find any significant changes in the external layers of cornea and within Bowman's membrane. Using EM data we investigate the structure of guinea pig corneas and analyse the difference between those groups. Low-angle x-ray data gives us a view of different collagen parameters such as: fibril diameter and interfibrillar spacing (IFS). These measurements are averages throughout the whole thickness of the tissue, and thus highlight any structural changes likely to affect the transparency of the tissue.

5.3 Materials and methods

5.3.1 Sample preparation: guinea pigs

Eight healthy male Albino guinea pigs (bred in Statens Serum Institut, Allerød, in Denmark) were used in our study. They were between 6 and 7 months old. The study was carried out in accordance with the Association for Research in Vision and Ophthalmology (ARVO) Statement for the Use of Animals in Ophthalmic and Vision Research.

The animals were reared by our collaborators at the National University of Cordoba, Argentina. They were kept in pairs in stainless steel cages with wood shavings on the floor for 3 months. The conditions under which the guinea pigs were kept remained constant: a temperature of 23°C and a humidity of 60%. All of the animals were reared on a homemade pellets diet which contained all the required nutrients: alfalfa, soybeans, oats and wheat. The level of vitamin C intake was regulated and served via micro-pipette (a single measured daily dose). Four guinea pigs received the normal recommended dose of Vitamin C which was 2mg/100g body weight/day) and the other four received a low dose of Vitamin C which was 0.07mg/100g body weight/day). All guinea pigs were exposed to the artificial light source from ceiling

lights (36W daylight fluorescent tubes) in a cycle: 12h light/12h dark. However four animals also received additional 40 minute dose of UVB which was 0.12J/cm^2/day).

In the experiment the animals were divided into four different groups: A) the first group was treated with UVB radiation and on a normal dose of ascorbate, B) the second group was also treated with UVB radiation but on low dose of ascorbate, C) the third group was not treated with UVB radiation and was on normal dose of ascorbate, and D) the fourth group was not treated with UVB radiation and was on low dose of ascorbate (Fig. 5.3).

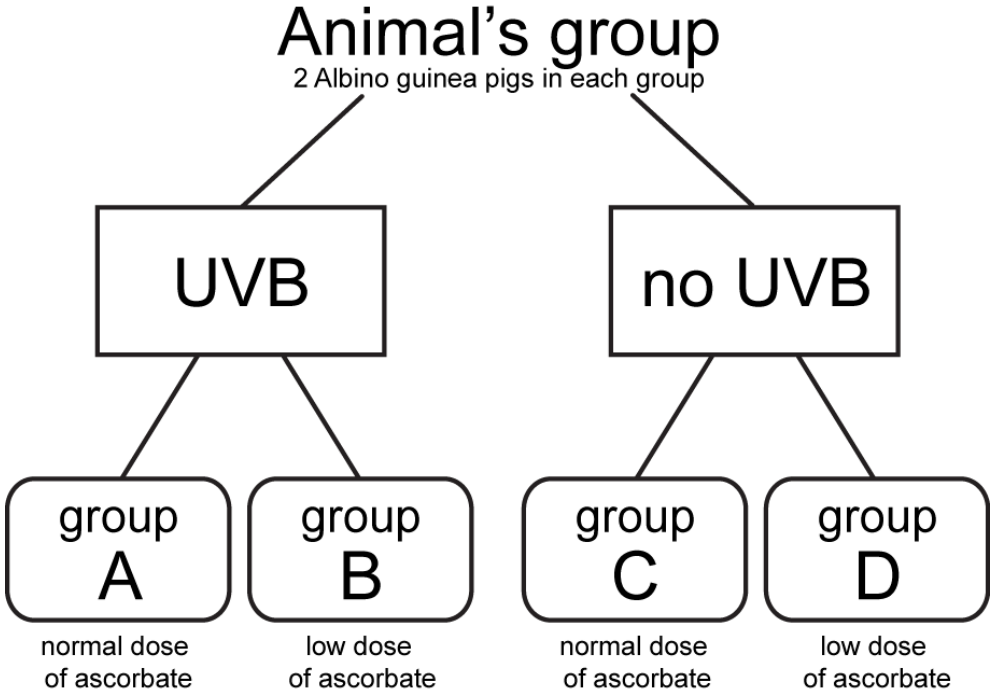

Figure 5.3. Diagram presenting relationship between two different diets and UVB exposure on animals divided into four experimental groups.

After treatment, the guinea pigs were euthanized with an overdose of ketamin. The corneas were removed from each eye with a 2-3mm sclera rim. To mark the superior of the cornea a small suture was placed at the 12 o'clock position in the sclera. Then the corneas were wrapped tightly in a thin plastic film (Ceranwrap), labelled and fozen at -80°C. The frozen corneas were shipped to Cardiff University (Wales, in UK) on dry ice. All together we had 16 corneas for further experiments.

5.3.2 Low-angle x-ray data collection and analysis

Each cornea was defrosted at room temperature and immediately processed to collect the data. Then each cornea was rewrapped in a single layer of Clingfilm and placed in its correct orientation (scleral suture at the 12 o'clock position) in a sealed polymethyl methacrylate chamber with mylar film windows.

Low-angle x-ray scattering data were collected at 1mm intervals for 11 of the 16 corneas (Group A = 3 corneas, Group B = 3 corneas, Group C = 3 corneas, Group D = 2 corneas) on Station I22 at the Diamond Light Source, Oxford, UK. The rest of the corneas were left for EM data collection. The patterns, each resulting from a 5s exposure to a 1Å wavelength x-ray beam with a cross sectional area at the specimen of 0.25 mm x 0.3 mm, were recorded on a RAPID2 detector positioned 6m behind the camera. The system was calibrated against the meridional x-ray reflections arising from the axial 67-nm repeat of collagen in moist rat-tail tendon.

The x-ray scatter patterns were analysed using Unix-based software, statistics and graphics packages (Fit2D, Excel, Statistica Statsoft) to obtain the most important measurements maintaining corneal transparency: fibril diameter, the average Bragg centre to centre collagen fibril separation distance (referred to here as the FSD), and axial D-period of corneal fibrillar collagen (calculated using position of third-order meridional reflection) (for the full method see the paper of Meek and Fullwood, 2001a).

5.3.3 TEM data collection

Four of the 16 corneas were immersed in 2.5% glutaraldehyde/2% paraformaldehyde in 0.1M Sörensen's phosphate buffer at pH 7.4. After 1 hour they were removed and cut into blocks approximately 1 x 5mm x full thickness. The samples were taken from peripheral and central corneal locations. Then these blocks were returned to fixative for another 3 hours. After that time they were dehydrated in ethanol and embedded in

Araldite CY212 epoxy resin. Then after washing and storage in buffer the blocks were postfixed in 1% osmium tetroxide, followed by 0.5% uranyl acetate. Ultrathin sections (~90nm) were collected on uncoated copper grids and stained with saturated uranyl acetate and lead citrate prior to examination in a Jeol 1010 tranmission electron microscope equipped with a Gatan Orius SC1000 digital camera.

A series of images were acquired at magnifications of x3000, x4000, x5000, x6000 and x12000 from outer, mid and posterior stromal sites in the central and peripheral cornea.

5.4 Results

5.4.1 Low-angle x-ray results

Because of lack of time, only one of each selected group was examined and the results are shown in figures 5.4 to 5.7.

In each of our four treatment groups the fibril diameter was lowest in the centre of the cornea (Figure 5.4 – 5.7, pictures b) and increased away from the centre. The same tendency was found for interfibrillar spacing: highest in the peripheral cornea and lowest in the centre of the cornea.

The biggest difference in the fibril diameter was found between animals fed on a normal ascorbic acid diet/exposed to UVB (group A) and animals fed on low dose of ascorbic acid/not exposed to UVB (group D). The last two groups B (fed an ascorbic acid deficient diet, exposure to UVB) and control group C (on normal level of ascorbic acid and not exposure to UVB) were not different from each other as it is seen in figure 5.4b and 5.7b. These two graphs show the same fibril diameter in the central and paracentral regions of their corneas. The lowest fibril diameter in these groups is between 36nm and 38nm. The fibril diameter increases peripherally and creates the circular shape of the corneal tissue.

For the interfibrillar spacing, the biggest differences were noticeable between group B and C (the control group) displaying results of two opposite treatments: no UVB and normal diet against UVB exposure and low ascorbate diet. This suggests that there is a strong effect of ascorbate and UVB exposure on the interfibrillar spacing.

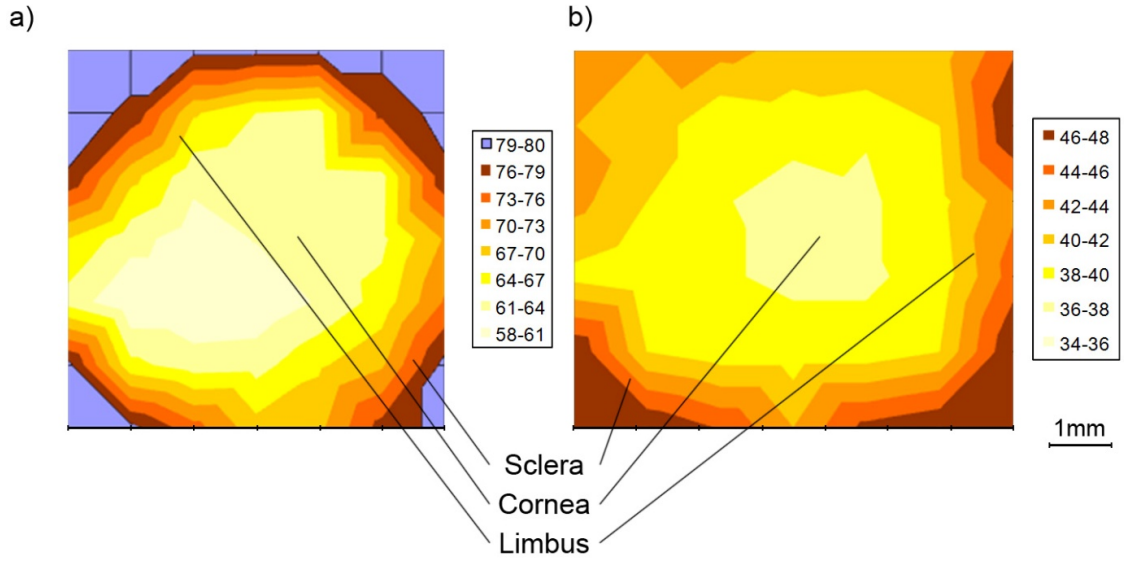

Figure 5.4. Group B (low dose of ascorbate, UVB exposure): **a)** interfibrillar spacing contour map; **b)** fibril diameter contour map. The collagen interfibrillar spacing (a) and fibril diameter (b) is shown in nanometres in the colour scale on a side of each graph.

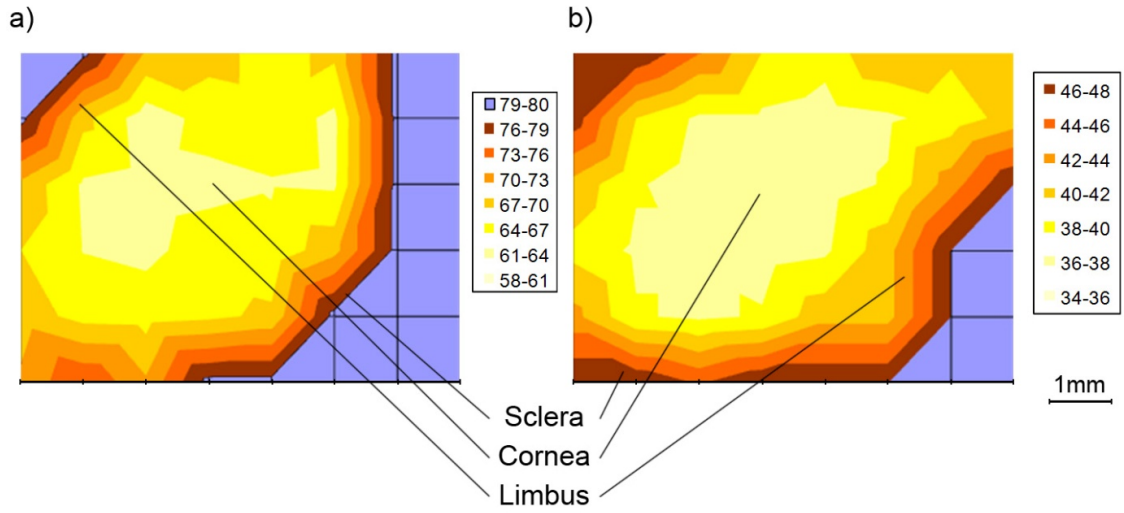

Figure 5.5. Group A (normal dose of ascorbate, UVB exposure): **a)** interfibrillar spacing contour map; **b)** fibril diameter contour map. The collagen interfibrillar spacing (a) and fibril diameter (b) is shown in nanometres in the colour scale on a side of each graph.

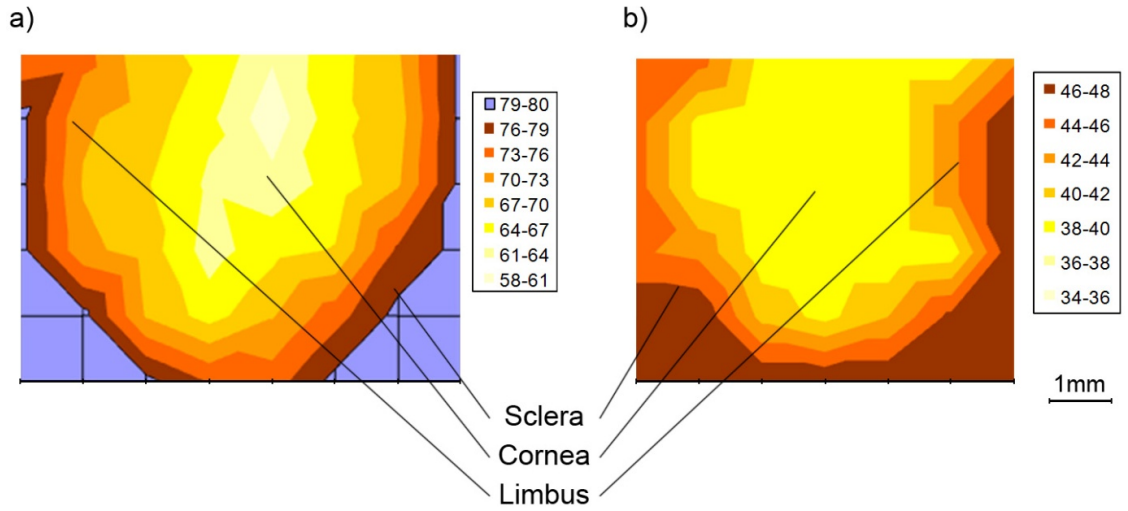

Figure 5.6. Group D (low dose of ascorbate, no UVB exposure): **a)** interfibrillar spacing contour map; **b)** fibril diameter contour map. The collagen interfibrillar spacing (a) and fibril diameter (b) is shown in nanometres in the colour scale on a side of each graph.

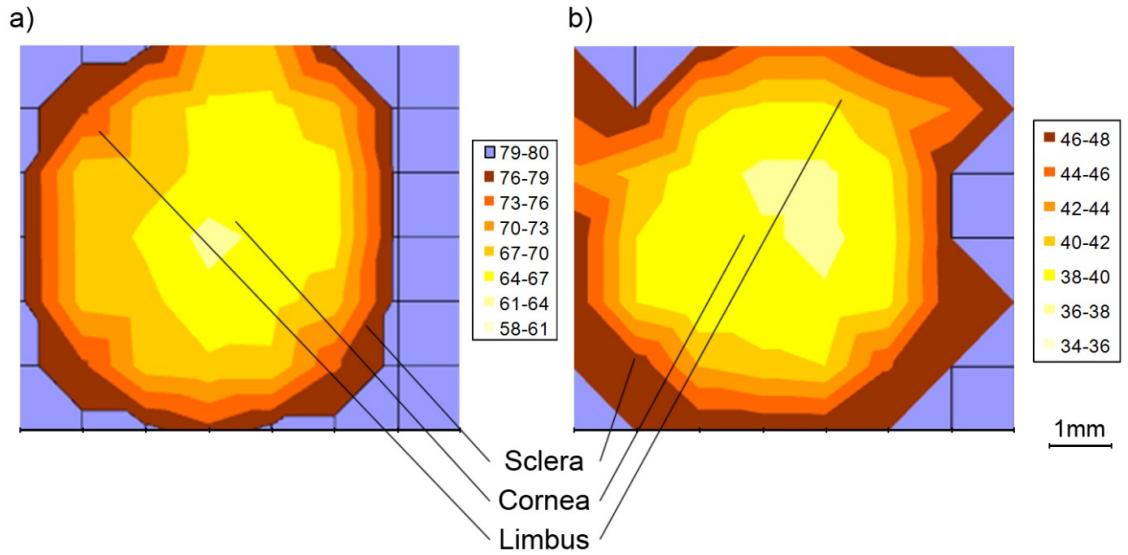

Figure 5.7. Group C (normal dose of ascorbate, no UVB exposure): **a)** interfibrillar spacing contour map; **b)** fibril diameter contour map. The collagen interfibrillar spacing (a) and fibril diameter (b) is shown in nanometres in the colour scale on a side of each graph.

5.4.2 Electron microscopy results

Using transmission electron microscopy, we collected pictures from four different groups of animals. The central and peripheral images are taken from the same eye of one individual. In general there were no strong and distinct differences between these two locations in the corneal stroma in all of collected pictures (Figure 5.8 – 5.11).

Normal lamellar structure of the stroma as well as evenly distributed collagen fibrils were noticed in both: 1) corneas from groups receiving normal dose of ascorbate but with UVB exposure – Group A (Fig. 5.8a) and no UVB radiation – Group C (Fig. 5.8b), 2) and also from groups with low ascorbate consumption – Group B treated with UVB (Fig. 5.10a) and Group D – with no UVB exposure (Fig. 5.10b).

Effect of UVB with normal AA

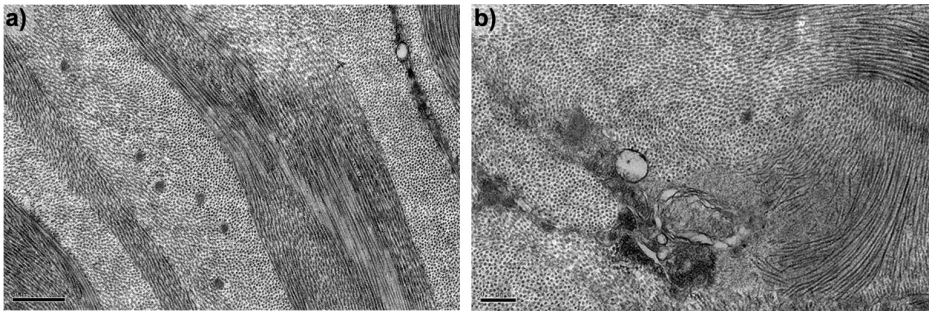

Figure 5.8. a) Normal dose AA (UVB) – centre (x3000); **b)** normal dose AA (no UVB) – centre (x3000).

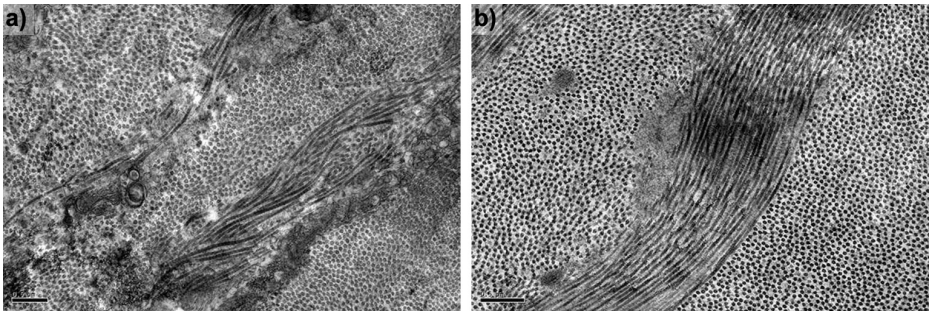

Figure 5.9. a) Normal dose AA (UVB) – peripheral (x3000); **b)** normal dose AA (no UVB) – peripheral (x3000)

Some evidence of cell disruption was clearly observed even at low magnification (x3000 or x4000) under TEM. Among these changes are the following: keratocyte disruption, swelling of endoplasmic reticulum and mitochondria (Fig. 5.10a), cell fragmentation which allows organelles and other membrane-bound vesicles to be released into the extracellular matrix (Fig.5.9a, Fig. 5.11a), and bubble formation inside the cell (Fig. 5.8b). It is possible however that freezing procedures and other actions

before and during fixation of the tissue could have affected the results. Frozen tissue is very fragile as it is but under a beam of electrons can be additionally easily broken.

Effect of UVB with low AA

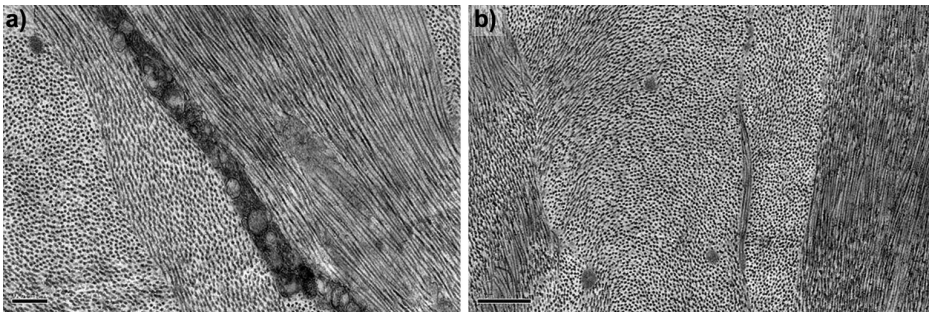

Figure 5.10. a) Low dose AA (UVB) – centre (x5000); **b)** low dose AA (no UVB) – centre (x5000).

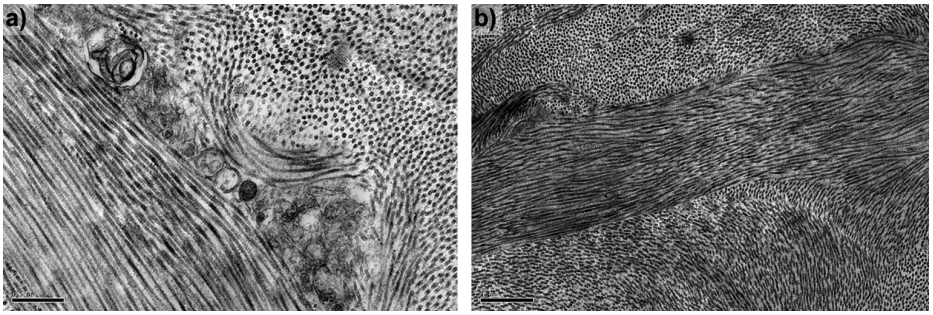

Figure 5.11. a) Low dose AA (UVB) – peripheral (x3000); **b)** low dose AA (no UVB) – peripheral (x3000).

5.5 Discussion

The aim of our study was to combine the results from two different studies: electron microscopy and x-ray diffraction on guinea pigs as a model of CDK disease and conclude how UVB radiation and diet affects the structure of the cornea. Climatic Droplet Keratopathy is a disease occurring mainly in hot climates where sunlight is active mostly throughout the whole year. Thus the cornea is much more exposed to wavelengths shorter than 300nm (UVB radiation is about 280-320nm). It is a well known fact that ultraviolet radiation causes many corneal changes including pathogenesis of corneal cells and opacity which is characterized for CDK. This in turn is closely related to the age of the patients (Gray et al., 1992, Kaji et al., 2007, Taylor et

al., 1989) as CDK develops normally in people over 40 years old in different parts of our globe in harsh climates.

One of the main roles of the cornea is that it acts as a special filter protecting deeper parts of the eye from radiation damage. The cornea, especially the epithelium, absorbs almost 80% of ultraviolet rays reaching the eye (Čejka et al., 2010, Podskochy, 2004). Leaving aside the protecting role of other antioxidants, ascorbic acid seems to be the best example of a UVB absorber and the component of the cornea that neutralizes free radicals. Generally, the problems caused by UVB are various: from induction of reactive oxygen species, peroxidation, and damage of proteins, lipids and DNA in corneal cells, to degradation of these cells (apoptosis) and other problems with transport system between cells within damaged area (Suh et al., 2008).

Ascorbate has the highest concentration in the human eye, especially in the corneal epithelium (in aqueous humor) compared with any other tissue in the human body (Brubaker et al., 2000, Wu et al., 2004). What is more, diurnal species (among which are humans and guinea pigs) have a higher level of ascorbate than nocturnal species (Brubaker et al., 2000, Reiss et al. 1986, Ringvold et al., 1998, Wu et al., 2004).

Our EM study confirmed the results from previous research by different authors. We found no significant changes in the epithelium of guinea pigs' corneas after treatment with UVB or low ascorbate diet. Wu et all. (2004) did not see the difference in ocular examination between groups of animals on normal and low ascorbic acid diet. Whereas they found that long-term UVB exposure caused some damage to the corneal epithelium, stroma and endothelium. They analysed corneal endothelium after 15 and 30 weeks of the treatment with UVB and observed that destruction was increased with the passing of time. The implication is that the longer the time of ultraviolet light exposition the better the results and the observed changes in cornea.

It is a fact that electron microscopy allows a tiny fraction of the tissue to be sampled, so gives us only a rough outline of the basic structure of the cornea. However, we could definitely notice some changes in the epithelium including cell fragmentation and disruption of different organelles (Fig. 5.11a). The same observations were made Podskochy et al. (2000) who found signs of cell apoptosis beneath the epithelial basement membrane: cell shrinkage, cellular blebbing and some structures that seem to be apoptotic bodies. What is more interesting, he observed a connection between the UV wavelength and the range of the corneal damage. This relationship was for wavelengths of 280nm and 310nm. While the 280nm UVR exposure caused only epithelial changes, the 310nm UVR exposure to the cornea caused considerably more serious damage.

Unlike the EM study, synchrotron x-ray scattering shows the picture of the whole cornea, and because the process takes a relatively short time (the synchrotron gives an opportunity to collect a large amount of data in a short time), the tissue is examined without any significant changes such as tissue shrinkage and cell destruction during preparation and fixation. On the other hand, considering the costs and time-limited access to the source of x-ray radiation, we collected data from only a few specimens, thus the results can only be regarded as preliminary.

Our x-ray diffraction results showed more significant differences between the examined groups. Collagen fibril diameter and interfibrillar spacing increased rapidly at the limbus in all groups but the largest value was noticed as follows: for fibril diameter in group A (normal diet, UVB) and for interfibrillar spacing in group B (low ascorbate diet, UVB). Increasing stromal collagen diameter and fibril spacing along with approaching to the limbus was noticed also by Boote et al. (2003) in human and guinea pig corneas. They suggested that it could be related to the differences in hydration

across the whole cornea (also without any effects on fibril diameter). Although the author was only able to analyse x-ray data from one cornea within each group, a colleague, Mr J. Harris, completed the analysis of the other three specimens within each group and a joint publication was written (see Appendix 5). From this it is clear that the greatest changes were in animals treated with a low ascorbate diet.

The x-ray diffraction results gave us a glimpse into the expected role of an ascorbate diet against the harmful effects of UVB on the cornea. The increased interfibrillar spacing closer to the limbus of the cornea suggested that, in the centre of the cornea where the packing density of collagen fibres is higher (more number of fibres per unit area), the tissue has additional strength. What is more, in this region, there can be found small proteoglycans which give the cornea increased transparency (Boote et al., 2003). Other authors (Meek et al., 1991) found a positive linear connection between fibril separation distance and corneal hydration. Their observation was that the water which enters the cornea is spread between the fibrils in a uniform arrangement. Hence, the space where there is lack of water is occupied by other compartments, e.g. keratocytes. These different elements could fill up the regions recognised by electron microscopy technique as parts destroyed by UVB exposure.

5.6 Conclusion

Taking into consideration the fact that in our study we had only limited animals numbers, the results are merely the introduction to future research on guinea pigs corneas as a model of CDK. From the EM study, we were only able to conclude tentatively that UVB treatment causes some damage to the cell and cell organelles of the corneal stroma. In the changed regions, we recognized signs of cell destruction and fragmentation of organelles e.g. keratocytes. The same results were found by Podskochy et al, (2000) in his research on the UVB influence on the corneal tissue, so

may not have been freezing artefacts. They also observed that UVB causes some damage in the control cornea.

Using x-ray diffraction we observed an increase of the average fibril diameter and interfibrillar spacing in the region closer to the limbus. The same study expanded by Hayes et al., (2011) showed that the greatest changes were in animals fed on low ascorbate diet. This gave rise to conclusion that ascorbic acid indeed plays a protecting role against UVB.

5.7 Future study

To have better and more detailed results we have to use more experimental animals as small numbers of treatment groups gives us only the base to the additional experiments. Climatic Droplet Keratopathy develops in harsh climates in men over forty and the inference is that there is need for longer experimental treatment. Longer UVB exposures to the guinea pigs corneas will give us more results to confirm those of Wu et al., (2004).

Another possibility is to use different wavelengths, as there is a connection (mentioned above) between this parameter and the corneal damage noticed by Podskochy et al, (2000). It would also be interesting to examine proteoglycans, as these are involved in corneal development and in the maintenance of structural integrity. As shown earlier in this thesis, the organisation of proteoglycans can be studied in 3D (to observe the three dimensional connections between collagen fibres and proteoglycans), to find more details about the basis of loss of corneal transparency in Climatic Droplet Keratopathy.

6 Concluding discussion

The corneal tissue is exceptionally transparent thanks to the regular arrangement of the stromal collagen fibrils. These fibrils stay in touch with proteoglycans which are suggested to be a control mechanism of the stromal arrangement.

The corneal stroma consists of about 250 stacked lamellae, each containing parallel collagen fibrils. Corneal transparency depends on the very well organized extracellular matrix within each lamella. This results from interactions between collagen fibrils and proteoglycans (PGs) around them leading to a consistent interfibrillar spacing (Chakravarti et al., 2000, Kao and Liu, 2003). The collagen fibrils in each of these lamellae produce destructive interference of scattered light (Meek, 2008). Thus scattered light is eliminated by mutual interference and only the light going forward is permitted to pass through the stromal layers.

There are four proteoglycans (PGs) occurring in the corneal stroma: **decorin, lumican, mimecan (osteoglycin) and keratocan** (Michelacci, 2003, Kao and Liu, 2003). They are responsible for the fact that collagen fibrils do not touch to each other by making a hydrated interfibrillar gel. This is achieved thanks to negative charges of PGs around collagen fibrils which prevent their aggregating (Meek, 2008). The exact mechanisms of this are unknown but will depend on the full three-dimensional arrangement of the collagen and the proteoglycans.

In Chapter 3 we therefore examined the arrangement of proteoglycans in the normal human cornea. In our project, the cornea was pre-stained with Cuprolinic Blue. This is a specific reagent for detecting proteoglycans (PGs) in the tissue. Our model presents normal human cornea in longitudinal sections (Fig. 3.13). Collagen fibrils have almost constant diameter. They are regularly spaced and the proteoglycans are located along the collagen fibrils' axis. Although there are two different kinds of them: KS and

CS/DS proteoglycans, they do not differ in length and size, unlike in the cow where KS aggregates appear smaller than CS/DS aggregates (Lewis et al., 2010). Comparing our results with bovine and mouse cornea we have come to the conclusion that, in spite of the fact that there is no regular arrangement of proteoglycans around the collagen fibrils, they are present in sufficient numbers along and around the fibrils to be responsible for the special distribution of collagen in corneal stroma and thus for corneal transparency.

Since, corneal shape and transparency depend on the collagen fibrils, and stromal arrangements (also spacing between fibrils) we decided to compare different fish species to each other and also to the mammals to have more general view of the corneal structure. Fish were of particular interest as the cornea has no refractive function in water so the structure is purely mechanical, unlike in air, where the cornea needs to have a precise shape. These results were presented in chapter 4. The fish is known to have smaller and more closely spaced fibrils (Gyi et al., 1998) and corneas with a different curvature to humans. The fish cornea is more flat, and thanks to that it can resist the water pressure, whereas the human cornea is more spherical in shape. The flat cornea has a smaller surface area and therefore less frictional resistance to water, compared to a curved cornea. There is also a difference in variation of the lamellar arrangement between these two species: the human cornea is orthogonal while the fish is more circular. However, the main difference is that the fish cornea has the spectacle – the goggle that protects the eyes from the water environment. We have also found many similarities, especially concerning fibril diameter and spacing. Both species display the increase in fibril diameter and collagen spacing towards the edge of the cornea. Consequently there is a reduction in transparency as we go from the centre to the periphery. We also noted several structural differences between different fish species.

These need further study but could relate to the habitats. Deep water fishes have to withstand greater pressures thus the cornea's structure needs to be stronger.

During the course of this study, the opportunity arose to study an animal model of a human pathology and to examine the potential cause and remedy for this condition. In chapter 5 we demonstrated the results from guinea pigs which have similar corneal structure to humans and also require ascorbic acid (AA or Vitamin C) to function normally. As in humans they are not able to synthesize ascorbate. This molecule is an excellent absorber of UVB which is thought to be one of the major factors affecting this human pathology which is known as Climatic Droplet Keratopathy (CDK). The aim was to understand more about the causes of transparency loss in this condition in terms of collagen changes. Also the results allowed us to see how ascorbate affects these changes. From the x-ray diffraction data we noticed that some unwanted structural changes associated with UVB were not present if ascorbate was included in the diet. Thus vitamin C could be good protection against some of the deleterious effects of UVB and could have an effect on the development and prevention of Climatic Droplet Keratopathy.

APPENDICES

Appendix 1 – Nomenclature

Symbol used for abbreviation	Original Term
2D	Two dimentional
3D	Three dimentional
ATPase	Adenosine triphosphate enzyme
CEC	Critical electrolyte concentration
Cl^-	Chlorine
CO_2	Carbon dioxide
CO_2H	Carboxyl group
CS	Chondroitin sulphate
DS	Dermatan sulphate
dd H_20	Double distilled water
ECD	Endothelial cell density
ECM	Extracellular matrix
FACIT	Fibril associated collagens with interrupted triple helices
GAG	Glycosaminoglycan
Gal	Galactose
GlaNAc	N-acetylogalactosamine
GlcA	Glucuronic acid
GlcNAc	N-acetyloglucosamine
Gly	Glycine
HCO_{3-}	Bicarbonate ion
HS	Heparan sulphate
Hyp	Hydroxyproline
IdoA	Iduronic acid
kDa	Kilodalton
KS	Keratan sulphate
K^+	Potassium ion
kV	Kilovolt
LOX	Lysyl oxidase
LRP	Leucine-rich repeat
$MgCl_2$	Magnesium chloride
min	Minutes
mm	Millimetre
mM	Millimolar
Na+	Sodium ion
nm	Nanometre

°C	Degree Celsius
OH^-	Hydroxide
OS	Oligosaccharides
PAPS	3'-Phosphoadenosine-5'phosphosulphate
PEI	Polyether amide
PG	Proteoglycans
PO_2	Propylene oxide
Pro	Proline
PTA	Phosphotungstic acid
RER	Rough endoplasmic reticulum
RT	Room temperature
SLRP	Small leucine-rich proteoglycans
SO_3^-	Sulphate group
TEM	Transmission electron microscope
UA	Uranyl acetate
UDP-galactose	Uridine diphosphate galactose
UDP-glucose	Uridine diphosphate glucose
UDP-N-acetylglucosamine	Uridine diphosphate-N-acetylgucosamine
µm	Micrometre
Xyl	Xylose

Appendix 2 – List of materials

Material	Supplier
Araldite Monomer	Agar Scientific
BDMA Accelerator	Agar Scientific
CCD camera (Kodak MegaPlus 1.4)	Gatan
Chloroform	Agar Scientific
Colloidal Gold (10 nm)	BBInternational
Cuprolinic Blue 0.05%	Agar Scientific
DDSA Hardener	Agar Scientific
EMKMR2 Glass maker	Leica
Ethanol (50%, 70%, 90%, 100%)	Sigma-Aldrich
Ethylene Dichloride (1,2 – Dichloroethane)	Sigma-Aldrich
Float glass	Leica
Glutaraldehyde 2.5%	Agar Scientific
JEM1010 TEM	Jeol
Magnesium chloride	TAAB
Microscope slides	TAAB
Petri dish (polypropylene)	Agar Scientific
Phospho-tungstate acid 1%	TAAB
Polyetherimide granules	Goodfellow
Propylene oxide	Agar Scientific
Razor blades (single edge)	Agar Scientific
Slot grids (Copper 3.05 mm, 2x1 mm)	Agar Scientific
Sodium acetate 0.5% (pH 5.7)	Aldrich
Sodium tungstate 0.5% (Ag.)	TAAB
Tweezers (Stainless steel, curved and fine points)	Dumont
Ultramicrotome Ultracut-E	Reichert-Jung
Uranyl acetate 2%	BDH

Appendix 3 – Solution preparation

I. 2.5% glutaraldehyde in 25mM sodium acetate, 0.1M $MgCl_2$, pH5.7

Weigh 0.246g sodium acetate and 2.436g $MgCl_2$
Add ~80ml distilled water and mix on magnetic stirrer.
Check pH. Make to pH 5.7 using 1M HCl droplets.
Make up to 120ml using distilled water.

Take:
36ml of sodium acetate, $MgCl_2$ buffer (out of 120ml)
4ml of 25% glutaraldehyde
It gives 40ml of required buffer.
Remaining 80ml of sodium acetate will be used to rinse the tissue.

II. Cuprolinic blue fix/staining solution

0.05% cuprolinic blue in 2.5% glutaraldehyde in 25mM sodium acetate,pH 5.7

Take 40ml of buffer from part I. (2.5% glutaraldehyde in 25mM sodium acetate, 0.1M $MgCl_2$, pH5.7).
Mix with 0.02g of cuprolinic blue.

III. Aqua 0.5% sodium tungstate

3x wash, 3ml per vial, 9 vials = 81 ml – make 100ml
Add 0.5g sodium tungstate to 100ml dd H_20.

IV. 50%EtOH 0.5% sodium tungstate

3ml per vial, 9vials, 1 change = 27ml – make 50ml
Add 0.25g of sodium tungstate to 25ml 100%EtOH and 25ml dd H_20.

V. Araldite resin

Allow 3ml, 6 changes, 9 vials =162ml + PO_2/resin (1.5ml, 9 vials) =67.5ml.
Make 180ml of resin

6 x 14ml araldite monomer = **84ml (resin)**
6 x 16ml DDSA Hardener = **96ml (hardener)**
6 x 0.6ml accelerator = **3.6ml (accelerator)**

Prewarm monomer and hardener in oven to facilitate measuring and pouring (10-15 min. before pouring).
Measure accelerator (BDMA) accurately with graduated pipette.
Add components to prewarmed conical flask, mixed thoroughly by swirling.

Appendix 4 – Routine sample processing for TEM

Quinolinic phthalocyanate (cuprolinic blue) Method for GAGs
Refs: Scott JE. (1980) Biochem J 187, 8-891.Scott JE & Orford CR (1981) Biochem J. 197, 213-16.

1. Fix/Stain tissue overnight in 2.5% glutaraldehyde in 25mM sodium acetate buffer, pH 5.7 containing 0.1M $MgCl_2$ and 0.05% cuprolinic blue (CB)
25mM sodium acetate – 0.205g/100ml 0.1M $MgCl_2$ – 2.03g/100ml
Adjust pH from ~7.5 to 5.7 with 0.1M HCl

2. Rinse 3x 5 mins in sodium actetate buffer, pH 5.7 (-) glutaraldehyde and CB

3. Wash 3x 5 mins in aq. 0.5% sodium tungstate

4. Dehydrate	50% etOH + 0.5% sodium tungstate		
	70%	)	
	90%	)	
*	100%	)	
	100%	)	15 mins
	Propylene oxide	)	
	Propylene oxide	)	
	1:1 Propylene oxide:Araldite resin mixture		1h

5. Resin infiltration:	Araldite resin I	early pm	on Rotator
	Araldite resin II	mid pm.	
	Araldite resin III	late pm.	
Take vial tops off, leave on rotator in fume hood → overnight			
	Araldite resin IV	early am.	
	Araldite resin V	mid am.	
	Araldite resin VI	midday	

6. Embed in moulds with further resin late pm.
7. Polymerise resin at 60°C for 24 hours (minimum)
8. Cut sections: stain with 0.5% aqueous Uranyl acetate 10-20 mins

* Make up **Araldite resin** mixture (allow approx 3ml per sample per change):
14 ml Araldite monomer CY212
16 ml DDSA Hardener
0.6 ml BDMA Accelerator
Prewarm monomer and hardener in oven to facilitate measuring and pouring
Measure accelerator (BDMA) accurately
Add components to prewarmed conical flask, mixed thoroughly by swirling.
Allow air bubbles to rise to surface and disperse before using.

Safety:
Most of the reagents used are hazardous; eg. osmium is poisonous, vapours can fix mucous membranes (eg.corneas); uranyl acetate is radioactive and toxic; propylene oxide is an irritant and explosive; BDMA carcinogenic; CY212 and DDSA are irritants.
All procedures must be carried out in a fume hood with all precautions.
Wear gloves, wipe up spillages, etc

Appendix 5 – paper published in 2011

Molecular Vision 2011; 17:3107-3115 <http://www.molvis.org/molvis/v17/a334>
Received 3 October 2011 | Accepted 22 November 2011 | Published 26 November 2011

The effect of vitamin C deficiency and chronic ultraviolet-B exposure on corneal ultrastructure: a preliminary investigation

Sally Hayes,[1] Thamara A. Cafaro,[2] Patrycja J. Boguslawska,[1] Christina S. Kamma-Lorger,[1] Craig Boote,[1] Jonathan Harris,[1] Robert Young,[1] Jennifer Hiller,[3] Nicholas Terrill,[3] Keith M. Meek,[1] Horacio M. Serra[2]

(The last two authors equally contributed to this work)

[1]School of Optometry and Vision Sciences, Cardiff University, Cardiff, United Kingdom; [2]CIBICI, Faculty of Chemistry, Universidad Nacional de Córdoba, Argentina; [3]Diamond Light Source, Didcot, Oxford, United Kingdom

Purpose: In the visually debilitating condition of climatic droplet keratopathy, corneal transparency is progressively lost. Although the precise cause of the disease and the mechanism by which it progresses are not known, a lifetime exposure to high solar radiation and a vitamin C–deficient diet may be involved in its development. This study examines the effect of dietary ascorbate levels and ultraviolet (UV)-B exposure on corneal stromal structure.

Methods: Eight guinea pigs were divided into four treatment groups (A, B, C, and D). For 15 weeks, Groups A and C were fed an ascorbate-rich diet (2 mg/100 g bodyweight/day), while Groups B and D received an ascorbate-deficient diet (0.07 mg/100 g bodyweight/day). For the last 12 weeks of the study, Groups C and D also experienced chronic UVB exposure (0.12 J/cm² for 40 min/day). Following euthanasia, the corneas were enucleated and their stromal ultrastructure examined using X-ray scattering and electron microscopy.

Results: UVB exposure resulted in an increased corneal thickness ($p<0.001$), but this was not accompanied by a widespread expansion of the collagen fibrillar array, and in the case of ascorbate-deficient animals, stromal thickening was associated with the compaction of collagen fibrils ($p<0.01$). Neither UVB exposure nor ascorbic acid deficiency caused any change in the average diameter or D-periodicity of the stromal collagen fibrils.

Conclusions: UVB-induced changes in the corneal ultrastructure were most pronounced in animals fed an ascorbic acid–deficient diet. This suggests that ascorbic acid may play a vital role in protecting the corneal stroma from the harmful effects of UVB.

Chronic exposure to ultraviolet (UV)-B light (290–320 nm) has been implicated in the development of several ocular disorders, such as pterygium [1,2], cataracts [1], and climatic droplet keratopathy [2,3]. Laboratory-based studies have shown that wavelengths below 290 nm (UVC) are almost completely absorbed by the corneal epithelium, whereas UVB penetrates deeper into the tissue and is absorbed by the corneal stroma and lens [4,5]. Corneal damage induced by chronic UVB exposure is thought to occur through a series of photooxidation reactions that result in the production of free radicals and reactive oxygen species. The presence of ascorbic acid in the corneal epithelium [6] is believed to limit damage to deeper ocular structures by absorbing UV radiation [7]. This is supported by the naturally high concentration of ascorbic acid in the corneas of diurnal species (especially those exposed to high solar radiation) compared to nocturnal species [8], as well as the reduced severity of corneal damage in UVB-exposed rabbits that are pretreated with ascorbic acid [9]. Moreover, in Norway, it was reported that corneal haze following photorefractive keratectomy (in which the ascorbate-rich epithelial layer is removed) only occurred during the summer months when the sun was visible 24 h per day [10], but when pre- and postoperative supplementation of vitamin C was used, the incidence of corneal haze reduced from 3.7% to zero [11]. We have also found that climatic droplet keratopathy patients in Patagonia (Argentina) experience a lifetime of constant intense winds, high solar radiation, and low humidity [12], and have abnormally low levels of ascorbate in their blood as a result of a low vitamin C diet (unpublished data).

In addition to its role as an antioxidant, ascorbic acid is also a cofactor in collagen synthesis reactions, where it is specifically needed for the hydroxylation of proline and lysine [13]. Without the hydroxylation of these amino acids, procollagen is unable to crosslink properly to form stable collagen fibrils [14], and glycosidic linkages between collagen and specific glycosaminoglycans may not be established [15]. Disturbing the precise organization of collagen in the corneal stroma may result in a loss of tissue transparency, since this property is largely dependent on the presence of uniformly narrow fibrils lying parallel to each other in layers (lamellae), which are themselves organized in a lattice-like configuration [16-18].

Correspondence to: Horacio M. Serra, CIBICI, Faculty of Chemistry, Universidad Nacional de Córdoba, Argentina; Phone: 54 351 4344973; FAX: 54 0351-4333048; email: hserra@bioclin.fcq.unc.edu.ar

Reference:

Aghamohammadzadeh, H., Newton, R.H., Meek, K.M., (2004), X-ray scattering used to map the preferred collagen orientation in the human cornea and limbus, Structure, vol. 12, 249-256.

Alberts, B., Johnson, A., Lewis, J. (2002), Molecular biology of the cell, Garland Science, 1091 – 1102.

Ameen, D.B., Bishop, M.F., McMullen, T., (1998), A Lattice Model for Computing the Transmissivity of the Cornea and Sclera, Biophysical Journal, vol. 75: 2520-2531.

Armitage, W.J., (1999), Anatomy and physiology of the cornea, In Oxford textbook of ophthalmology , edited by Easty, D.L., Sparrow, J.M., Oxford University Press, vol.1, sections 1-2.10: 373-380.

Benedek, G.B., (1971), Theory of transparency of the eye, Appl. Opt., 10: 459-473.

Beuerman, R.W., Pendoza L. (1996), Ultrastructure of the Human cornea, Microscopy and research technique, 33: 320 – 335.

Birk, D.E., (2009), Regulation of Corneal Stromal Assembly, The 9th Corneal Conference in Cardiff.

Bone, Q., Marshall, N.B., (1982), Biology of fishes, published by Blackie (Glasgow and London), 253 pages.

Bonnano, J.A., (2003), Identity and regulation of ion transport mechanisms in the corneal endothelium, Progress in Retinal and Eye Research, 22: 69-94.

Bonnano, J.A., Srinivas, S.P., (1997), Cyclic AMP Activates Anion Channels in Cultured Bovine Corneal Endothelial Cells, Experimental Eye Research, 64: 953-962.

Bonnano, J.A., Giasson, C., (1992), Intracellular ph Regulation in Fresh and Cultured Bovine Corneal Endothelium. II. Na^+: HCO_3^- Cotransport and Cl^-/HCO_3^- Exchange, Investigative Ophthalmology & Visual Science, vol. 33, no.11: 3068-3079.

Boote, C., Hayes, S., Abahussin, M., Meek, K.M., (2006), Mapping collagen organization in the human cornea: left and right eyes are structurally distinct, Investigative Ophthalmology & Visual Science, vol. 47, no. 3, 901-908.

Boote, C., Dennis, S., Meek, K.M., (2004), Spatial mapping of collagen fibril organization in primate cornea – an X-ray diffraction investigation, Journal of Structural Biology, 146, 359-367.

Bozzano, A., Catalán, I.A., (2002), Ontogenetic changes in the retinal topography of the European hake, Merluccius merluccius: implications for feeding and depth distribution, Marine Biology, 141 (3), 549-559.

Bozzola, J.J., 2002, Electron Microscopy, Encyclopedia of life science, John Wiley & Sons, 1-10.

Brubaker, R.F., Bourne, W.M., Bachman, L.A., McLaren, J.W., (2000), Ascorbic acid content of human corneal epithelium, Investigative Ophthalmology & Visual Science, 41, 1681-1683.

Cafaro, T.A., Ortiz, S.G., Maldonado, C., Espósito, F.A., Croxatto, J.O., Berra, A., Ale, O.L., Torrealday, J.I., Urrets-Zavalia, E.A., Urrets-Zavalia, J.A., Serra, H.M., (2009), The cornea of Guinea pig: structural and functional studies, Veterinary Ophthalmology, volume 12, issue 4, 234-241.

Carlson, E.C., Chia-Yang Liu, Tai-ichiro Chikama, Hayashi, Y., Kao Candace, W.-C., Birk, D.E., Funderburgh, J.L., Jester, J.V., Winston W.-Y. Kao, (2005), Keratocan, a Cornea-specific Keratan Sulfate Proteoglycan, Is Regulated by Lumican, The Journal of Biological Chemistry, vol. 280, no. 27, Issue of July 8: 25541-25547.

Čejka, Č, Ardan, T., Širc, J., Michálek, J., Brůnová, B., Čejková, J., (2010), The influence of various toxic effects on the cornea and changes in corneal light transmission, Graefe's Archive for Clinical and Experimental Ophthalmology, vol. 248, issue 12, 1749-1756.

Chakravarti, S., (2006), Focus on Molecules: Keratocan (KERA), Experimental Eye Research, 82: 183-184.

Chakravarti, S., Petroll, W.M., Hassell, J.R., Jester, J.V., Lass, J.H., Paul J., Birk, D.E., (2000), Corneal Opacity in Lumican-Null Mice: Defects in Collagen Fibril Structure and Packing in the Posterior Stroma, Investigative Ophthalmology & Visual Science, vol. 41, no.11: 3365-3373.

Collin, P., Collin, H.B., (2006), The corneal epithelial surface in the eyes of vertebrates: environmental and evolutionary influences on structure and function, Journal of Morphology, 267:273-291.

Collin, S.P., Collin, H.B., (2001), The Fish Cornea: Adaptation for Different Aquatic Environments, In Sensory biology of jawed fishes: new insights, Kapoor, B.G., Hara, T.J., Science Publishers, 57-96.

Connon, C.J., Meek, K.M., Kinoshita, S., Quantock, A.J., (2004), Spatial and temporal alterations in the collagen fibrillar array during the onset of transparency in the avian cornea, Experimental Eye Research, 78: 909-915.

Davies, Y., Davies, L., Fullwood N.J., Nieduszynski, I.A., Marcyniuk, B., Albon, J., Tullo, A., (1999), Proteoglycans on Normal and Migrating Human Corneal Endothelium, Exp. Eye Res., 68: 303-311.

Daxer, A., Fratxl, P., (1997), Collagen fibril orienatation in the human corneal stroma and its implication in keratoconus, Investigative Ophthalmology & Visual Science, vol. 38, no. 1.

Doutch, J., Quantock, A.J., Smith, V.A., Meek, K.M., (2008), Light Transmission in the Human Cornea as a Function of Position across the Ocular Surface: Theoretical and Experimental Aspects, Biophysical Journal, vol. 95, 5092-5099.

Edelhauser, H.F., (2006), The Balance between Corneal Transparency and Edema, Investigative Ophthalmology & Visual Science, vol. 46, no. 5, 1755-1767.

Ehlers, N., Hjortdal, J., (2006), The cornea. Epithelium and stroma, In The Biology of the Eye, red. Fischbarg, J., Elsevier B.V., 83-111.

Fischbarg, J., (2006), The corneal endothelium, In The Biology of the Eye, red. Fischbarg, J., Elsevier B.V., 113-125.

Fischbarg, J., Diecke, F.P.J., (2005), A Mathematical Model of Electrolyte and Fluid Transport across Corneal Endothelium, The Journal of Membrane Biology, 203: 41-56.

Fischbarg, J., Maurice, D.M., (2004), An update on corneal hydration control, Experimental Eye Research, 78: 537-541.

Fischbarg, J., (2003), On the Mechanism of Fluid Transport Across Corneal Endothelium and Epithelia in General, Journal of Experimental Zoology, 300A: 30-40.

Fischbarg, J., (1997), Mechanism of fluid transport across corneal endothelium and other epithelial layers: a possible explanation based on cyclic cell volume regulatory changes, British Journal of Ophthalmology, 81: 85-89.

Fischbarg, J., Hernandez, J., Liebovitch, L.S., Koniarek, J.P., (1985), The mechanism of fluid and electrolyte transport across corneal endothelium: Critical revision and update of a model, Current Eye Research, vol. 4, no. 4: 351-360.

Fischer, F.H., Zadunaisky, J.A., (1977), Electrical and hydrophilic properties of fish corneas, Experimental Eye Research, vol. 25, issue 2, 149-161.

Funderburgh, J.L., (2000), Keratan sulphate: structure, biosynthesis, and function, Glycobiology, vol. 10, no. 10: 951-958.

Funderburgh, J.L., Corpuz, L.M., Roth, M.R., Funderburgh, M.L., Tasheva, E.S., Conrad, G.W., (1997), Mimecan, the 25-kDa Corneal Keratan Sulfate Proteoglycan, Is a Product of the Gene Producing Osteoglycin, The Journal of Biological Chemistry, vol. 272, no. 44, Issue of October 31: 28089-28095.

Gray, R.H., Johnson, G.J., Freedman, A., (1992), Climatic Droplet Keratopathy, Survey of Ophthalmology, vol. 36, no. 4, 241-253.

Guthrie, D.M., Muntz, W.R.A., (1993), Role of vision in fish behaviour, in Behaviour of Teleost Fishes, Edited by Tony J. Pitcher, Chapman & Hall, Second Edition, 89-128.

Gyi, T.J., Meek, K.M., Elliot, G.F., (1998), Collagen interfibrillar distances in corneal stroma using synchrotron X-ray diffraction: a species study, Int. J. Biol. Macromol., vol. 10, 265-269.

Harris, A., Cardone, G., Winkler, D.C., Heymann, J.B., Brecher, M., White, J.M., Steven, A.C., (2006), Influenza virus pleiomorphy characterized by cryoelectron tomography, PNAS, vol. 103, no. 50, 19123-19127.

Hart, R.W., Farrell, R.A., (1969), Light scattering in the cornea, J. Opt. Soc. Am., 59: 766-774.

Hawryshyn, C.W., (1998), Vision, In Physiology of Fishes, Second Edition, Evans, D.H., CRC Press LLC, 345-374.

Hayes, S., Cafaro, T.A., Boguslawska, P.J., Kamma-Lorger, C.S., Boote, C., Harris, J., Young. R.D., Hiller, J., Terrill, N., Meek, K.M., Serra, H.M., (2011), The effect of vitamin C deficiency and chronic ultraviolet-B exposure on corneal ultrastructure: a preliminary investigation, Molecular Vision, 17, 3107-3115.

Hayes, S., Boote, C., Lewis, J., Sheppard, J., Abahussin, M., Quantock, A.J., Purslow, C., Votruba, M., Meek, K.M., (2007), Comparative study of fibrillar collagen arrangement in the corneas of primates and other mammals, The anatomical record, vol. 290: 1542-1550.

Hodson, S., Miller, F., (1976), The bicarbonate ion pump in the endothelium which regulates the hydration of rabbit cornea, J. Physiol. 263, 563-577.

Hulmes, D.J.S., (2008), Collagen Diversity, Synthesis and Assembly, In Collagen. Structure and Mechanics, Fratzl. P., Springer, 15-47.

Ihanamäki, T., Pelliniemi, L.J., Vuorio, E., (2004), Collagens and collagen-related matrix components in the human and mouse eye, Progress in Retinal and Eye Research, 23: 403-434.

Iozzo, R.V., (1999), The Biology of the Small Leucine-rich Proteoglycans, The Journal of Biological Chemistry, vol. 274, no. 27, Issue of July 2: 18843-18846.

Iozzo, R.V., (1998), Matrix Proteoglycans: From Molecular Design to Cellular Function, Annu. Rev. Biochem., 67: 609-652.

Jentsch, T.J., Keller, S.K., Koch, M., Wiederholt M., (1984), Evidence for Coupled Transport of Bicarbonate and Sodium in Cultured Bovine Corneal Endothelial Cells, The Journal of Membrane Biology, 81: 189-204.

Junqueira, L.C.U., Montes, G.S., (1983), Biology of Collagen-Proteoglycan Interaction, Arch. histol. jap., vol. 46, no 5, 589-629.

Kaji, Y., Nagai, R., Amano, S., Takazawa, Y., Fukayama, M., Oshika, T., (2007), Advanced glycation end product deposits in climatic droplet keratopathy, British Journal of Ophthalmology, 91, 85-88.

Kao, Winston W.-Y., Funderburgh, J.L., Ying Xia, Chia-Yang Liu, Conrad, G.W., (2006), Focus on molecules: Lumican, Experimental Eye Research, 82: 3-4.

Kao, Winston W.-Y., Chia-Yang Liu (2003) , Roles of lumican and keratocan on corneal transparency, Glycoconjugate Journal, 19: 275-282.

Kjellen, L., Lindahl, U., (1991), Proteoglycans: Structures and Interactions, Annu. Rev. Biochem., 60: 443-475.

Knupp, C., Pinali C., Lewis, P.N., Parfitt, G.J., Young, R.D., Meek, K.M., Quantock, A.J., (2009), The architecture of the Cornea and Structural Basis of Its Transparency, Structural Biology, vol. 78, 25-49.

Koster, A.J., Grimm, R., Typke, D., Hegerl, R., Stoschek A., Walz, J., Baumeister, W., (1997), Perspectives of Molecular and Cellular Electron Tomography, Journal of Structural Biology, 120: 276-308.

Kremer, J.R., Mastronarde, D.N., McIntosh, J.R., (1996), Computer Visualization of Three-Dimensional Image Data Using IMOD, Journal of Structural Biology, 116: 71-76.

Lewis P.N., Pinali, C., Young, R.D., Meek, K.M., Quantock, A.J., Knupp, C., (2010), Structural interactions between collagen and proteoglycans are elucidated by three-dimensional electron tomography of bovine cornea, Structure, vol. 18, issue 2, 239-245.

Mastronarde, D.N., (2006), Tomographic reconstruction with the IMOD software package, Microscopy & Microanalysis, 12 (Supp 2), 178-179.

Maurice, D.M., (1957), The structure and transparency of the cornea, The Journal of Physiology, 136, 263-286.

McEwan, P.A., Scott, P.G., Bishop, P.N., Bella, J., (2006), Structural correlations in the family of small leucine-rich repeat proteins and proteoglycans, Journal of Structural Biology, 155: 294-305.

McIntosh, R., Nicastro, D., Mastronarde, D., (2005), New views of cells in 3D: an introduction to electron tomography, Trends in Cell Biology, vol.15, no. 1, 43-51.

McLaughlin, S.H., Bulleid, N.J., (1998), Molecular Recognition in Procollagen Chain Assembly, Matrix Biology, vol. 16, issue 7: 369-377.

Meek, K.M., (2008), The Cornea and Sclera, In Collagen. Structure and Mechanics, Fratzl, P., Springer, 359-396.

Meek, K.M., Leonard, D.W., Connon, C.J., Dennis, S., Khan, S., (2003), Transparency, swelling and scarring in the corneal stroma, Eye, 17: 927-936.

Meek, K.M., (2002), The cornea, In Signal and perception. The fundamentals of human sensation, Roberts, D., Palgrave Macmillan, The Open University, 103 – 114.

Meek, K.M., Fullwood, N.J., (2001a), Corneal and scleral collagens – a microscoist's perspective, Micron, 32: 261-272.

Meek, K.M., Quantock A.J., (2001b), The Use of X-ray Scattering Techniques to Determine Corneal Ultrastructure, Progress in Retinal and Eye Research, vol. 20, no. 1, 95-137.

Meek, K.M., Leonard, D.W., (1993), Ultrastructure of the corneal stroma: a comparative study, Biophys. J., 64: 273-280.

Menegay, M., Lee, D., Tabbara, K.F., Cafaro, T.A., Urrets-Zavalia, J.A., Serra, H.M., Bhattacharya, S.K., (2008), Proteomic Analysis of Climatic Keratopathy Droplets, Investigate Ophthalmology & Vision Science, vol. 49, no. 7, 2829-2837.

Mergler, S., Pleyer, U., (2007), The human corneal endothelium: New insights into electrophysiology and ion channels, Progress in Retinal and Eye Research, 26: 359-378.

Michelacci, Y.M., (2003), Collagens and proteoglycans of the corneal extracellular matrix, Brazilian Journal of Medical and Biological Research, 36: 1037 – 1046.

Midgley, P.A., Weyland, M., (2003), 3D electron microscopy in the physical sciences: the development of Z-contrast and EFTEM tomography, Ultramicroscopy, 96: 413-431.

Müller, L.J., Pels, E., Schurmans, L.R.H.M., Vrensen, G.F.J.M., (2004), A new three-dimensional model of the organization of proteoglycans and collagen fibrils in the human corneal stroma, Experimental Eye Research, 78: 493-501.

Munk, O., (1965), Ocular degeneration in deep-sea fishes, Galathea Rep, vol. 8, 21-32.

Newton, R.H., Meek, K.M., (1998), Circumcorneal annulus of collagen fibrils in the human limbus, Investigative Ophthalmology & Visual Science, vol. 39, no. 7, 1125-1134.

Nicol, J.A.C., Somiya, H., (1989), Sclera, Cornea, And Spectacle, Lens And Accommodation, Intraocular Fluids, In The Eyes of fishes, Nicol, J.A.C, Somiya, H., Oxford Science Publications, Clarendon Press, 25-39.

Oyster, C.W. (1999) The human eye. Structure and function, Sinauer Associates, Inc, 325 – 378.

Parfitt, G.J., Pinali, C., Young, R.D., Quantock, A.J., Knupp, C., (2010), Three-dimensional reconstruction of collagen-proteoglycans interactions in the mouse corneal stroma by electron tomography, Journal of Structural Biology, 170, 392-397.

Podskochy, A., (2004), Protective role of corneal epithelium against ultraviolet radiation damage, Acta Ophthalmologica, vol. 82, issue 6, 714-717.

Poole, A.R., (1986), Proteoglycans in health and disease: structures and function, Biochem. J., 236: 1-14.

Prydz, K., Dalen, K.T., (2000), Synthesis and sorting proteoglycans, Journal of Cell Science, 113: 193-205.

Quantock, A.J., Young, R.D., (2008), Development of the corneal stroma, and the collagen-proteoglycan associations that help define its structure and function, Developmental Dynamics, 237: 2607-2621.

Reiss, G.R., Campbell, R.J., Bourne, W.M., (1986), Infectious crystalline keratopathy, Survey of Ophthalmology, vol. 31, issue 1, 69-72.

Ress, D.B., Harlow, M.L., Marshall, R.M., McMahan, U.J., (2004), Methods for Generating High-Resolution Structural Models from Electron Microscope Tomography Date, Structure, vol. 12, 1763-1774.

Ringvold A., (1998), Corneal epithelium and UV-protection of the eye, Acta Ophthalmologica, vol. 76, issue 2, 149-153.

Robert, L., Legeais, J.M., Robert, A.M., Renard, G. (2001), Corneal collagens, Pathol Biol, 49: 353-363.

Ruoslahti, E., (1988), Structure and Biology of Proteoglycans, Ann. Rev. Cell Biol., 4: 229-255.

Scott, J.E., (2001), Structure and function in extracellular matrices depend on interactions between anionic glycosaminoglycans, Pathol Biol, 49: 284-289.

Scott, J.E., (1995), Extracellular matrix, supramolecular organization and shape, Journal of Anatomy, 187: 259-269.

Scott, J.E., (1993), Proteoglycan-fibrillar collagen interactions in tissues: dermatan sulphate proteoglycan as a tissue organizer; in Dermatan Sulphate Proteoglycans, Chemistry, Biology, Chemical Pathology, Portland Press Ltd, 165-181.

Scott, J.E., (1992a), Morphometry of Cupromeronic blue-stained proteoglycan molecules in animal corneas, versus that of purified proteoglycans stained in vitro, implies that tertiary structures contribute to corneal ultrastructure; Journal of Anatomy, 180: 155-164.

Scott, J.E., (1992b), Supramolecular organization of extracellular matrix glycosaminoglycans, in vitro and in the tissue, The FASEB Journal, June, vol.6, 2639-2645.

Scott, J.E., (1991), Proteoglycan: collagen interactions in connective tissues. Ultrastructural, biochemical, functional and evolutionary aspects, Int. J. Biol. Macromol., vol. 13: 157-161.

Scott, J.E. (1988), Proteoglycan – fibrillar collagen interactions, Biochemical Journal, 252: 313-323.

Scott, J.E., Haigh, M., (1988), Identification of specific binding sites for keratan sulphate proteoglycans and chondroitin-dermatan sulphate proteoglycans on collagen fibrils in cornea by use of Cupromeronic Blue in 'critical-electrolyte-concentration' techniques, Biochem. J., 253: 607-610.

Scott, J.E., Haigh, M., (1985), 'Small'-proteoglycan: collagen interactions: Keratan sulphate proteoglycan associates with rabbit corneal collagen fibrils at the 'a' and 'c' bands, Bioscience Reports, 5: 765-774.

Scott, J.E., Orford, C.R., (1981), Dermatan sulphate-rich proteoglycans associates with rat tail-tendon collagen at the d band in the gap region, Biochem. J., 197: 213-216.

Shidar, M.S., Garg, P., Das, S., Vemuganti, G., Gopinathan, U., Rao, G.N., (2000), Infectious Keratitis in Climatic Droplet Keratopathy, Cornea, 19(4), 455-458.

Smelser, G.K., (1962), Corneal hydration. Comparative physiology of fish and mammals, The Proctor Award Lecture, Investigative Ophthalmology, vol.1, no. 1, 11-32.

Stiemke, M.M., Watsky, M.A., Kangas, T.A., Edelhauser, H.F., (1995), The Establishment and Maintenance of Corneal Transparency, Progress in Retinal and Eye Research, vol. 14, no.1: 109-140.

Suh, M.H., Kwon Ji-Won, Wee, W.R., Han, Y.K., Kim, J.H., Lee, J.H., (2008), Protective Effect of Ascorbic Acid Against Corneal Damage by Ultraviolet B Irradiation: A Pilot Study, Cornea, vol. 27, issue 8, 916-922.

Tai Gui-Hua, Nieduszynski, I.A., Fullwood, N.J., Huckerby, T.N., (1997), Human Corneal Keratan Sulfates, The Journal of Biological Chemistry, vol. 272, no. 45, Issue of November 7: 28227-28231.

Tamura Y., Konomi, H., Sawada, H., Takashima, S., Nakajima, A., (1991), Tissue distribution of type VIII Collagen in human adult and fetal eyes, Investigative Ophthalmology & Visual Science, vol. 32, no. 9, 2636-2644.

Trowbridge, J.M., Gallo, R.L., (2002), Dermatan sulphate: new function from an old glycosaminoglycan, Glycobiology, vol. 12, no. 9: 117R-125R.

Urrets-Zavalia, J.A., Maccio, J.P., Knoll, E.G., Cafaro, T.A., Urrets-Zavalia, E.A., Serra, H.M., (2007), Surface Alterations, Corneal Hypoesthesia, and Iris Atrophy in Patients with Climatic Droplet Keratopathy, Cornea, vol. 26, no. 7, 800-804.

Urrets-Zavalia, J.A., Knoll, E.G., Maccio, J.P., Urrets-Zavalia, E.A., Saad, J.A., Serra, H.M., (2006), Climatic Droplet Keratopathy in the Argentine Patagonia, American Journal of Ophthalmology, vol. 141, no. 4, 744-746.

Volpi, N., (2006), Therapeutic Applications of Glycosaminoglycans, Current Medicinal Chemistry, 13: 1799-1810.

Warrant, E.J., Locket, N.A., (2004), Vision in the deep sea, Biological Reviews, vol. 79, issue 3, 671-712.

Weber, I.T., Harrison, R.W., Iozzo, R.V., (1996), Model Structure of Decorin and Implications for Collagen Fibrillogenesis, The Journal of Biological Chemistry, vol. 271, no. 50, Issue of December 13: 31767-31770.

Winkler, H., Taylor, K.A., (2006), Accurate marker-free alignment with simultaneous geometry determination and reconstruction of tilt series in electron tomography, Ultramicroscopy, 106: 240-254.

Worthington, C.R., Inouye H., (1985), X-ray diffraction study of the cornea, International Journal of Biological Macromolecules, vol. 7, issue 1, 2-8.

Wu, K., Kojima, M., Shui, Y.B., Sasaki, H., (2004), Ultraviolet B-Induced Corneal and Lens Damage in Guinea Pigs on Low-Ascorbic Acid Diet, Ophthalmic Research, 36, 277-283.